APPLICATION OF THE DENSITY FUNCTIONAL THEORY: FROM BIOMOLECULES TO TRANSITION METAL COMPLEXES

by

JUN ZHANG

(Under the Direction of Henry F. Schaefer III)

ABSTRACT

Density functional theory (DFT), as the most popular method in the modern quantum chemistry field, has been applied to two molecular systems.

The first work performs a systematic structure optimization and vibronic analysis of hydrogenated DNA bases (cytosine tautomers and guanine) and base pair (guanine cytosine base pair). A reliable approach combined B3LYP functional with DZP++ basis sets was applied consistently to all structures. The electron affinities of each hydrogenated structure were also predicted. The results have been reported from the Chapter 2 to Chapter 4.

In the second work, the heterometallic binuclear cyclopentadienylironnickel carbonyls $Cp_2FeNi(CO)_n$ ($n$ = 3, 2, 1; Cp = $\eta^5$-$C_5H_5$) have been studied by DFT BP86 functional for comparison with the isoelectronic homometallic dicobalt derivatives $Cp_2Co_2(CO)_n$. A high spin open-shell structure was found for $Cp_2FeNi(CO)$ to have lower total energy than closed-shell structure with multiple Fe-Ni bond, while homometallic $Cp_2Co_2(CO)$ prefers closed-shell structure with multiple Co-Co bond.

INDEX WORDS: Density Functional Theory, Electron Affinity, Gaunine, Cytosine, Guanine-Cytosine Base Pair, Cyclopentadienylironnickel Carbonyls

# APPLICATION OF THE DENSITY FUNCTIONAL THEORY: FROM BIOMOLECULES TO TRANSITION METAL COMPLEXES

by

JUN ZHANG

B. S., Nankai University, Tianjin, China, 1996

M.S., State University of New York at Stony Brook, Stony Brook, NY, 2004

A Dissertation Submitted to the Graduate Faculty of The University of Georgia in Partial Fulfillment of the Requirement for the Degree

DOCTOR OF FHILOSOPHY

ATHENS, GEORGIA

2007

# APPLICATION OF THE DENSITY FUNCTIONAL THEORY: FROM BIOMOLECULES TO TRANSITION METAL COMPLEXES

by

JUN ZHANG

| | |
|---|---|
| Major Professor: | Henry F. Schaefer III |
| Committee: | Nigel G. Adams<br>Geoffrey D. Smith |

Electronic Version Approved:

Maureen Grasso
Dean of the Graduate School
The University of Georgia
December 2007

DEDICATION

To my beloved wife, daughter, and parents

ACKNOWLEDGEMENTS

During the course of my research at the Center for Computational Chemistry (CCC), there are so many people who deserve my special thanks.

First of all, I want to gratefully thank my research advisor Professor Schaefer for recruiting me and giving me an opportunity to work in the CCC's world-class research environment that he created. He builds a wonderful academic research environment at CCC for graduate students. He has a kind and pleasure personality; he is generous, trustworthy, and always helpful; He is a true role model of scientist. I also thank three research scientists. Dr. Xie, Professor Allen and Dr. Yamaguchi are all great teachers and scientists in helping us to understand the subtle details of quantum mechanics. Dr Xie is also my mentor in application and development of the Density Functional Theory. I owe a lot to Dr. Xie for his kindness, patience and willingness to help.

I would like to sincerely thank Professor Nigel Adams and Professor Geoffrey Smith for being my committee members. They are very nice and respectful. I would like to thank Professor R. Bruce King and Professor Paul Schleyer, and Dr. Zhongfang Chen for their great effort in our collaborated papers and very helpful discussion on my research projects. I thank Dr. Qiong Luo and Professor Qian-Shu Li from the Beijing Institute of Technology for their great work in two collaborated papers. I also thank Dr. Jiande Gu from the Shanghai Institute of Materia Medica for his help in my research.

I can't forget to thank the members of CCC supporting stuff Mrs. Linda Rowe, Amy Peterson, Karen Branch and Dr. Richard Remington for insulating me from all the often difficulties. Special thank goes to Dr. Justin Turney for all prompt help with any computer problems. I also want to thank many of past and current graduate students of CCC. Dr. Joseph Larkin was my tutor. Dr. Martin Kim, Dr. Suyun (Holly) Wang and Dr. Ge (Eric) Yan often answered my lots of scientific questions. Heather and Frank have been wonderful officemates for many helpful and fruitful discussions.

I would like to cordially thank my parents, Yaoxian Zhang and Jinmei Ma for giving me a warm home and supporting my study abroad. Finally, my deepest thank goes to my wife Ling Yang. Without her foremost support, I would have never had the courage to finish my graduate study. Her love and consideration is reflected in every accomplishment of mine. I also thank another member of my family, my three years old daughter Mandy. She is such a cute angle. Her smile lives in my mind and brings me joy and hope.

TABLE OF CONTENTS

Page

LIST OF TABLES

Page

LIST OF FIGURES

Page

# CHAPTER 1

# INTRODUCTION AND LITERATURE REVIEW

The goal of computational chemistry is to solve the chemistry problems using computer clusters instead of bench instruments. With the developing of sophisticated theoretical methods and ever-increasing CPU power in recent decades, computational chemistry has evolved into an era where computations can not only confirm and explain experimental results, but also predict and venture experimentally unsolved problems: properties of not-yet-synthesized molecule and dynamics of immeasurable reaction. A combination of state-of-art high level *ab initio* methods and large basis sets can usually yield results that achieve chemical accuracies for small molecules. For larger molecules and molecular clusters (~100 atoms), Density Functional Theory (DFT) methods combined with medium size basis sets can routinely provide reliable results. In a sense like analytical instruments, computation has become an indispensable tool to help chemists explore and understand the world.

This dissertation focuses on the application of DFT methods to explore various "larger" biological and transition metal systems. These systems are yet to be investigated experimentally. The results of DFT computation have provided a foundation for future experimental measurements and further higher-level computations.

## 1.1 THE DEVELOPMENT OF DFT METHODS

### 1.1.1 EARLY ORIGINATION

The earliest approach of using electron density to express the energetic information of atomic system started from 1927. In that year, Thomas and Fermi published two papers in which they proposed that the kinetic energy of heavy atoms could be derived based on the density of electrons in an infinite potential.[1,2] In 1930, Dirac added exchange-energy part to the Thomas

and Fermi's formula.[3] The combined energetic expression is the called Thomas-Fermi-Dirac (TFD) model, which works fine for non-interacting electron system, but failed for molecules. In 1951, Slater introduced the Xα method[4] in order to simplify Hartree-Fock (HF) theory.[5,6] The average exchange potential is approximated from an operator based on the local electron density of uniform-electron-gas. The major breakthrough of the development of DFT is in 1964 when Hohenberg and Kohn proved that the electron density both corresponds to a Hamiltonian with external potential v(r) and can be obtained from antisymmetric wavefunction.[7] In the next year, Kohn and Sham reformulate the DFT equation to allow exact solution of kinetic energy functional and introduced orbitals to DFT, which are called Kohn-Sham orbitals.[8] Apart from previous TFD-DFT which represents both kinetic and exchange-correlation energy by the function of the electron density, the Kohn-Sham DFT only proposes exchange-correlation energy as the function of the electron density while the kinetic energy is still the function of the electronic wave functions as in the traditional HF theory. However, the exact form of exchange-correlation functional has been unknown. The Kohn-Sham DFT provides the foundation of the development of modern DFT.

### 1.1.2 DFT FUNTIONALS

The formalism of the DFT equation can be divided into five components:

$$E[\rho(r)] = E_T + E_V + E_J + E_X + E_C$$

where the five components represent the kinetic energy of the non-interacting electron, the electron-nuclei coulombic interaction, the electron-electron coulombic repulsion, the correction to the kinetic energy deriving from the interacting nature of the electrons (exchange correction), and all non-classical corrections to the electron-electron repulsion energy (correlation correction),

respectively. Both the exchange and correlation correction usually combined together called exchange-correlation energy ($E_{XC}$). The $E_{XC}$ are most difficult terms for implementation and various exchange and correlation functionals have been proposed to treat the corrections in the modern DFT. One of the earliest is the Local Spin Density Approximation (LSDA), which treats electron density locally as a uniform electron gas. This functional combines the Vosko, Wilki, and Nusair's 1980 correlation functional (VWN) [9] and Slater's exchange functional.[10] The LSDA functional was known to over-bind molecules. There are two types of functionals which added further corrections to LSDA: the Generalized Gradient Approximation (GGA) which formulates the derivative of the local density as a no non-local component. The later includes some mixing with the HF theory and so-called the Hybrid functional.

The presented research in this dissertation mainly uses the following functionals: namely BHLYP, B3LYP, BLYP, and BP86. The first three are combinations of the half-and-half hybrid functional (BH),[11] Becke's three parameter exchange functional (B3),[12] or Becke's 1988 pure DFT exchange functional (B),[13] respectively, with the correlation functional of Lee, Yang, and Parr (LYP).[14] The last functional combines the B exchange with Perdew's correlation functional (P86).[15-16]

## 1.2 COMPUTATIONAL DETAILS

The Gaussian 94[17] suites of program were used to perform all theoretical computations in this dissertation. The Huzinaga-Dunning DZP[18-19] basis sets were used for the transition metal complexes studies and the DZP++[20] basis sets were used for all the electron affinity prediction for damaged DNA bases and base pairs studies. The DFT with DZP++ basis sets approach for electron affinity prediction has been tested within 0.2 eV of the experimentally reported.[21]

## 1.3 OVERVIEW OF CHAPTERS

### 1.3.1 HYDROGENATED AND HYDRIDED DNA SUBUNITS

In Chapter 2, the structures, energetics, and electron affinities of eighteen H-addition cytosine radical isomers $(C+H)^{\bullet}$ are predicted using carefully calibrated density functional methods.[21] Radical rO1 in which H is attached at the N3 site of amino-oxo cytosine, has the lowest energy. The lowest energy anion is aO2, in which $H^{-}$ is attached to the C5 site of amino-oxo cytosine. The theoretical adiabatic electron affinities (AEAs) for the eighteen radicals range from -0.20 eV to 2.59 eV. Radical rO4, where the additional H atom is at C4 site has the largest AEA. In contrast, when H is attached to the N3 site of *trans* amino-hydroxy form, the resulting radical rA1 has a negative AEA, –0.20 eV. The radical rB1**,** in which H is appended on the N1 atom of *cis* amino-hydroxy form, also has the negative AEA value -0.16 eV. Generally, the AEA values for the cytosine H-addition radicals are rather smaller than those of the earlier studied H-abstraction cytosine radicals, which range from 2.22 eV to 3.00 eV.

In Chapter 3, The structures, energetics, and vibrational frequencies of nine hydrogenated 9H- *keto*-guanine radicals $(G+H)^{\bullet}$ and closed-shell anions $(G+H)^{-}$ are predicted using the B3LYP density functional method in conjunction with a DZP++ basis set. These radical and anionic species come from consecutive electron attachment to the corresponding protonated $(G+H)^{+}$ cations in low pH environments. The $(G+H)^{+}$ cations are studied using the same level of theory. The proton affinity (PA) of guanine computed in this research (228.1 kcal/mol) is within 0.7 kcal/mol of the latest experiment value. The radicals range over 41 kcal/mol in relative energy, with radical r1, in which H is attached at the C8 site of guanine, having the lowest energy. The lowest energy anion is a2, derived by hydride ion attachment at the C2 site of

guanine. No stable N2-site hydride should exist in the gas phase. Structure a9 was predicted to be dissociative in this research. The theoretical adiabatic electron affinities (AEA), vertical electron affinities (VEA), and vertical detachment energies (VDE) were computed, with AEAs ranging from 0.07 eV to 3.12 eV for the nine radicals.

In Chapter 4, The radicals generated by hydrogen atom addition to the Watson-Crick Guanine-Cytosine (G-C) DNA base pair were studied theoretically using an approach that has proved effective in predicting molecular structures and energetics. All optimized structures were confirmed to be minima via vibrational frequency analysis. The dissociation energies of the base pair radicals are predicted and compared with that of neutral G-C base pair. The lowest energy base pair radical is that with the hydrogen atom attached to the C8 position of guanine, resulting in the nitrogen radical designated G(C8)-C. In this the most favorable radical, the G-C pair C8=N7 distance of 1.310 Å increases to 1.453 Å when the π bond is broken upon hydrogen atom addition. This radical has a dissociation energy of 28 kcal/mol, which may be compared with 27 kcal/mol for neutral G-C. The other $(GC+H)^{\bullet}$ radical dissociation energies range downward to 8 kcal/mol. Significant structural changes were observed when the hydrogen was added to the sites where the inter-strand hydrogen bonds are formed. For example, “butterfly” shape structures were found when the hydrogen atom adds to the C4 or C5 sites of guanine. The formation of radical G(C2)-C may cause single strand break because of significant strain in the closely stacked base pairs. Radical G(C8)-C is of biological importance because it may be an intermediate in the formation of 8-oxo guanine.

In Chapter 5, The anionic species resulting from hydride addition to the Watson-Crick Guanine-Cytosine (GC) DNA base pair are investigated theoretically. Proton transferred structures of GC hydride, in which proton H1 of guanine or proton H4 of cytosine migrates to the

complementary base pair side, have been also studied. All optimized geometrical structures are confirmed to be minima via vibrational frequency analyses. The lowest energy structure places the additional hydride on the C6 position of Cytosine coupled with proton transfer, resulting in the closed-shell anion designated **1T** ($G^{-}C(C6)$). Energetically, the major groove side of the GC pair has a greater propensity toward hydride/hydrogen addition than does the minor grove side. The pairing (dissociation) energy and electron attracting ability of each anionic structure are predicted and compared with those of the neutral GC and the hydrogenated GC base pairs. Anion 8T ($G(O6)C^{-}$) is a water-extracting complex and has the largest dissociation energy. Anion 2 ($GC(C4)^{-}$) and the corresponding open-shell radical GC(C4) have the largest vertical electron detachment energy and adiabatic electron affinity, respectively. From the difference between the dissociation energy and electron removal ability of the normal GC anion and the most favorable structure of GC hydride, it is clear that one may dissociate the GC anion and maintain the integrity of the GC hydride.

### 1.3.2 ISOELECTRONIC HETEROMETALLIC AND HOMOMETALLIC BINUCLEAR CYCLOPENTADIENYLMETAL CARBONYLS

In Chapter 6, The heterometallic binuclear cyclopentadienylironnickel carbonyls $Cp_2FeNi(CO)_n$ ($n$ = 3, 2, 1; Cp = $\eta^5$-$C_5H_5$) have been studied by density functional theory (BP86) for comparison with the isoelectronic homometallic dicobalt derivatives $Cp_2Co_2(CO)_n$. The FeNi tricarbonyl is shown to be the doubly bridged isomer $Cp_2Fe(CO)Ni(\mu\text{-}CO)_2$ with an Fe–Ni distance of 2.455 Å (BP86), in accord with experiment and in contrast to $Cp_2Co_2(CO)_3$ where singly and triply bridged but not doubly bridged isomers are found. The dicarbonyls $Cp_2FeNi(\mu\text{-}CO)_2$ and $Cp_2Co_2(\mu\text{-}CO)_2$ both have analogous doubly bridged structures with M=M

distances around 2.35 Å, suggesting formal M=M double bonds. The monocarbonyls have analogous singly bridged axial structures $Cp_2FeNi(\mu\text{-}CO)$ and $Cp_2Co_2(\mu\text{-}CO)$ with metal-metal distances in the range 2.05 Å ($M_2 = Co_2$) to 2.12 Å ($M_2$ = FeNi) consistent with the formal M≡M triple bonds required for the favored 18-electron configuration. Open-shell states of $Cp_2FeNi(\mu\text{-}CO)$ are found to have even lower energies than the closed-shell structure, which indicates that the ground state of $Cp_2FeNi(\mu\text{-}CO)$ might be a high spin structure. However, the global minimum for the monocarbonyl is found to be a singlet "hot dog" perpendicular $Cp_2NiFe(CO)$ structure with a terminal CO group bonded to the iron atom. Other higher energy perpendicular structures are also found for $Cp_2FeNi(CO)_n$ ($n$ = 3, 2, 1) with terminal CO groups and bridging Cp rings.

## 1.4 REFERENCES


1. Fermi, E. *Rend. Accad. Lincei*, **1927**, *6*, 602.
2. Thomas, L. H. *Proc. Cambridge Phil. Soc.* **1927**, *23*, 542.
3. Dirac, P. A. M. *Proc. Cambridge Phil. Soc.* **1930**, *26*, 376.
4. Slater, J. C. *Phys. Rev.* **1951**, *81*, 385.
5. Hartree, D. R. *Proc. Cambridge Phil. Soc.* **1928**, *24*, 426.
6. Slater, J. C. *Phys. Rev.*, **1951**, *81*, 385.
7. Hohenberg, P.; Kohn, W. *Phys. Rev.*, **1964**, *136*, B864.
8. Kohn, W.; Sham, L. J. *Phys. Rev.*, **1965**, *137*, 1697.
9. Vosko, S. H.; Wild, L.; Nusair, M. *Can. J. Phys.*, **1980**, *58*, 1200.
10. Slater, J. C. *Quantum Theory of Molecules and Solids: The Self-Consistent Field for Molecules and Solids, Vol. IV.* McGraw-Hill, New York, **1974**.

11. Becke, A. D. *J. Chem. Phys.* **1993**, *98*, 1372.

12. Becke, A. D. *J. Chem. Phys.* **1993**, *98*, 5648.

13. Becke, A. D. *Phys. Rev. A* **1988**, *38*, 3098.

14. Lee, C.; Yang, W.; Parr, R. G. *Phys. Rev. B* **1988**, *37*, 785.

15. Perdew, J. P. *Phys. Rev. B* **1986**, *33*, 8822.

16. Perdew, J. P. *Phys. Rev. B* **1986**, *34*, 7406.

17. Frisch, M. J.; Trucks, G. W.; Schlegel, H. B.; Scuseria, G. E.; Robb, M. A.; Cheeseman, J. R.; Zakrzewski, V. G.; Montgomery, J. A.; Stratmann, R. E.; Burant, J. C.; Dapprich, S.; Millam, J. M.; Daniels, A. D.; Kudin, K. N.; Strain, M. C.; Farkas, O.; Tomasi, J.; Barone, V.; Cossi, M.; Cammi, R.; Mennucci, B.; Pomelli, C.; Adamo, C.; Clifford, S.; Ochterski, J.; Petersson, G. A.; Ayala, P. A.; Cui, Q.; Morokuma, K.; Salvador, P.; Dannenberg, J. J.; Malick, D. K.; Rabuck, A. D.; Raghavachari, K.; Foresman, J. B.; Cioslowski, J.; Ortiz, J. V.; Baboul, A. G.; Stefanov, B. B.; Liu, G.; Liashenko, A.; Piskorz, P.; Komaromi, I.; Gomperts, R.; Martin, R. L.; Fox, D. J.; Keith, T.; Al-Laham, M. A.; Peng, C. Y.; Nanayakkara, A.; Challacombe, M.; Gill, P. M. W.; Johnson, B. G.; Chen, W.; Wong, M. W.; Andres, J. L.; Gonzalez, C.; Head-Gordon, M.; Replogle, E. S.; Pople, J. A. *Gaussian 94*, revision c.3; Gaussian, Inc.: Pittsburgh, PA, **1995**.

18. Huzinaga, S. *J. Chem. Phys.* **1965**, *42*, 1293.

19. Dunning, T. H. *J. Chem. Phys.* **1970**, *53*, 2823.

20. Lee, T. J.; Schaefer, H. F. *J. Chem. Phys.* **1985**, *83*, 1784.

21. Rienstra-Kiracofe, J. C.; Tschumper, G. S.; Schaefer, H. F.; Nandi, S.; Ellison, G. B. *Chem. Rev.* **2002**, *102*, 231.

# CHAPTER 2

# ADDITION OF HYDROGEN ATOM/HYDRIDE ANION TO THE DOUBLE BONDS OF CYTOSINE TAUTOMERS: RADICAL AND ANION STRUCTURES AND ENERGETICS[1]

[1] Zhang, J. D.; Xie, Y.; Schaefer, H. F., III; Luo, Q.; Li, Q.-S. To be submitted to Molecular Physics.

## 2.1 ABSTRACT

The structures, energetics, and electron affinities of eighteen H-addition cytosine radical isomers $(C+H)^{\bullet}$ are predicted using carefully calibrated density functional methods (*Chem. Rev.* **2002**, *102*, 231). Radical **rO1** in which H is attached at the N3 site of amino-oxo cytosine, has the lowest energy. The lowest energy anion is **aO2**, in which $H^-$ is attached to the C5 site (see Figure 2.1) of amino-oxo cytosine. The theoretical adiabatic electron affinities (AEAs) for the eighteen radicals range from -0.20 eV to 2.59 eV. Radical **rO4**, where the additional H atom is at C4 site has the largest AEA. In contrast, when H is attached to the N3 site of *trans* amino-hydroxy form, the resulting radical **rA1** has a negative AEA, –0.20 eV. The radical **rB1,** in which H is appended on the N1 atom of *cis* amino-hydroxy form, also has the negative AEA value -0.16 eV. Generally, the AEA values for the cytosine H-addition radicals are rather smaller than those of the earlier studied H-abstraction cytosine radicals, which range from 2.22 eV to 3.00 eV.

## 2.2 INTRODUCTION

One aspect of DNA damage[1] can be represented by hydrogen atom addition to the double bonds of the nucleic acid bases (NABs)[2]. The resulting H-adduct radicals can undergo fast transformation to cause further DNA lesions such as single strand breaks (SSB)[3], double strand breaks (DSB)[4] and mutations[5]. Greenberg's recent research shows DNA radicals may result in damages, including tandem lesions[6] and interstrand cross-links[7]. It is interesting and challenging to explore the chemistry of these transient radical intermediates during the process of altering and repairing genetic information.

Net hydrogen gain and loss in NABs can also be represented by protonation or deprotonation processes involving the pyrimidines and purines within the DNA strand. As noted by Steenken in his influential 1989 review,[8] the reactivity of DNA radicals is related to the tendency of the radicals to undergo protonation or deprotonation. In Bernhard's early research,[9] the protonation and deprotonation processes were found to have drastic effects on the chemical reactivities of the species involved. More recently, in Leszczynski's[10-11] exploration of proton transfer between DNA base pairs, non-planar base pairs are predicted theoretically.

Among the four DNA bases, cytosine has been the focus of much research along these lines, because cytosine is the primary reduction site in DNA.[8] For the standard numbering of atoms in cytosine tautomers see Figure 2.1. Experimentally, the radical arising from hydrogenation on the C5 site $(C5+H)^{\bullet}$ in 1-methylcytosine (1-MeC) was characterized by Wyard and Elliott in 1973[12] by electron paramagnetic resonance (EPR) methods. In 2002, Debije and Bernhard observed the hydrogen adducts at the C5 and C6 positions of both cytosine and thymine in EPR spectroscopy experiments.[13] In the same year, Debije and Bernhard also detected the radical cation $Cyt(C6+H, N3+H)^{+\bullet}$ in crystalline $d(CGCG)_2$ by EPR, in which there is a net gain of a hydrogen atom at C6 and a proton at N3 following X irradiation.[14] There are few theoretical studies of hydrogenated cytosine radicals. Colson and Sevilla estimated the enthalpies associated with hydrogen radical addition to nucleic acid bases, using both ab initio ROHF/6-31G* and semiempirical PM3 methods in 1997.[15] Turecek and Yao explored hydrogenated cytosine systems both theoretically and experimentally, and the energetic order of the radical isomers was predicted in 2003.[16a] An analogous experiment/theory paper[16b] on adenine radicals appeared in 2005. In their most recent paper[17], the methyl cytosine derivatives $Cyt\ (N1+Me,\ N3+H)^{+}$ and $Cyt\ (N1+Me,\ N5+H)^{+}$ were characterized by Turecek from

collisionally activated dissociation (CAD) mass spectra that showed characteristic differences in ion-dissociation patterns.

Theoretically, the adiabatic electron affinity (AEA) of cytosine in the gas phase has been predicted to be essentially zero (0.03 eV, B3LYP/DZP++) by Wesolowski and co-workers.[18] However, the anionic structures and AEAs of hydrogenated cytosine *radicals* are unclear. The purpose of the present research is to carry out a comprehensive theoretical investigation of the possible radical isomers derived from three cytosine isomers by adding a hydrogen atom. Compared to Turecek and Yao's paper[16a], more H-adduct conformers are considered in this research. Further, we consider all the anions arising from attaching an electron to the above cytosine radicals.

## 2.3 THEORETICAL METHODS

The total energies, equilibrium geometries, and vibrational frequencies for the radicals and anions considered in this study are predicted using four density functional methods, namely BHLYP, B3LYP, BLYP, and BP86. The first three are combinations of the half-and-half hybrid functional (BH),[19] Becke's three parameter exchange functional (B3),[20] or Becke's 1988 pure DFT exchange functional (B),[21] respectively, with the correlation functional of Lee, Yang, and Parr (LYP).[22] The last functional combines the B exchange with Perdew's correlation functional (P86).[23-24] Double- ζ quality basis sets with added polarization and diffuse functions, denoted DZP++, were used with the DFT methods. The DZP++ basis sets were constructed by augmenting the Huzinaga-Dunning[25-26]contracted double-ζ set with one set of *p*-type polarization functions for each H atom and one set of five *d*-type polarization functions for the C, N, and O atoms [$\alpha_p$ (H) = 0.75, $\alpha_d$ (C) = 0.75, $\alpha_d$ (N) = 0.80, $\alpha_d$ (O) = 0.85]. To complete the DZP++ basis

sets, one even-tempered diffuse *s* function is added to each H atom, while sets of even-tempered *s* and *p* diffuse functions are centered on each heavy atom. The even-tempered orbital exponents were determined by the convention of Lee and Schaefer.[27] In the final DZP++ basis set, 6 contracted functions per H atom and 19 functions per C, N, or O atom are included. The total number of basis functions for the cytosine radicals $(C+H)^{\bullet}$ is 188. The geometry optimizations are performed using analytic gradients with keyword tight convergence criteria. All computations were carried out with the GAUSSIAN 94 and GAUSSIAN 03 program packages.[28]

The electron affinities were determined in the following manner. The adiabatic electron affinity (AEA) is defined as the energy difference between the neutral and corresponding anion species at their respective optimized geometries

AEA = *E*(optimized neutral) – *E*(optimized anion).

the vertical electron affinity (VEA) of the radical is defined as

VEA = *E*(optimized neutral) – *E*(anion at optimized neutral geometry).

and the anion vertical detachment energy (VDE) is determined via

VDE = *E*(neutral at optimized anion geometry) – *E*(optimized anion).

## 2.4 RESULTS AND DISCUSSION

### 2.4.1 RADICALS

Three cytosine isomers were considered, the standard amino-oxo form and two rotamers (*trans* and *cis* designated as A and B, respectively) of the amino-hydroxy form. Sketches of these three closed-shell singlet cytosine isomers are displayed in Figure 2.1 with heavy atoms numbered following previous studies[29]. Although these three cytosine isomers should be observable in the gas phase, only the standard amino-oxo form is pertinent to the Watson-Crick

structure. This is because in the DNA pyrimidine base the N1 atom is the position at which the glycosidic bond is attached. There are also two imino-oxo rotamers[30] of cytosine, but the latter have not been considered in the present research. As discussed in the pioneering experimental study of Bowen and coworkers,[31] non-Watson-Crick structures must be invoked to understand the spectroscopy of bio-molecules in the gas phase. There are three double bonds for each of the three cytosine isomers considered here. Thus, by attaching one hydrogen atom to break a double bond, six isomers can be generated from the each cytosine structure. The total 18 isomers may be designated as **rO1-rO6** (derived from the amino-oxo form of cytosine), **rA1-rA6** (derived from amino-hydroxy *trans* form of cytosine) and **rB1-rB6** (derived from amino-hydroxy *cis* form of cytosine). All these hydrogenated isomers are shown in Table 2.1 with the formal radical center indicated.

The optimized geometries for each particular structure using various functional methods are in general very similar. The present discussion of the structural and energetic features is made primarily from the B3LYP results. The optimized geometries, total energies, and the zero-point vibrational energies predicted by all four functional methods (B3LYP, BHLYP, BLYP, and BP86) are accessible in the supporting information.

*1. Radicals Derived From Amino-Oxo Cytosine (rO1–rO6)*

The geometries of the **rO1**–**rO6** radicals are displayed in Figure 2.2. For the radical **rO1** ($C_s$ symmetry), corresponding to the attachment of H to the N3 site of amino-oxo cytosine, the amino group hydrogen atoms are out of plane. The CN bond distances N1-C2 (1.385 Å) and C2-N3 (1.387 Å) are very similar, and the C4-C5 and C5-C6 bond lengths are nearly the same (1.391 Å). This confirms the presence of delocalized π bonding interactions around the ring. As shown in Figure 2.7, the spin density in **rO1** is mainly delocalized on the C4 and C6 atoms with

0.54 “electrons” at C6 in **rO1**, in excellent agreement with the experimental deduction of 0.53.[32] It is also shown in Figure 2.7 that the unpaired electron distribution for **rO3** is slightly more delocalized than that of **rO2**, perhaps explaining why **rO3** is more energetically stable than **rO2** (by 2.1 kcal/mol, Table 2.2).

When a hydrogen atom adds to the C2 position to break the carbonyl double bond, there are two radicals formed, **rO5** and **rO6** as *trans* and *cis* isomers, respectively (Figure 2.2). The two radicals derived from the amino-oxo form of cytosine, **rO1** and **rO2**, keep their six-member rings planar after the hydrogen atom appendage. For the other radicals, the ring planarity is slightly disturbed due to pyramidization at the hydrogen addition site (Figure 2.2).

*2. Radicals Derived From Amino-Hydroxy Cytosine (rA1–rA6 and rB1–rB6)*

The structures of the H-addition radicals (**rA1**–**rA6 and rB1**–**rB6)** derived from amino-hydroxy cytosine conformers are shown in the Figure 2.3. When a hydrogen atom adds to N3, only the *trans* radical **rA1** could be optimized. The reason is that the *cis* adduct will experience a heavy steric effect between atom $H_{7'}$ and the hydrogen atom on N3 (see Table 2.1). For the same reason, **rB1** is the only radical derived from hydrogen atom addition to the N1 site.

The other radicals from the amino-hydroxy cytosines necessarily form two possible conformers corresponding *trans* and *cis* forms of amino-hydroxy cytosine, such as the **rA3** and **rB3** pair (H-addition at the C5 site), the **rA2** and **rB2** pair (at the C6 site) and the **rA4** and **rB4** pair (at the C4 site). Similar to hydrogen addition to atom C2 of the amino-oxo form, *trans* and *cis* isomers are obtained for both amino-hydroxy radical rotamers, which are named as **rA5**, **rA6** and **rB5, rB6**, respectively.

*3. Energies*

The total and relative energies for the eighteen radicals at the B3LYP/DZP++ level of theory are reported in Table 2.2. These results are summarized schematically in Figure 2.9. Radical **rO1** is predicted to have the lowest energy. This result is consistent with the experimental observation that the $(N3+H)^{\bullet}$ amino-oxo cytosine radical and $(N1–H)^{\bullet}$ uracil radical were derived from single crystals of 1-MeC:5-FU via X-irradiation[32]. Of course, comparison of the present results (strictly relevant to gas phase processes) with condensed phase experiments must be done cautiously.

The BLYP and BP86 methods predict the same energetic order for the radicals as B3LYP, while BHLYP assigns a different order between **rB3** and **rB1**. The three radicals derived from the two amino-oxo isomers, **rO1**, **rO3**, and **rO2**, lie lowest in energy followed by the twelve radicals from the amino-hydroxy conformers. The *trans* and *cis* radical pairs from the amino-oxo isomer, **rO5** and **rO6**, have the highest energies, namely 43 and 44 kcal/mol higher than the minimum **rO1** (Table 2.2). Benefiting from delocalized π bonding, **rO1** is the most stable radical, indicating that atom N3 of amino-oxo cytosine is the most favored site for H addition.

Energies of radicals derived from amino-hydroxy cytosine ranged from 9.7 to 26.5 kcal/mol when compared with the most favorable minimum **rO1** (B3LYP/DZP++). As shown in Table 2.2, the energy differences between paired conformers, such as **rA1** and **rB1**, **rA2** and **rB2**, etc. are only around 1 kcal/mol. Moreover, when the additional hydrogen atom adds to the C2 site, the resulting four isomers, labeled **rA5**, **rB5**, **rA6** and **rB6** have even smaller energy gaps, within only 0.4 kcal/mol, which indicates that the actual C2 hydrogenated adducts could be very complex. Thus the biochemical selectivity would play a key role in deciding the final products.

Turecek and Yao[16] predicted 11 of our 18 possible double bond breaking hydrogen addition products at the B3LYP/6-31+G(d,p) level theory (Table 2.2). Their energetic order is confirmed in the present paper except for switching **rA3** and **rB3**. Sevilla and co-workers[33] predicted the relative stability of **rO1** and **rB1** with the HF/6-31G*//HF/3-21G method. Radical **rO1** was predicted by Sevilla to be the most stable radical, and **rB1** to lie energetically higher by 13.7 kcal/mol. The same energetic order of the two radicals is shown in the present study, though the predicted energy gap between the two radicals is somewhat less than that of Sevilla. Specifically, **rB1** is predicted to lie at 11.4 kcal/mol (B3LYP), 11.7 kcal/mol (BHLYP), 11.5 kcal/mol (BLYP) and 11.2 kcal/mol (BP86), a remarkably consistent array of predictions.

### 2.4.2 ANIONS

The optimized geometries for the eighteen $(C+H)^-$ anions at the B3LYP/DZP++ level of theory are displayed in Figure 2.4 (Labeled as **aO1-aO6)** and Figure 2.5, (labeled as **aA1-aA6** and **aB1-aB6**), and the total and relative energies are reported in Table 2.3. These results are summarized energetically in Figure 2.9. Only the closed-shell singlet states are considered for these anions. All anions are marked as "**a**" in contrast to "**r**" for radicals.

The optimized geometry of **aO5** from the BLYP method is inconsistent with other three functionals. A N1-C2 broken bond minimum is found with BLYP **(Figure 2.6a)**. This minimum is not confirmed by the other functionals. Note also that the same optimized geometry is obtained for the **aA6** and **aB6** anions with the BHLYP method **(**Figure 2.6b**)**, while two distinct structures are optimized separately under the other three functionals with energetic differences about 0.53 kcal/mol.

Figures 4 and 5 shows that adding one electron to the neutral radicals leads to significant changes in the geometries. For example, the six-member ring in anion **aO1** seriously deviates from planarity compared to **rO1**, and the bond distances between the heavy atoms in **aO1** differ significantly from those of **rO1**. These considerable structural changes between the radicals and their related anions confirm that all anions are of distinctly covalent character. It is intriguing to compare the geometry alterations between **aO2** and **rO2**. The bond distances change from **rO2** to **aO2** in the following way: $C_2$-$N_3$ 1.403 → 1.355 Å, $N_3$-$C_4$ 1.322 → 1.371 Å, $C_4$-$N_5$ 1.428 → 1.372 Å, and $C_2$-$O_7$ 1.228 → 1.255 Å. It is seen that shorter bond lengths in the radical become longer in the anions, while some longer distances become shorter. This reflects the character of increasing delocalization for the anions, and may be the reason why **rO2** is the global minimum among all the anions (Table 2.3).

It is shown in Table 2.3 that the energetic order of the anions differs significantly from that of the analogous radicals. Anion **aO2** is the most favored energetically, followed by **aO4**. Unlike the radical systems, a**A4** and a**B4 (**the anions with H-addition at the C4 site) are more stable than **aA2** and **aB2** (H-addition at the C5 site). Quite different from the radicals **rA1** and **rB1**, the negative ions **aA1** and **aB1** have the highest energies among the anions, lying 54 and 52 kcal/mol, respectively, above the global minimum **aO2**.

### 2.4.3 ELECTRON AFFINITIES

Three kinds of neutral-anion energy separations, the adiabatic electron affinities (AEA), the vertical electron affinities (VEA), and the vertical detachment energies (VDE) for the related anions, are reported in Tables 4 - 6. The results predicted by the B3LYP, BLYP, and BP86 methods are close to each other, with a few exceptions, but the BHLYP results are rather

different. The B3LYP method is often considered to be the most reliable,[34-35] so our discussion is based on the results from B3LYP. The adiabatic electron affinities with and without zero-point vibrational energy (ZVPE) corrections are reported in Table 2.4. Note that the ZPVE corrections are quite small. The relative energies of anions $(C+H)^-$ and radicals $(C+H)^\bullet$ also showed in Figure 2.9, the energy gap between radical and anion characterizing the magnitude of the AEA.

Compared to the AEA values for the earlier studied cytosine H-abstraction radicals[29], the electron affinities for the H-addition radicals are rather smaller. The **rO4** radical studied here has the largest AEA (2.59 eV), while **rA1** and **rB1** have negative AEA values -0.20 eV and -0.16 eV, respectively. The values of AEA for **rA3** and **rB3**, the two conformers of the $(C5+H)^\bullet$ radical, are very close to each other, within 0.01 eV. The analogous situation occurs for **rA2**/**rB2** and **rA4**/**rB4**. The most stable radical **rO1** has a very small positive AEA of 0.13 eV.

The VEA values for **rO1**, **rO3**, **rA1** and **rB1** are negative. These radicals at their equilibrium geometries will not bind an electron. The vertical detachment energies (VDE) for the anions are necessarily higher than the AEAs for the relative radicals, and they are predicted to be positive except for **aB1** at BHLYP (with –0.06 eV). The highest B3LYP VDE is 2.94 eV for **aO4,** and the lowest is 0.75 eV for **aO1** (Table 2.6). The VEA and VDE values are quite different (Tables 5 and 6), because the significant changes in the structures between the cytosine radicals and their corresponding anions.

## 2.5 CONCLUSION

In the present work, eighteen radical isomers $(C+H)^{\bullet}$ are generated from H atom attachment to cytosine (six from amino-oxo and twelve from the two amino-hydroxy conformers). The theoretical electron affinities are predicted by four carefully calibrated density functionals,[35] B3LYP, BHLYP, B3LYP, and BP86 in conjunction with DZP++ basis sets.

The attachment of H at the N3 site of amino-oxo cytosine produces the lowest energy radical **rO1**. For amino-hydroxy cytosine, H-addition yields two possible conformers. For instance, structures **rA3** and **rB3** are OH rotamers, with H attached at the C5 site; similarly **rA2** and **rB2** involve H addition at the C6 site, and radicals **rA4** and **rB4** have H added at the C4 site. C5 is the favored site for hydrogen atom addition compared to C6, either for amino-oxo cytosine or amino-hydroxy cytosine.

The energetic order for the anions differs very significantly from that of the analogous radicals. Anion **aO2** has the lowest energy. Using the B3LYP method, adiabatic electron affinities are predicted for the eighteen radicals in the range –0.20 eV to 2.59 eV. The ZPVE corrections are generally small (Table 2.4). Radical **rO4** has the largest AEA (2.59 eV), while **rA1** and **rB1** do not bind an electron (-0.16 eV and -0.20 eV, respectively). The AEA values for the earlier studied H-abstraction radicals $(C–H)^{\bullet}$ from amino-oxo cytosine ranged from 2.22 eV to 3.00 eV,[29] generally larger than those for the H-addition radicals $(C+H)^{\bullet}$ examined in this work. The theoretical VEA and VDE values are quite different from the adiabatic electron affinities (See Figure 2.10), due to the considerable geometrical changes between the radicals $(C+H)^{\bullet}$ and the corresponding anions $(C+H)^{-}$.

## 2.6 ACKNOWLEDGEMENTS

We appreciate the generous support of the U. S. National Science Foundation, Grant CHE-0451445.

## 2.7 REFERENCES

1. von Sonntag, C. The Chemical Basis of Radiation Biology; Taylor and Francis; New York, **1987.**
2. (a). O'Neill, P.; Fielden, M. Advancss in Radiation Biology. **1993**, vol. 17, pp 53-120 (b). Becker, D.; Sevilla, M.D. Advances in Radiation Biology. **1993**, vol. 17 pp, 121-131 (c). Colson, A.O.; Sevilla, M.D. *Int. J. Radiat. Biol.* **1995**, 67, 627 (d). Sanche, L. *Mass Spectrometry Reviews* **2002**, *21*, 349.
3. Ahnstroem, G. *Intern. J. Radiat. Biol.* **1988**, *54*, 695.
4. Karagiannis, T.C.; El-Osta, A. *Cell. Mol. Life Sci.,* **2004**, *61*, 2137.
5. Llano, J.; Eriksson, L.A. *Phys. Chem. Chem. Phys.* **2004**, *6*, 4707.
6. Cater, K.N.; Greenberg, M. M. *J. Am. Chem. Soc.* **2003**, *125*, 13376.
7. Hong, I. S.; Greenberg, M. M. *J. Am. Chem. Soc.* **2005**, *127*, 3692.
8. Steenken, S. *Chem. Rev.* **1989**, *89*, 503.
9. Bernhard, W. A. *Adv. Radiat. Biol.* **1981**, *9*, 199.
10. Gorb, L.; Podolyan, Y.; Dziekonski, P.; Sokalski, W. A.; Leszczynski, J. *J. Am. Chem. Soc.* **2004**, *126*, 10119.
11. Gu, J.; Wang, J.; Leszczynski, J. *J. Am. Chem. Soc.* **2004**, *126*, 12651.
12. Wyard, S. J.; Elliott, J. P. *Ann. N.Y. Acad. Sci.* **1973**, *222*, 628.
13. Debije, M.D.; Bernhard, W.A. *J. Phys. Chem. A* **2002**, *106*, 4608.

14. Debije, M. G.; Close, D. M.; Bernhard, W. A. *Radiation Research* **2002**, *157*, 235.

15. Colson, A.O.; Becker, D.; Eliezer, I.; Sevilla, M.D. *J. Phys. Chem. A* **1997**, *101*, 8935.

16. (a). Turecek, F.; Yao, C. *J. Phys. Chem. A* **2003**, *107*, 9221. (b). Chen, X.; Syrstad, E. A.; Nguyen, M. T.; Gerbaux, P. G.; Turecek, F. *J. Phys. Chem. A* **2005**, *109*, 8121.

17. Yao, C.; Cuadrado-Peinado, M. L.; Polasek, M.; Turecek, F. *Angew. Chem. Int. Ed.* **2005**, *44*, 6708.

18. Wesolowski, S. S.; Leininger, M. L.; Pentchev, P. N.; Schaefer, H. F. *J. Am. Chem. Soc.* **2001**, *123*, 4023.

19. Becke, A. D. *J. Chem. Phys.* **1993**, *98*, 1372.

20. Becke, A. D. *J. Chem. Phys.* **1993**, *98*, 5648.

21. Becke, A. D. *Phys. Rev. A* **1988**, *38*, 3098.

22. Lee, C.; Yang, W.; Parr, R. G. *Phys. Rev. B* **1988**, *37*, 785.

23. Perdew, J. P. *Phys. Rev. B* **1986**, *33*, 8822.

24. Perdew, J. P. *Phys. Rev. B* **1986**, *34*, 7406.

25. Huzinaga, S. *J. Chem. Phys.* **1965**, *42*, 1293.

26. Dunning, T. H. *J. Chem. Phys.* **1970**, *53*, 2823.

27. Lee, T. J.; Schaefer, H. F. *J. Chem. Phys.* **1985**, *83*, 1784.

28. (a) Frisch, M. J.; Trucks, G. W.; Schlegel, H. B.; Scuseria, G. E.; Robb, M. A.; Cheeseman, J. R.; Zakrzewski, V. G.; Montgomery, J. A.; Stratmann, R. E.; Burant, J. C.; Dapprich, S.; Millam, J. M.; Daniels, A. D.; Kudin, K. N.; Strain, M. C.; Farkas, O.; Tomasi, J.; Barone, V.; Cossi, M.; Cammi, R.; Mennucci, B.; Pomelli, C.; Adamo, C.; Clifford, S.; Ochterski, J.; Petersson, G. A.; Ayala, P. A.; Cui, Q.; Morokuma, K.; Salvador, P.; Dannenberg, J. J.; Malick, D. K.; Rabuck, A. D.; Raghavachari, K.;

Foresman, J. B.; Cioslowski, J.; Ortiz, J. V.; Baboul, A. G.; Stefanov, B. B.; Liu, G.; Liashenko, A.; Piskorz, P.; Komaromi, I.; Gomperts, R.; Martin, R. L.; Fox, D. J.; Keith, T.; Al-Laham, M. A.; Peng, C. Y.; Nanayakkara, A.; Challacombe, M.; Gill, P. M. W.; Johnson, B. G.; Chen, W.; Wong, M. W.; Andres, J. L.; Gonzalez, C.; Head-Gordon, M.; Replogle, E. S.; Pople, J. A. *Gaussian 03*, Revision B.04; Gaussian, Inc.: Pittsburgh PA, **2003** (Used in Beijing).

(b) Frisch, M. J.; Trucks, G. W.; Schlegel, H. B.; Scuseria, G. E.; Robb, M. A.; Cheeseman, J. R.; Zakrzewski, V. G.; Montgomery, J. A.; Stratmann, R. E.; Burant, J. C.; Dapprich, S.; Millam, J. M.; Daniels, A. D.; Kudin, K. N.; Strain, M. C.; Farkas, O.; Tomasi, J.; Barone, V.; Cossi, M.; Cammi, R.; Mennucci, B.; Pomelli, C.; Adamo, C.; Clifford, S.; Ochterski, J.; Petersson, G. A.; Ayala, P. A.; Cui, Q.; Morokuma, K.; Salvador, P.; Dannenberg, J. J.; Malick, D. K.; Rabuck, A. D.; Raghavachari, K.; Foresman, J. B.; Cioslowski, J.; Ortiz, J. V.; Baboul, A. G.; Stefanov, B. B.; Liu, G.; Liashenko, A.; Piskorz, P.; Komaromi, I.; Gomperts, R.; Martin, R. L.; Fox, D. J.; Keith, T.; Al-Laham, M. A.; Peng, C. Y.; Nanayakkara, A.; Challacombe, M.; Gill, P. M. W.; Johnson, B. G.; Chen, W.; Wong, M. W.; Andres, J. L.; Gonzalez, C.; Head-Gordon, M.; Replogle, E. S.; Pople, J. A. *Gaussian 94*, revision c.3; Gaussian, Inc.: Pittsburgh, PA, **1995** (Used in Georgia).

29. Luo, Q.; Li, J.; Li, Q. S.; Kim, S.; Wheeler, S. E.; Xie, Y.; Schaefer, H.F. *Phys. Chem. Chem. Phys.* **2005**, *6*, 1.

30. (a). Les, A.; Adamowicz, L.; Bartlett, R. J. *J. Phys. Chem.* **1989**, *93*, 4001.

(b). Gorb, L.; Podolyan, Y.; Leszczynski, J.; *J. Mol. Struct.* **1999**, *487*, 47.

31. Radisic, D.; Bowen, K. H.; Dabkowska, I.; Storoniak, P.; Rak, J.; Gutowski, M. *J. Am. Chem. Soc.* **2005**, *127*, 6443.

32. Close, D. M.; Eriksson, L. A.; Hole, E. O.; Sagstuen, E.; Nelson, W. H. *J. Phys. Chem. B* **2000**, *104*, 9343.

33. Colson, A.-O.; Besler, B.; Close, D. M.; Sevilla, M. D. *J. Phys. Chem.* **1992,** *96*, 661.

34. Smith, D. M. A.; Jalbout, A. F.; Smets, J.; Adamowicz, L. *Chem. Phys.* **2000,** *260*, 45.

35. Rienstra-Kiracofe, J. C.; Tschumper, G. S.; Schaefer, H. F.; Nandi, S.; Ellison, G. B. *Chem. Rev.* **2002**, *102*, 231.

Table 2.1: Hydrogenated cytosine radicals $(C+H)^{\bullet}$ derived from three cytosine tautomers.

| Cytosine | Hydrogenated Cytosine Radicals $(C+H)^{\bullet}$ (● shows the formal radical center) | | | | | | |
|---|---|---|---|---|---|---|---|
| 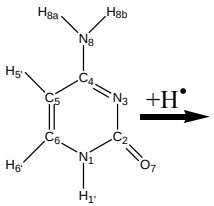 amino-oxo (A-O) | rO1 | rO2 | rO3 | rO4 | rO5 | rO6 | |
| | 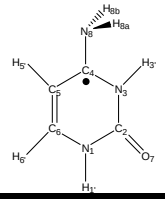 | 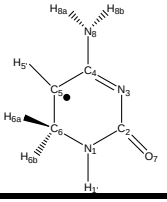 | 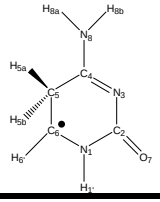 | 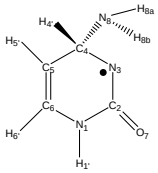 | 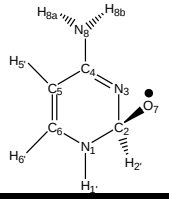 | 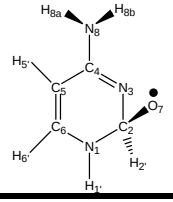 | |
| 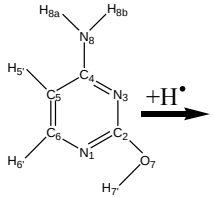 amino-hydroxy (A-H) Trans | rA1 | rA2 | rA3 | rA4 | rA5 | rA6 | rB1 |
| | 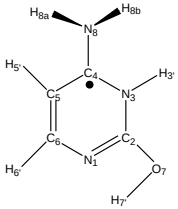 | 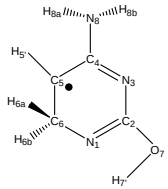 | 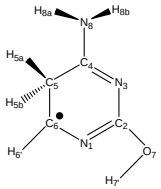 | 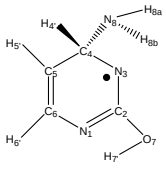 | 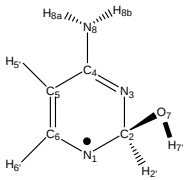 | 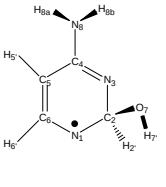 | 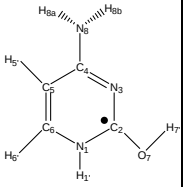 |
| 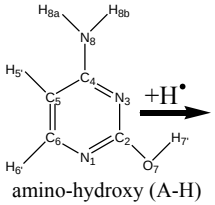 amino-hydroxy (A-H) Cis | | rB2 | rB3 | rB4 | rB5 | rB6 | |
| | | 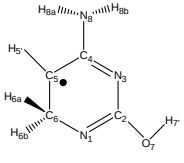 | 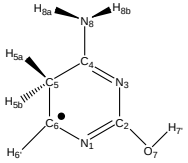 | 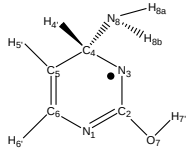 | 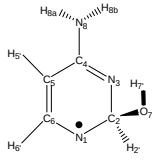 | 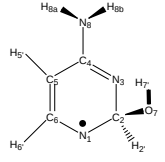 | |

Table 2.2: Total and relative energies of the radicals derived from cytosine (ZPVE corrected relative energies in parentheses) at the B3LYP/DZP++ level of theory.

| Structure | Rel. Energy (kcal/mol) | Total Energy ($E_h$) | Turecek's Rel. Energy (kcal/mol)[16] | | |
|---|---|---|---|---|---|
| | | | $\Delta H_0$[a] | $\Delta H_0$[b] | $\Delta H_0$[c] |
| **rO1** | 0.0 (0.0) | -395.57852 | 0.0 | 0.0 | 0.0 |
| **rO3** | 6.3 (6.2) | -395.56846 | 7.4 | 8.6 | 7.4 |
| **rO2** | 8.4 (8.0) | -395.56521 | 8.8 | 10.5 | 10.3 |
| **rA3** | 9.7 (9.3) | -395.56303 | 11.7 | 12.4 | |
| **rB3** | 10.6 (10.1) | -395.56162 | 11.0 | 13.4 | |
| **rB1** | 11.4 (11.0) | -395.56029 | 12.9 | 12.2 | |
| **rA1** | 12.6 (12.7) | -395.55850 | 14.6 | 14.3 | |
| **rA2** | 14.6 (14.3) | -395.55521 | 15.8 | 17.0 | |
| **rB2** | 15.7 (15.3) | -395.55350 | 16.7 | 17.9 | |
| **rB4** | 26.0 (26.2) | -395.53709 | | | |
| **rA6** | 26.0 (25.5) | -395.53707 | | | |
| **rB6** | 26.1 (25.5) | -395.53694 | | | |
| **rB5** | 26.4 (25.8) | -395.53646 | | | |
| **rA5** | 26.4 (25.8) | -395.53642 | | | |
| **rA4** | 26.5 (26.5) | -395.53634 | | | |
| **rO4** | 30.1 (29.8) | -395.53060 | 33.9 | 37.0 | |
| **rO5** | 43.0 (41.7) | -395.51002 | 42.3 | 48.5 | |
| **rO6** | 44.0 (44.2) | -395.50838 | | | |

a. B3LYP/6-31+G(d,p) results with ZPVE corrections.
b. B3-MP2/6-311++G(3df,2p) results from spin-projected MP2 energies, with ZPVE corrections.
c. Estimated CCSD(T)/6-311++G(3df,2p) results, from the formula: E[CCSD(T)/6-311++G(3df,2p)]≈E[CCSD(T)/6-31G(d,p)]+E[PMP2/6-111++G(3df,2p)]-E[PMP2/6-31G(d,p)]. with ZPVE corrections.|

Table 2.3: Total and relative energies of the anions derived from cytosine (ZPVE corrected relative energies in parentheses) at the B3LYP/DZP++ level of theory.

| Structure | Rel. Energy (kcal/mol) | Total Energy ($E_h$) |
|---|---|---|
| **aO2** | 0.0 (0.00) | -395.63759 |
| **aO4** | 7.5 (7.6) | -395.62566 |
| **aB4** | 11.9 (12.1) | -395.61865 |
| **aA4** | 11.9 (12.1) | -395.61862 |
| **aA2** | 14.1 (13.7) | -395.61517 |
| **aB2** | 14.3 (14.1) | -395.61475 |
| **aA5** | 15.1 (14.7) | -395.61355 |
| **aB5** | 15.3 (14.8) | -395.61323 |
| **aA6** | 15.3 (14.9) | -395.61316 |
| **aB6** | 15.9 (15.4) | -395.61231 |
| **aO5** | 26.0 (25.3) | -395.59608 |
| **aO6** | 26.2 (25.4) | -395.59588 |
| **aO3** | 29.1 (28.4) | -395.59120 |
| **aO1** | 34.1 (33.5) | -395.58319 |
| **aA3** | 36.5 (34.8) | -395.57938 |
| **aB3** | 37.3 (35.4) | -395.57821 |
| **aB1** | 52.2 (50.7) | -395.55441 |
| **aA1** | 54.2 (52.5) | -395.55116 |

Table 2.4. Adiabatic electron affinities (in eV) of the radicals $(C+H)^{\bullet}$ derived from cytosine (ZPVE corrected EAs in parentheses).

| Structure | B3LYP | BHLYP | BLYP | BP86 |
|---|---|---|---|---|
| **rO1** | 0.13 (0.16) | -0.23 (-0.21) | 0.15 (0.20) | 0.27 (0.31) |
| **rO2** | 1.97 (1.96) | 1.77 (1.75) | 1.83 (1.83) | 2.01 (2.01) |
| **rO3** | 0.62 (0.65) | 0.07 (0.10) | 0.47 (0.53) | 0.62 (0.68) |
| **rO4** | 2.59 (2.58) | 2.37 (2.37) | 2.42 (2.44) | 2.61 (2.62) |
| **rO5** | 2.34 (2.33) | 1.83 (1.86) | 2.67 (2.69) | 2.36 (2.34) |
| **rO6** | 2.38 (2.43) | 1.84 (1.88) | 2.29 (2.35) | 2.46 (2.51) |
| **rA1** | -0.20 (-0.11) | -0.63 (-0.56) | -0.15 (-0.04) | 0.01 (0.11) |
| **rB1** | -0.16 (-0.11) | -0.88 (-0.84) | -0.41 (-0.35) | -0.29 (-0.23) |
| **rA2** | 1.63 (1.64) | 1.44 (1.44) | 1.49 (1.51) | 1.66 (1.68) |
| **rB2** | 1.67 (1.67) | 1.49 (1.48) | 1.52 (1.53) | 1.69 (1.70) |
| **rA3** | 0.44 (0.51) | 0.00 (0.06) | 0.47 (0.55) | 0.63 (0.71) |
| **rB3** | 0.45 (0.52) | 0.00 (0.06) | 0.48 (0.56) | 0.64 (0.72) |
| **rA4** | 2.24 (2.24) | 1.99 (1.98) | 2.12 (2.13) | 2.31 (2.31) |
| **rB4** | 2.22 (2.23) | 1.96 (1.96) | 2.11 (2.12) | 2.30 (2.31) |
| **rA5** | 2.10 (2.10) | 1.77 (1.77) | 1.99 (2.00) | 2.16 (2.17) |
| **rB5** | 2.09 (2.09) | 1.79 (1.78) | 2.01 (2.02) | 2.19 (2.20) |
| **rA6** | 2.07 (2.08) | 1.77 (1.77) | 1.99 (2.00) | 2.16 (2.17) |
| **rB6** | 2.05 (2.06) | 1.76 (1.76) | 1.97 (1.99) | 2.15 (2.16) |

Table 2.5: Vertical electron affinities (in eV) of the radicals $(C+H)^{\bullet}$ derived from cytosine (C).

| Structure | B3LYP | BHLYP | BLYP | BP86 |
|---|---|---|---|---|
| **rO1** | -0.33 | -0.72 | -0.30 | -0.17 |
| **rO2** | 1.63 | 1.39 | 1.53 | 1.70 |
| **rO3** | -0.02 | -0.49 | 0.10 | 0.24 |
| **rO4** | 2.10 | 1.74 | 2.09 | 2.24 |
| **rO5** | 1.52 | 1.34 | 1.52 | 1.64 |
| **rO6** | 1.78 | 1.34 | 1.85 | 1.99 |
| **rA1** | -0.55 | -1.06 | -0.42 | -0.30 |
| **rB1** | -0.91 | -1.52 | -0.73 | -0.66 |
| **rA2** | 1.36 | 1.12 | 1.25 | 1.42 |
| **rB2** | 1.41 | 1.18 | 1.29 | 1.45 |
| **rA3** | 0.01 | -0.50 | 0.11 | 0.26 |
| **rB3** | 0.01 | -0.52 | 0.10 | 0.27 |
| **rA4** | 2.04 | 1.77 | 1.95 | 2.13 |
| **rB4** | 2.00 | 1.70 | 1.92 | 2.10 |
| **rA5** | 1.81 | 1.53 | 1.72 | 1.89 |
| **rB5** | 1.80 | 1.50 | 1.72 | 1.88 |
| **rA6** | 1.81 | 1.53 | 1.72 | 1.89 |
| **rB6** | 1.80 | 1.51 | 1.72 | 1.88 |

Table 2.6: Vertical detachment energies (in eV) of the anions $(C+H)^-$ derived from cytosine (C).

| Structure | B3LYP | BHLYP | BLYP | BP86 |
|---|---|---|---|---|
| **aO1** | 0.75 | 0.47 | 0.71 | 0.84 |
| **aO2** | 2.30 | 2.14 | 2.12 | 2.31 |
| **aO3** | 1.37 | 0.70 | 0.86 | 1.03 |
| **aO4** | 2.94 | 2.77 | 2.71 | 2.91 |
| **aO5** | 2.82 | 2.59 | 2.57 | 2.71 |
| **aO6** | 2.86 | 2.37 | 2.54 | 2.72 |
| **aA1** | 0.81 | 0.48 | 0.67 | 0.98 |
| **aB1** | 1.06 | -0.06 | 0.25 | 0.41 |
| **aA2** | 1.90 | 1.73 | 1.75 | 1.93 |
| **aB2** | 1.93 | 1.76 | 1.78 | 1.96 |
| **aA3** | 0.88 | 0.50 | 0.84 | 1.03 |
| **aB3** | 0.90 | 0.52 | 0.86 | 1.04 |
| **aA4** | 2.43 | 2.20 | 2.27 | 2.47 |
| **aB4** | 2.43 | 2.20 | 2.28 | 2.48 |
| **aA5** | 2.39 | 2.11 | 2.27 | 2.47 |
| **aB5** | 2.38 | 2.10 | 2.28 | 2.48 |
| **aA6** | 2.38 | 2.05 | 2.27 | 2.47 |
| **aB6** | 2.36 | 2.05 | 2.26 | 2.45 |

Figure 2.1: The amino-oxo and amino-hydroxy tautomers of cytosine

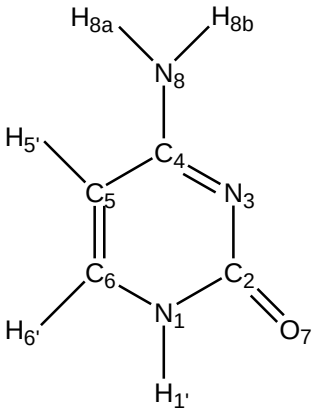


Amino-Oxo (A-O)

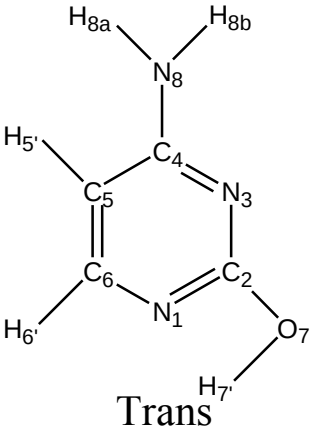


Trans

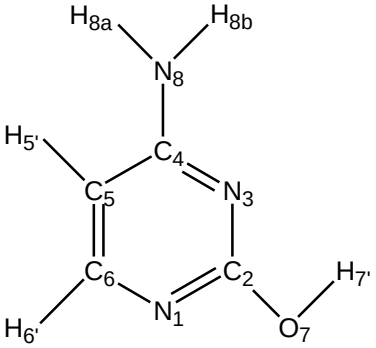


Cis

Amino-Hydroxy (A-H)

Figure 2.2: Bond lengths (in angstroms) and selected dihedral angles (in degrees) of the radicals (C+H)• from amino-oxo cytosine (B3LYP/DZP++). A dot (●) shows the formal radical center position in each qualitative valence structure.

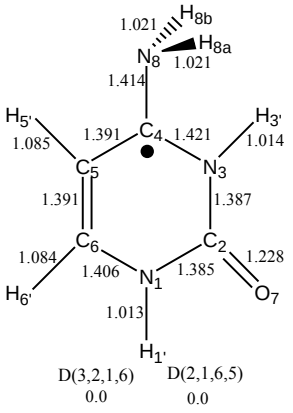


rO1

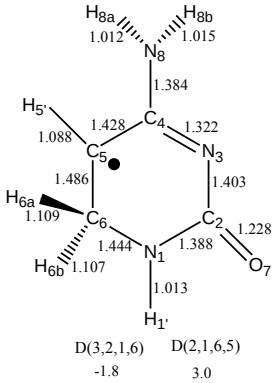


rO2

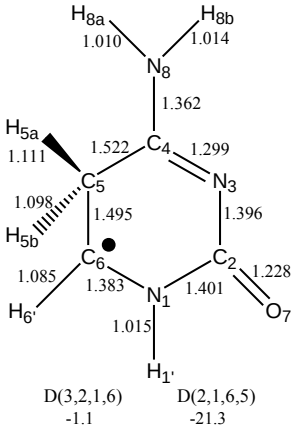


rO3

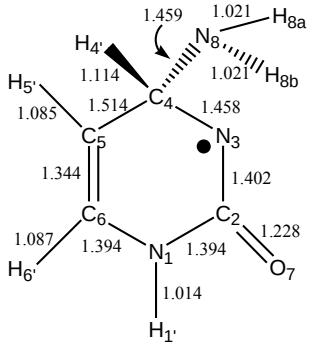


rO4

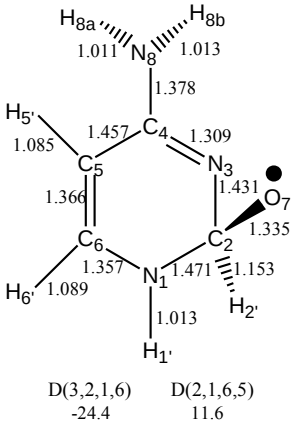


rO5

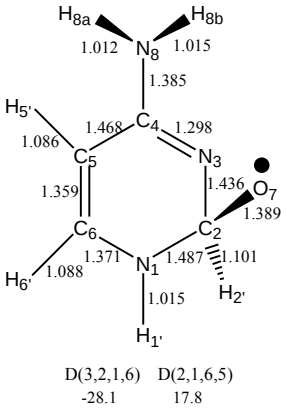


rO6

Figure 2.3: Bond lengths (in angstroms) and selected dihedral angles (in degrees) of the radicals (C+H)$^{\bullet}$ from amino-hydroxy cytosine (B3LYP/DZP++). A dot (●) shows the formal radical center position in each qualitative valence structure.

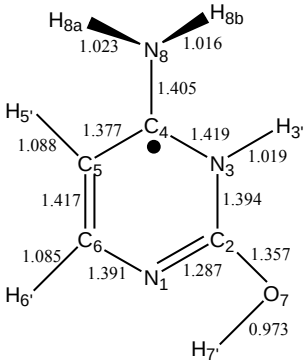


D(3,2,1,6) D(2,1,6,5)
3.4 0.8

rA1

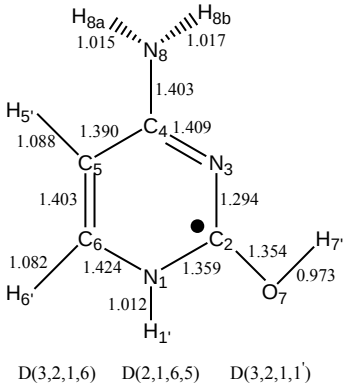


D(3,2,1,6) D(2,1,6,5) D(3,2,1,1')
1.5 -1.5 176.6

rB1

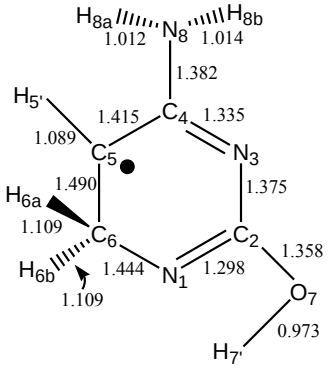


D(3,2,1,6) D(2,1,6,5)
0.4 0.4

rA2

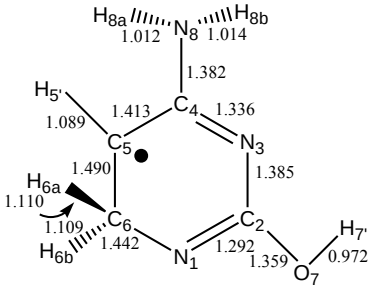


D(3,2,1,6) D(2,1,6,5)
0.4 0.5

rB2

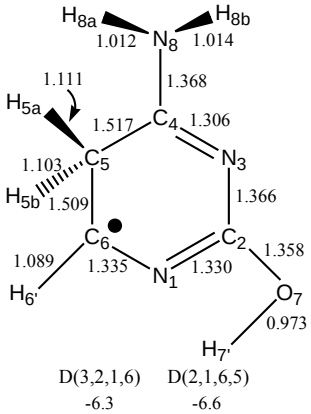


D(3,2,1,6) D(2,1,6,5)
-6.3 -6.6

rA3

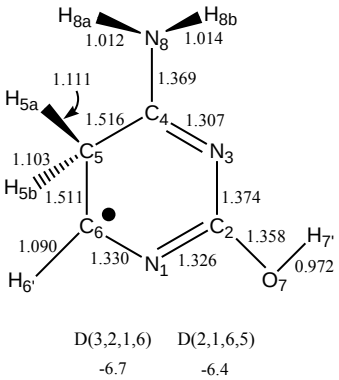


D(3,2,1,6) D(2,1,6,5)
-6.7 -6.4

rB3

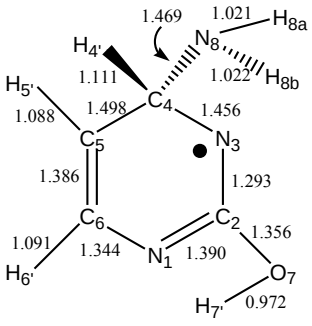


| D(3,2,1,6) | D(2,1,6,5) | D(4,3,2,1) |
|---|---|---|
| 1.4 | -1.0 | 2.0 |

rA4

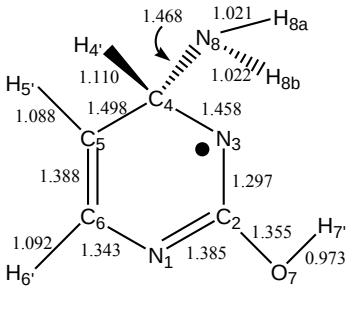


| D(3,2,1,6) | D(2,1,6,5) | D(4,3,2,1) |
|---|---|---|
| 1.2 | -0.7 | 1.6 |

rB4

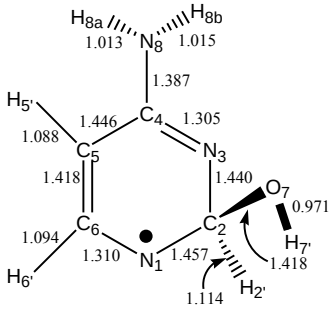


| D(3,2,1,6) | D(2,1,6,5) | D(4,3,2,7) | D(4,3,2,2') |
|---|---|---|---|
| 10.9 | -4.2 | -135.9 | 107.3 |

rA5

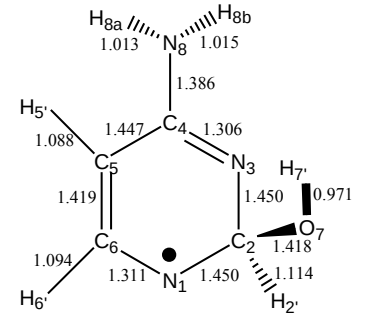


| D(3,2,1,6) | D(2,1,6,5) | D(4,3,2,7) | D(4,3,2,2') |
|---|---|---|---|
| 12.2 | -5.3 | -135.9 | 106.8 |

rB5

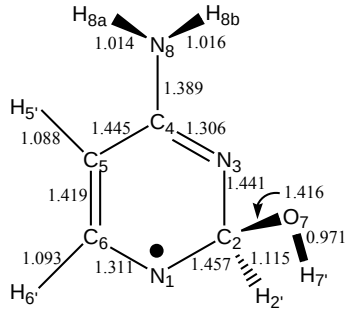


| D(3,2,1,6) | D(2,1,6,5) | D(4,3,2,7) | D(4,3,2,2') |
|---|---|---|---|
| -15.4 | 4.3 | 141.6 | -101.5 |

rA6

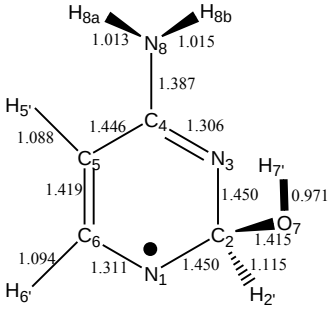


| D(3,2,1,6) | D(2,1,6,5) | D(4,3,2,7) | D(4,3,2,2') |
|---|---|---|---|
| -16.6 | 5.3 | 141.5 | -100.9 |

rB6

Figure 2.4: Bond lengths (in angstroms) and selected dihedral angles (in degrees) of the anions $(C+H)^-$ from amino-oxo cytosine at the B3LYP/DZP++ level of theory. A minus sign (⊖) shows the formal negative charge position in each qualitative valence structure.

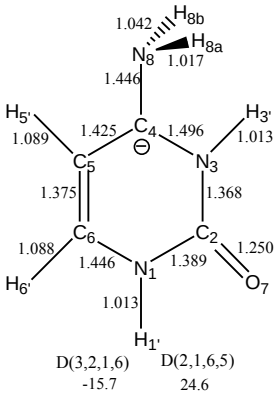


aO1

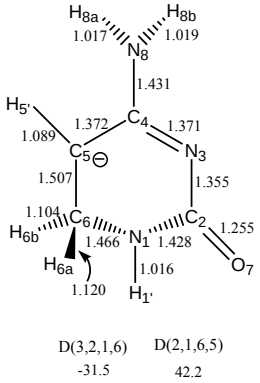


aO2

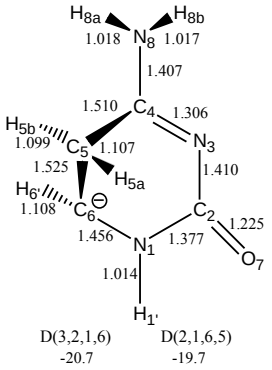


aO3

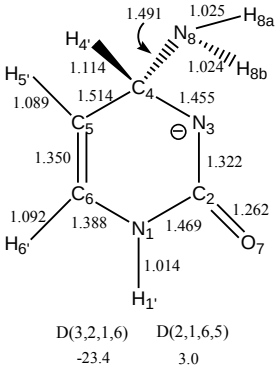


aO4

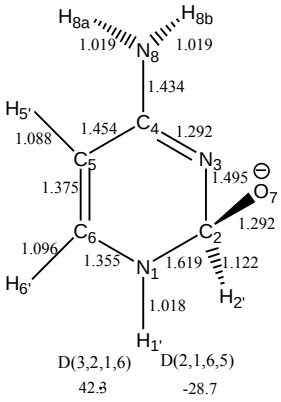


aO5

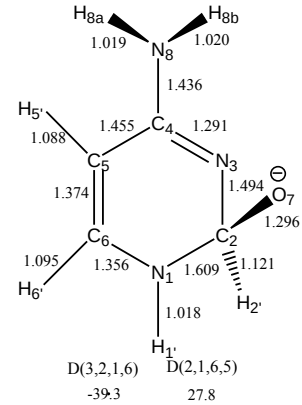


aO6

Figure 2.5: Bond lengths (in angstroms) and selected dihedral angles (in degrees) of the anions $(C+H)^-$ from amino-hydroxy cytosine at the B3LYP/DZP++ level of theory. A minus sign (⊖) shows the formal negative charge position in each qualitative valence structure.

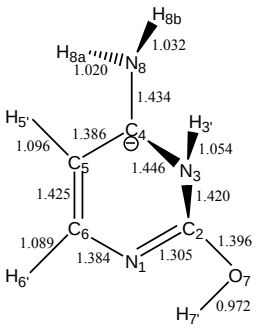


D(3,2,1,6) D(2,1,6,5)
18.6 17.5

aA1

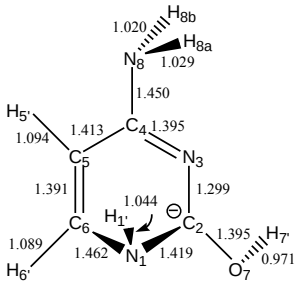


D(3,2,1,6) D(2,1,6,5) D(3,2,1,1') 
49.3 -48.1 -66.3

aB1

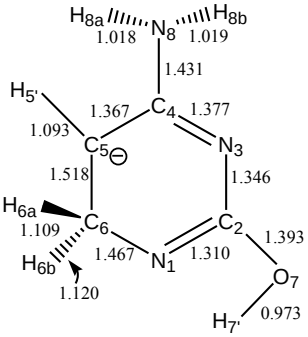


D(3,2,1,6) D(2,1,6,5)
6.0 -16.4

aA2

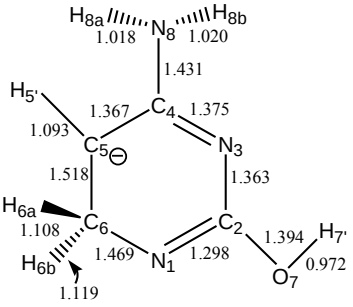


D(3,2,1,6) D(2,1,6,5)
6.6 -19.4

aB2

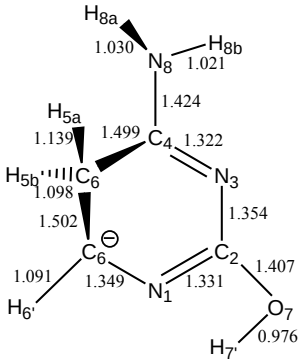


D(3,2,1,6) D(2,1,6,5)
-19.0 -21.1

aA3

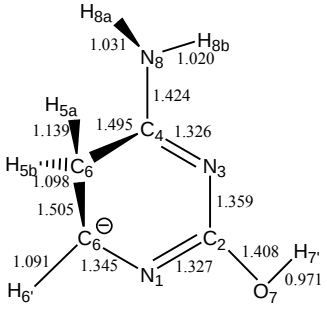


D(3,2,1,6) D(2,1,6,5)
-20.0 -20.0

aB3

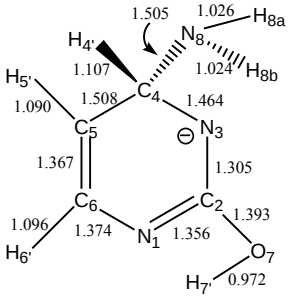


| D(3,2,1,6) | D(2,1,6,5) | D(4,3,2,1) |
|---|---|---|
| -1.9 | 4.1 | -8.4 |

aA4

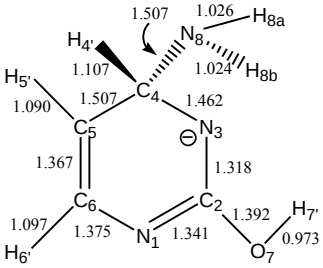


| D(3,2,1,6) | D(2,1,6,5) | D(4,3,2,1) |
|---|---|---|
| -1.6 | 3.8 | -8.7 |

aB4

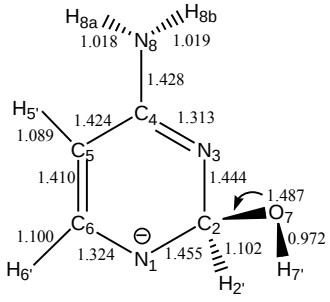


| D(3,2,1,6) | D(2,1,6,5) | D(4,3,2,7) | D(4,3,2,2') |
|---|---|---|---|
| -26.9 | 8.3 | -94.7 | 152.4 |

aA5

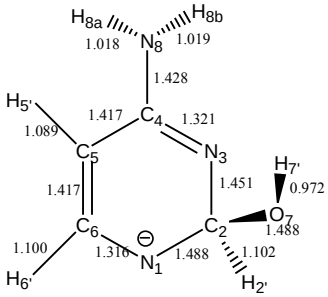


| D(3,2,1,6) | D(2,1,6,5) | D(4,3,2,7) | D(4,3,2,2') |
|---|---|---|---|
| -27.1 | 8.1 | -94.7 | 152.7 |

aB5

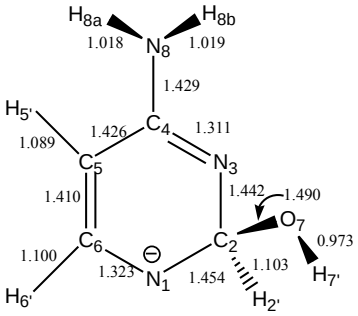


| D(3,2,1,6) | D(2,1,6,5) | D(4,3,2,7) | D(4,3,2,2') |
|---|---|---|---|
| 24.0 | -7.7 | 97.9 | -149.6 |

aA6

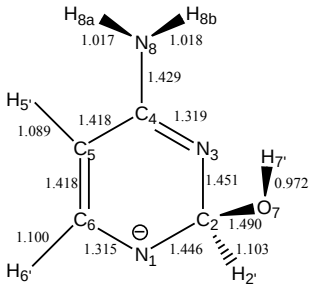


| D(3,2,1,6) | D(2,1,6,5) | D(4,3,2,7) | D(4,3,2,2') |
|---|---|---|---|
| 23.6 | -7.4 | 98.7 | -149.0 |

aB6

Figure 2.6: (a). **aO5** N1-C2 bond breaking minimum at the BLYP/DZP++ level of theory. A minus sign (⊖) shows the formal negative charge position.
(b). Optimized geometry of both **aA6** and **aB6** at BHLYP/DZP++ level of theory. A minus sign (⊖) shows the formal negative charge position.

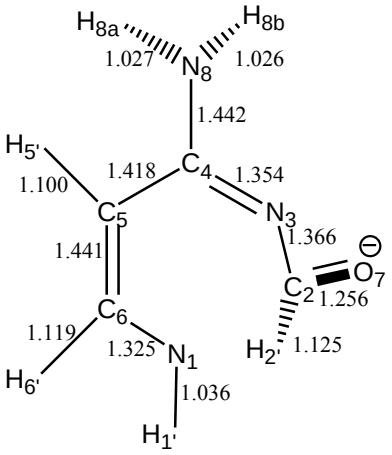


| D(3,4,5,6) | D(4,5,6,1) | D(4,3,2,7) | D(4,3,2,2') |
|---|---|---|---|
| 9.3 | 3.3 | 25.1 | -160.7 |

(a)

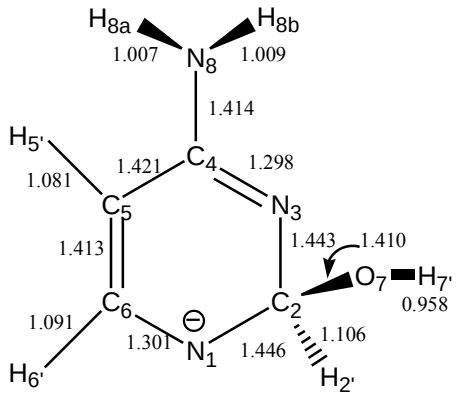


| D(3,2,1,6) | D(2,1,6,5) | D(4,3,2,7) | D(4,3,2,2') |
|---|---|---|---|
| -45.5 | 10.7 | 170.7 | -75.5 |

(b)

Figure 2.7: Atomic spin densities for the radicals $(C+H)^{\bullet}$ derived from amino-oxo cytosine.

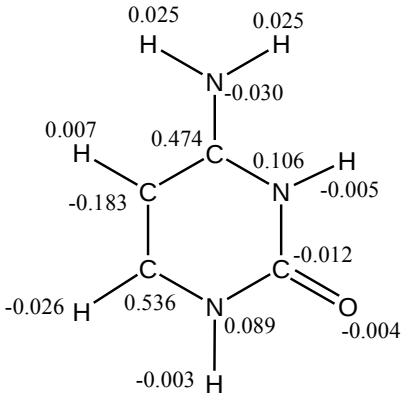


**rO1**

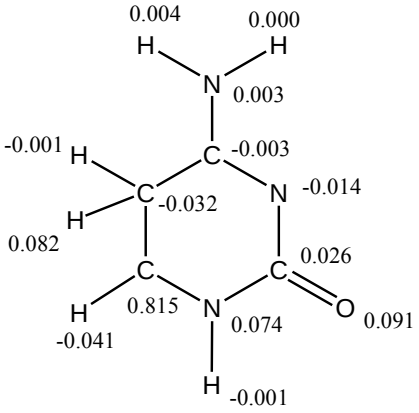


**rO3**

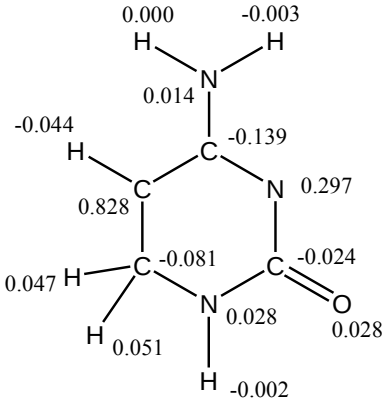


**rO2**

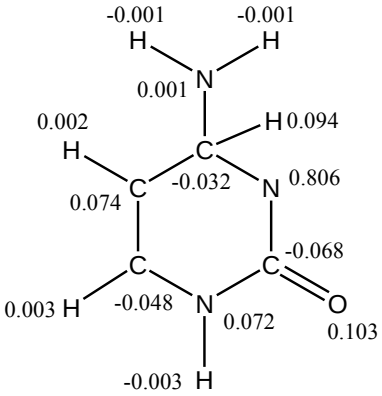


**rO4**

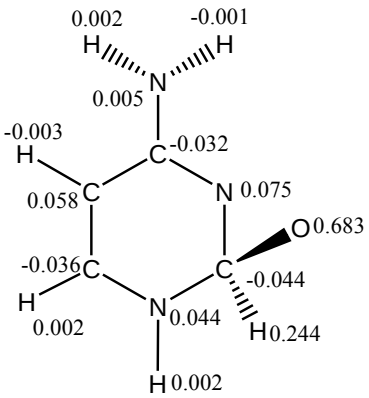


**rO5**

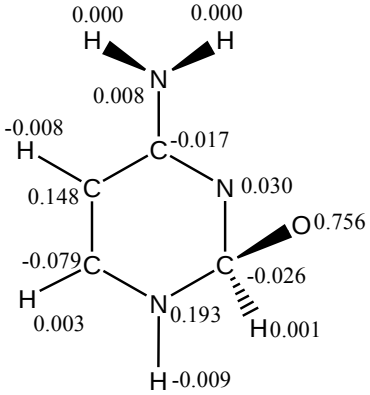


**rO6**

Figure 2.8: Atomic spin densities for the radicals $(C+H)^{\bullet}$ derived from amino-hydroxy cytosine.

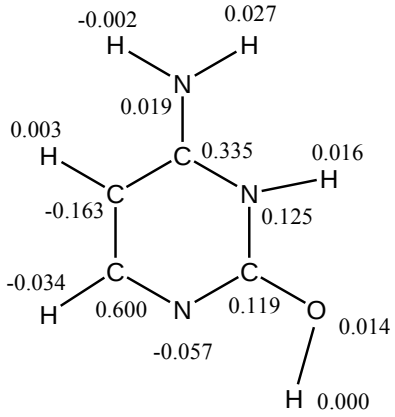


**rA1**

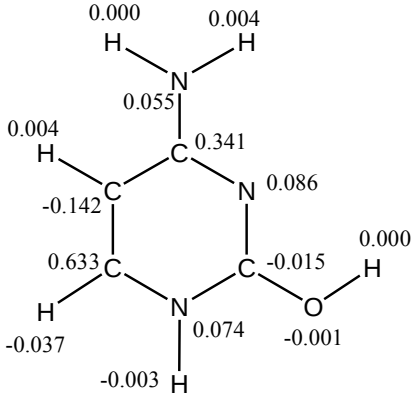


**rB1**

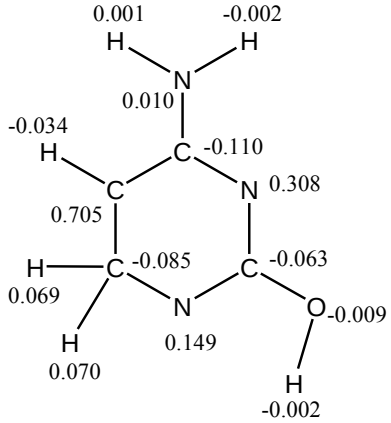


**rA2**

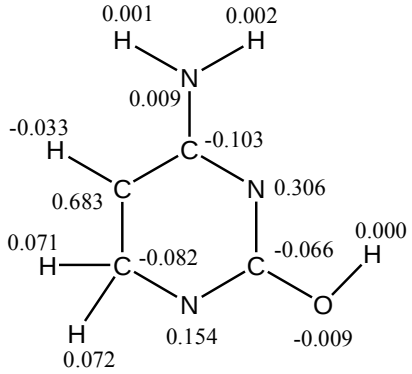


**rB2**

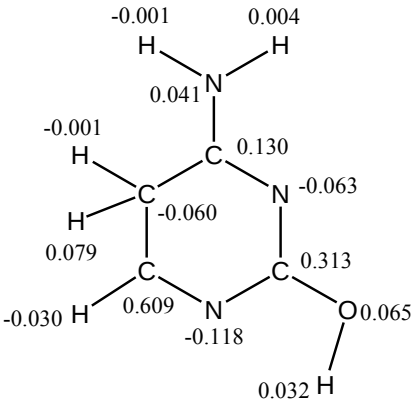


**rA3**

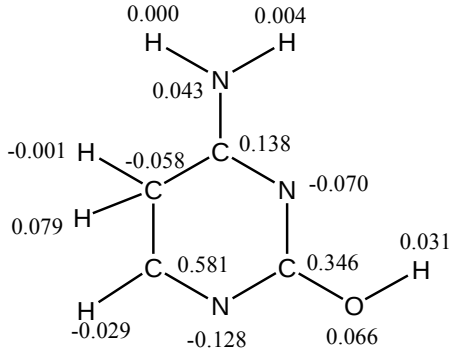


**rB3**

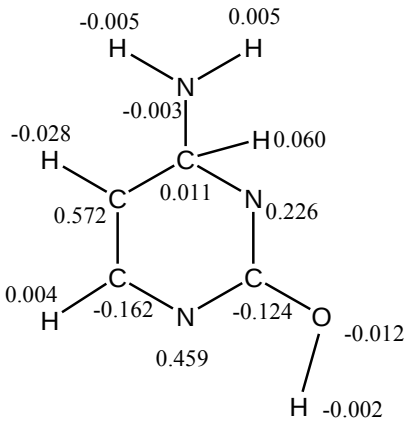


**rA4**

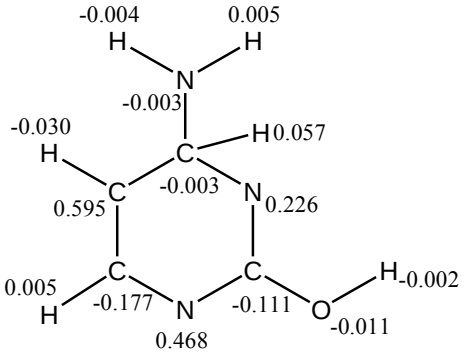


**rB4**

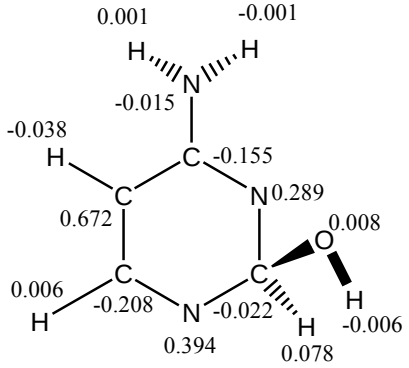


**rA5**

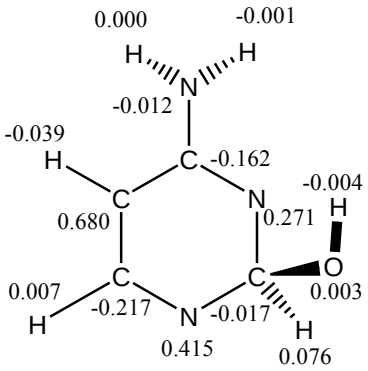


**rA5**

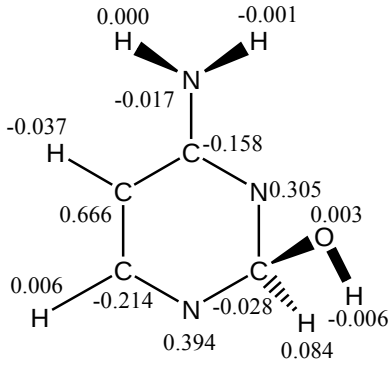


**rA6**

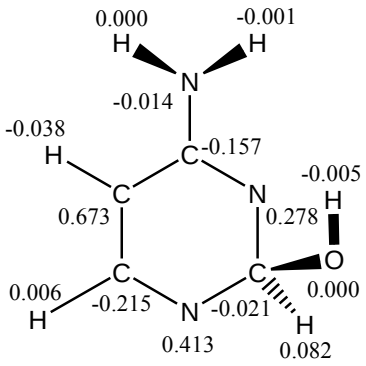


**rB6**

Figure 2.9: Relative Energies of $(C+H)^{\bullet}$ Radicals and $(C+H)^{-}$ Anions Derived from Cytosine (C).

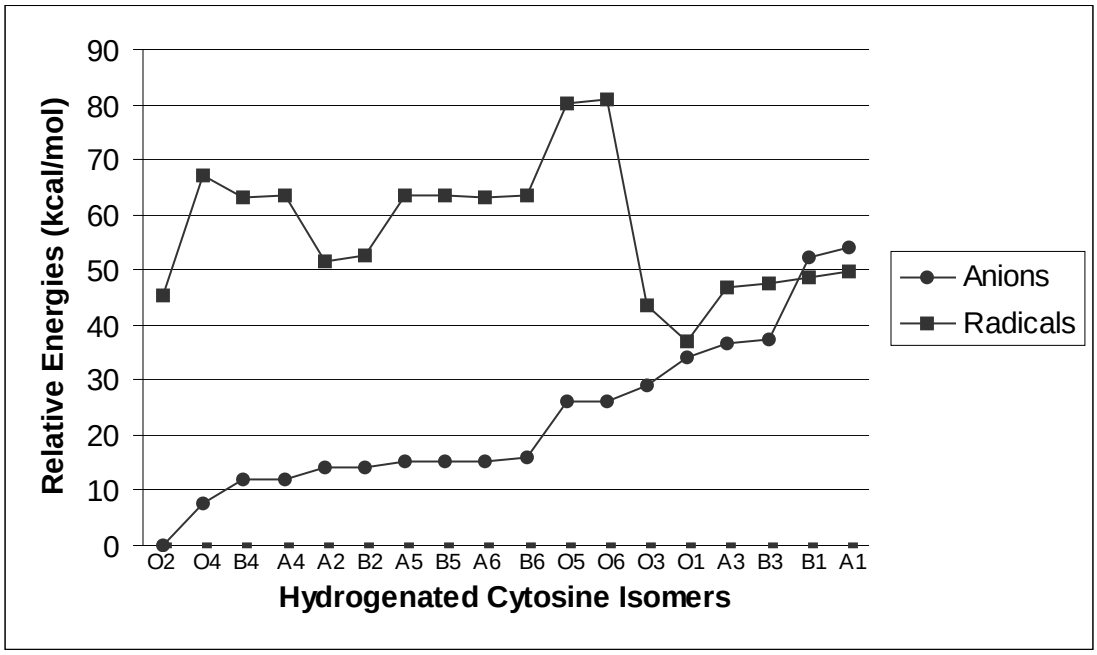

Figure 2.10: Electron Attracting Properties for $(C+H)^{\bullet}$ Radicals and $(C+H)^{-}$ Anions Derived from Cytosine (C).

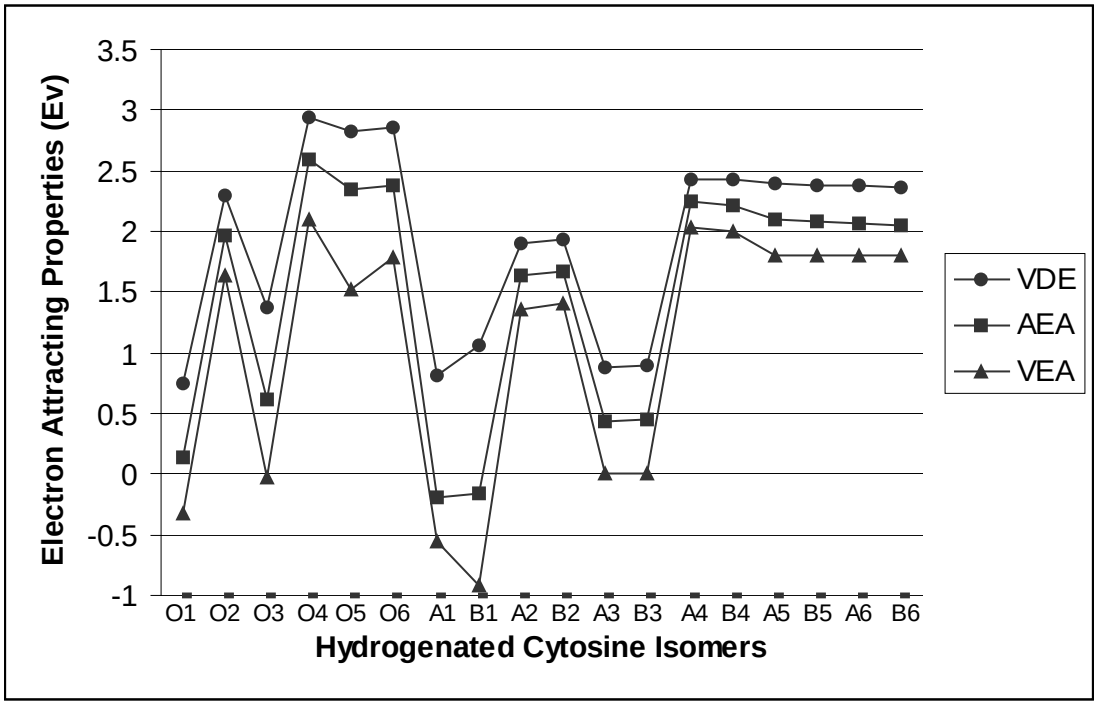

CHAPTER 3

# SUCCESSIVE ATTACHMENT OF ELECTRONS TO PROTONATED GUANINE: $(G+H)^{\bullet}$ RADICALS AND $(G+H)^{-}$ ANIONS[2]

[2] Zhang, J. D.; Xie, Y.; Schaefer, H. F., III. Journal of Physical Chemistry A, 2006, 110(43), 12010-12016. Reprinted here with permission of the American Chemical Society.

## 3.1 ABSTRACT

The structures, energetics, and vibrational frequencies of nine hydrogenated 9H- *keto*-guanine radicals $(G+H)^{\bullet}$ and closed-shell anions $(G+H)^{-}$ are predicted using the carefully calibrated (*Chem. Rev.* **2002**, *102*, 231) B3LYP density functional method in conjunction with a DZP++ basis set. These radical and anionic species come from consecutive electron attachment to the corresponding protonated $(G+H)^{+}$ cations in low pH environments. The $(G+H)^{+}$ cations are studied using the same level of theory. The proton affinity (PA) of guanine computed in this research (228.1 kcal/mol) is within 0.7 kcal/mol of the latest experiment value. The radicals range over 41 kcal/mol in relative energy, with radical **r1**, in which H is attached at the C8 site of guanine, having the lowest energy. The lowest energy anion is **a2**, derived by hydride ion attachment at the C2 site of guanine. No stable N2-site hydride should exist in the gas phase. Structure **a9** was predicted to be dissociative in this research. The theoretical adiabatic electron affinities (AEA), vertical electron affinities (VEA), and vertical detachment energies (VDE) were computed, with AEAs ranging from 0.07 eV to 3.12 eV for the nine radicals.

## 3.2 INTRODUCTION

The initial step in DNA radiation damage is known to involve the interaction between ionizing sources (photons, electrons, and chemical radicals) and the poly-nucleotide. The intermediates resulting from electron trapping on nucleic acid bases,[1] identified as charged radicals, will cause further DNA lesions such as strand breaks,[2] base pair mutations[3], and interstrand cross-links[4]. These lesions, if not repaired, may lead to lethal living cell damage. Thus, a reliable and comprehensive understanding of these transient radicals may shed light on the damage recognition processes and repair mechanisms. The base-centered radicals play a key

role in the modified nucleobase formation processes when normal pyrimidine and purine base molecular structures alternate.[5] In recent investigations, guanine has been a focus, due to its having the highest propensity of reduction among the four bases.[6] Single guanine or guanine sequences have been detected as hole (radical cation) trapping sites in DNA strand charge transport experiments.[7] The 8-oxo-guanine molecule, which is the usual guanine oxidation product, has been the subject of great interest due to its mispairing ability with adenine (A) and cytosine (C).[8] Recent research has also shown that the electron capturing probability scales with the number of guanines in a single strand DNA oligomer.[9] Theoretical studies of gas phase anionic guanine have demonstrated that guanine tautomers have near zero electron affinities, whether the end product is the dipole bound or valence bound anion.[10]

In acid environments, the interaction between protons and guanine may be attributed to the simple acid-base chemical equilibrium, both in the gas phase and condensed phases. Guanine has been recognized as the most readily protonated base, due to having the highest proton affinity (PA) among the four DNA nucleobases.[11] The site specific PAs and p$K_a$ values of guanine have been studied extensively.[12-14] Gas phase data for the proton affinity of guanine has been obtained from Greco and co-workers'[11] FAB-MS (Fast Atom Bombardment Tandem Mass Spectrometry) experiments. In 2000, Podolyan, Gorb and Leszczynski[13] preformed comprehensive theoretical studies to determine the gas phase PAs of various nucleobases using post-Hartree-Fock methods. More recently, the absolute p$K_a$ values of guanine in water have been predicted by Jang, Goddard and co-workers.[14]

Despite the different methods used, all investigations have indicated that the N7 site protonated guanine (see Scheme 1) is the dominating form among the possible tautomers. However, previous investigations have not considered the possibility that protonated guanine

tautomers may be electron trapping sites, in which the radical or anionic guanine-hydrogen complex may be formed after consecutive attachment of electrons to protonated guanine. The resulting guanine derivative species, classified as hydrogenated guanine radicals or anions, may lead to permanent DNA lesions. This is because the added hydrogen atom is covalently bound to guanine, except for protonated guanine, where the proton may be appended to the induced dipole of guanine. In the gas phase, the hydrogenated guanine radicals have been examined in Wetmore, Boyd and Eriksson's EPR/ENDOR experiments and DFT computations.[15] The neutral and anionic states of the dehydrogenated guanine isomers have been studied by Luo and co-wokers.[16]

We focus here on the radicals $(G+H)^{\bullet}$ and anions $(G+H)^{-}$ formed by electrons attaching to protonated 9H-*keto*-guanine $(G+H)^{+}$ cations in the gas phase. The molecular structures and thermodynamic properties of all species have been predicted by using a carefully calibrated theoretical approach B3LYP/DZP++. The aim of this research is to complement the previous work on base centered DNA radicals ($(Base-H)^{\bullet}$ and $(Base+H)^{\bullet}$)[16,17] and contribute to the studies of induced DNA fragment damage by low energy electron attachment in the gas phase.[18] Thus we do not incorporate solvent effects in our theoretical approach. The structure and numbering scheme of guanine used in this work are depicted in Scheme 1 (showing the IUPAC numbering of the atoms).

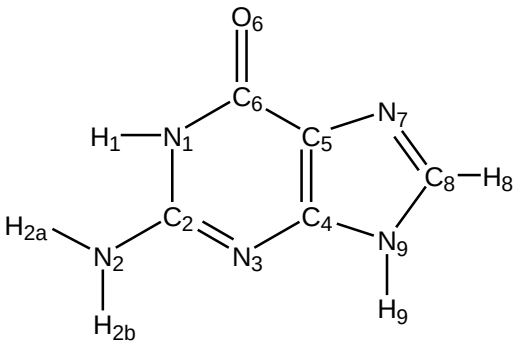


Guanine

**Scheme 1**

In Scheme 1, as a building block of DNA, the 9H-*keto*-guanine molecule (ordinary guanine) connects the furanose sugar through the glycosidic bond at the N9 position. The guanine *enol* tautomers were not considered in this research, since they are less important biochemically compared to 9H-*keto*-guanine. An understanding of molecular structures and energetic features of these critical molecules will help us to understand more complex DNA fragments.

## 3.3 THEORETICAL METHODS

A carefully calibrated DFT approach[19] has been used in this research to optimize the many geometries and to predict vibrational frequencies. The method chosen is B3LYP, a combination of the exchange treatment from Becke's three parameter HF/DFT exchange functional (B3)[20] with the dynamic correlation functional of Lee, Yang, and Parr (LYP).[21] The GAUSSIAN 94 system of DFT programs was used for the computations.[22] All computations were performed using double-ζ quality basis sets with polarization and diffuse functions (DZP++). The DZP++ basis sets were constructed by augmenting the Huzinaga-Dunning set of contracted double-ζ Gaussian functions with one set of p-type polarization functions for each H atom and one set of five d-type polarization functions for each C, N, and O atom [$\alpha_p$(H) = 0.75, $\alpha_d$(C) = 0.75, $\alpha_d$(N) = 0.80, $\alpha_d$(O) = 0.85].[23,24] To complete the DZP++ basis, one even tempered

diffuse s function was added to each H atom while sets of even tempered diffuse s and p functions were centered on each heavy atom. The even tempered orbital exponents were determined by the convention of Lee and Schaefer.[25]

The final DZP++ set contains six functions per H atom (5s1p/3s1p) and nineteen functions per C, N, or O atom (10s6p1d/5s3p1d), yielding a total of 245 contracted Gaussian functions for each $(G+H)^{\bullet}$ hydrogenated base radical. This basis set has a significant tactical advantage, since it has been systematically examined in comprehensive calibrative studies of a wide range of electron affinities with average errors less than 0.12 eV for the case of a closed-shell anion and the corresponding open-shell neutral.[19]

The electron affinities were determined in the following manner. The adiabatic electron affinity (AEA) is defined as the energy difference between the neutral and corresponding anion species at their respective optimized geometries

AEA = *E*(optimized neutral) – *E*(optimized anion).

The vertical electron affinity (VEA) of the radical is defined as

VEA = *E*(optimized neutral) – *E*(anion at optimized neutral geometry).

The anion vertical detachment energy (VDE) is determined via

VDE = *E*(neutral at optimized anion geometry) – *E*(optimized anion).

To analyze the unpaired electron distributions, Kohn-Sham molecular orbitals and spin density plots were constructed from the appropriate B3LYP/DZP++ density. Natural Population Atomic (NPA) charges were determined using the Natural Bond Order (NBO) analysis of Reed and Weinhold.[26-29]

## 3.4 RESULTS AND DISCUSSION

The proposed reaction path for consecutive electron attachment to $(G+H)^+$, leading to the formation of hydrogenated guanine neutrals $(G+H)^\bullet$ and anions $(G+H)^-$, is represented in Scheme 2.

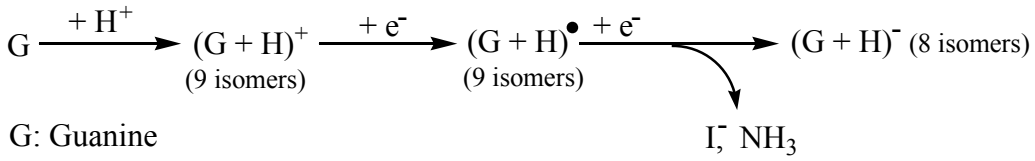


G: Guanine
I: Inosine

**Scheme 2**

We considered nine different protonated guanine isomers (**c1**-**c9**; these isomers are labeled in order of increasing energy) in the present research, involving the different heavy atoms of guanine as proton acceptors. The neutral (**r1**-**r9**) and anionic (**a1**-**a9**) forms of these structures may be envisioned as having been formed following electron attachment (neutrals and anions are labeled in the same manner as the corresponding cations). The relative energies of cation, radical and anion are shown in Figure 3.2. Eight of the nine isomers display anionic structure, while anion **a9** has been found to be a dissociative complex. In what follows we will focus the present research on understanding the thermodynamic properties of these neutral and charged species, as well as those of the complex of 2-dehydrogenated inosine (Scheme 3) anion ( $I - H)^-$ with ammonia ($NH_3$).

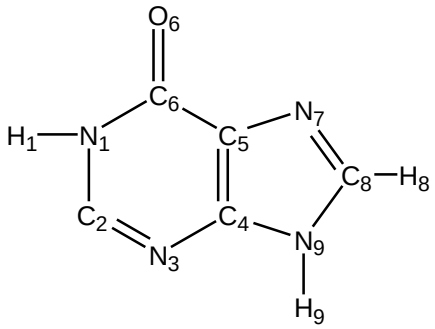


2-Dehydrogenated Inosine (I-H)

**Scheme 3**

Vibrational frequencies were employed to characterize all optimized geometrical structures as stationary points on the potential energy surfaces.

### 3.4.1 THE $(G+H)^+$ CATIONS AND THE PROTON AFFINITIES OF GUANINE

The formation of protonated guanine $(G+H)^+$ cations is directly related to the gas phase basicity of guanine. Generally, the proton is likely to attach to heavy atoms with lone pair electrons. The site specific proton affinities of guanine have been studied extensively.[11-14] The cation **c1** (Figure 3.1), associated with the appendage of a proton to atom N7 of guanine (Scheme 1), has lowest energy on the potential energy surface, confirmed both theoretically and experimentally. The corresponding radical and anion isomers are labeled as **r1** and **a1**, respectively. The proton affinity of guanine leading to **c1** is computed as 228.1 kcal/mol in this research, in good agreement with the Greco's[11] FAB-MS (Fast Atom Bombardment Tandem Mass Spectrometry) gas phase experiment, 227.4 ± 0.1 kcal/mol. The other eight cations, labeled as **c2** to **c9**, are also displayed in the Figure 3.1. The relative energies and proton affinities of the nine cations at B3LYP/DZP++ level of theory are presented in Table 3.1. These results include ZPVE corrections.

### 3.4.2 THE $(G+H)^\bullet$ RADICALS

The $(G+H)^\bullet$ radical structures may be imagined as arising from electrons being appended to the $(G+H)^+$ cations. The energetics associated with such electron capture range from 4.6 eV to 7.8 eV and are identical to the ionization potentials of the $(G+H)^\bullet$ structure. The relative energies (with ZPVE corrections) of the resulting nine neutral radicals at the B3LYP/DZP++ level of theory are presented in Table 3.2. From the geometrical structures of the $(G+H)^\bullet$ isomers

displayed in Figure 3.1, it may be noticed that all isomers undergo significantly geometric change when compared to corresponding $(G+H)^+$ structures. The present energetic ordering of $(G+H)^\bullet$ may be compared to the results of Wetmore, Boyd and Eriksson at the B3LYP/6-311G(2df,p)//B3LYP/6-31G(d,p) level of theory[15] (Table 3.2). In Wetmore's work, their ordering qualitatively agrees with our findings except for the radical **r5**, which they predict to be a ring open structure with higher energy (20 kcal/mol) than that found in our studies.

Structure **r2** has the lowest total energy, and this radical arises from hydrogen atom addition to the C8 site. The N7-C8 bond length increases significantly from 1.312 Å in neutral guanine and 1.446 Å in **c2** to 1.453 Å for **r2**. The energetic favorability of the **r2** radical may due to the conjugation between the radical center N7 and the neighboring

double bond C4=C5, as shown in Scheme 4. The spin density distributions are positive for both the N7 (0.53) and C4 (0.16) sites. A similar conjugation scheme may occur for radical **r8**, which is about 9.2 kcal/mol (ZPVE corrected) above the global minimum **r2** at the B3LYP/DZP++ level. The unpaired electron is has significant contributions from N3, C5 and C8, with spin densities 0.46, 0.38 and 0.26, respectively.

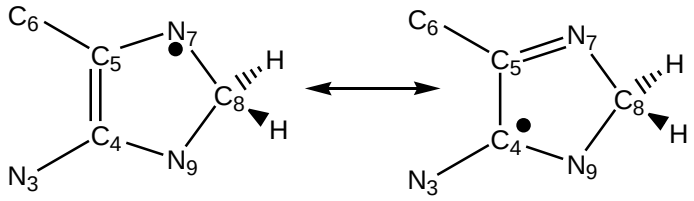


**Scheme 4**

Radical **r1** lies 10.4 kcal/mol above the global minimum **r2**. The unpaired electron is mainly localized on the C8 atom with spin density 0.74. This radical is of potential biological importance because it may be an intermediate in the formation of 8-oxo-guanine. Radicals **r6** and **r5** are predicted lie 13.9 and 15.4 kcal/mol, respectively, above the global minimum **r2** in

the gas phase. The two species undergo significant geometrical distortions on formation compared to the planar guanine molecule. Sevilla[30] described these structures as "butterfly" conformations, in which the pyrimidine and imidazole rings remain planar but both are tilted about the C4-C5 bond. The spin density for radical **r6** is predicted to reside primarily on the C5 (0.50) and C8 (0.25) atoms and that for **r5** resides in large part on C4 (0.42) and C2 (0.34), due to the conjugation effects discussed above.

The radical **r4** is predicted to lie 20.9 kcal/mol higher than **r2**. The significant structural feature of this radical is that the N2 amino group is out-of-plane (following hydrogen atom addition) compared to closed-shell neutral guanine. There are two radical isomers arising from hydrogen atom addition to the carbonyl group of guanine. These are **r3** associated with the hydrogen attached to atom O6 and **r7** with the additional hydrogen atom on C6. The total energy of **r3** is 16.9 kcal/mol higher than that of the global minimum **r2**. The resulting hydroxyl group is significantly out of the ring plane (by about 35 degrees; the O6-C6-C5-C4 dihedral angle is 145.2 degrees) due to the pyramidization of C6. Radical **r7** is the isomer with 31.1 kcal/mol higher than **r2**. Hydrogen atom addition to C6 results in an oxygen atom centered radical, comparable to that predicted to have the highest total energy for hydrogenated cytosine[17c]. Radical **r9** is the isomer with the highest total energy, namely 40.6 kcal/mol higher than **r2**. Hydrogen addition to amino group causes C2-N2 bond distance increasing significantly by 0.191 Å compared with neutral guanine.

### 3.4.3 THE $(G+H)^-$ ANIONS AND THE $(I-H)^-\cdots NH_3$ COMPLEX

We are the first to report the anionic structures for the hydrogenated guanine isomers. The eight open-shell neutral $(G+H)^\bullet$ isomers (**r1** to **r8**), may form closed-shell anions $(G+H)^-$

upon capturing electrons. Radical **r9** is predicted to extrude $NH_3$ leading to a 2-dehydrogenated inosine (Scheme 3) anion and an ammonia molecule following electron attachment in the gas phase. The predicted geometrical structures of all anions are displayed in Figure 3.1 (labeled as **a1** to **a9**), and the relative energies (ZPVE corrected) are reported in Table 3.3. Only the conventional closed-shell singlet state anions are considered in this research. Figures 1 shows that adding one electron to the neutral radicals leads to significant geometrical changes, confirming that all anions are of distinctly covalent character.

It is shown in Table 3.2 that the energetic order of the anions differs significantly from that of the analogous radicals. Anion **a8** is the most favored energetically. The anion **a9**, with *C*s symmetry, is a complex of 2-dehydrogenated inosine anion with ammonia. As the hydrogen donor, the ammonia forms a very weak hydrogen bond with the inosine N3 atom, which has a –0.70 negative charge in the NBO analysis. The very long $H_a\cdots N3$ hydrogen bond distance is 3.081 Å, and the bond angle $N_a–H_a\cdots N3$ is 152.3°. The distance between $H_a$ with inosine C2 atom is 2.165 Å, represented as a plausible hydrogen bond pattern $N_a–H_a\cdots C2$, since the C2 atom has a positive charge with 0.11 "electrons" from the NBO analysis. The Scheme 5 shows the relative energies profile of guanine, protonated guanine **c9**, hydrogenated guanine **r9**, the inosine-ammonia complex **a9,** and the energy when inosine and ammonia are separated infinitely. The theoretical results presented here should contribute to the understanding of guanine deamination reaction mechanisms via consecutive electron attachment to protonated guanine in the gas phase.

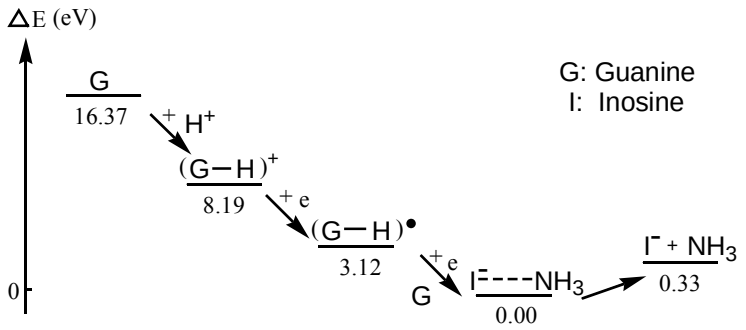


**Scheme 5**

The anions **a7**, **a6** and **a2** lie a narrow energy range 18-20 kcal/mol above the global minimum. A large energy difference (20 kcal/mol) between these three anions and remaining four anions, namely **a5**, **a4**, **a1** and **a3**, is predicted in the gas phase at the B3LYP/DZP++ level theory. Accordingly, these four anions are predicted to lie 40-53 kcal/mol above the global minimum **a8** energetically.

### 3.4.4 ELECTRON AFFINITIES OF $(G+H)^{\bullet}$ AND VERTICAL DETACHMENT ENERGIES OF $(G+H)^{-}$

Three kinds of neutral-anion energy separations, namely the adiabatic electron affinities (AEA with and without ZPVE corrections), the vertical electron affinities (VEA), and the vertical detachment energies (VDE), are reported in Table 3.4 and 5. Compared to the AEA values for the earlier studied *dehydrogenated* guanine radicals (AEA ranges from 2.22 to 2.97 eV for five isomers )[16], the electron affinities for the hydrogen addition radicals lie in a broader range (AEAs range from 0.07 to 3.12 eV for nine isomers with ZPVE). The **r9** radical studied here has the largest AEA (3.12 eV), while **r1** has a nearly zero AEA value 0.07 eV, indicating that radical **r1** has a very low propensity to bind an electron. The theoretical VEA and VDE values are quite different from the adiabatic electron affinities (See Figure 3.3), due to the

considerable geometrical changes between the radicals $(G+H)^{\bullet}$ and the corresponding anions $(G+H)^{-}$. Compared to the AEA value, the VEA of **r9** is quite small (0.60 eV). This is because the optimized neutral geometrical structure is significantly different from the optimized anionic complex structure.

## 3.5 CONCLUSION

In the present work, 27 hydrogenated guanine isomers in cationic, neutral, and anionic states have been studied theoretically. The structures, energetics and theoretical electron affinities are predicted using the carefully calibrated[19] B3LYP density functional method in conjunction with DZP++ basis sets. Our main findings include the following:

1. The computational results for nine protonated guanine cations are compared with experiment and with previous theoretical studies. The proton affinity of **c1** quantitatively matches the latest gas phase experimental measurement, within 1 kcal/mol. Protons are found likely to bind on the nitrogen and oxygen sites of guanine with an energetic range of 39 kcal/mol, while the guanine carbon sites are less favorable to protonation, since the energies range as high as 70 kcal/mol (Table 3.1).
2. Nine neutral hydrogenated guanine radicals have been examined. Radical **r2**, with the H atom attached at the guanine C8 site, is predicted to be the global minimum on the potential energy surface. Radical **r9**, with the additional hydrogen atom at N2, has the highest energy, namely 40.6 kcal/mol above **r2** (Table 3.2).
3. The energetic order for the anions differs from that of the analogous radicals (Table 3.3, Figure 3.2). The global minimum among all the anion structures is **a8**, associated with a hydride ion at the guanine C2 position. Eight of the nine anions are valence bound and

should be stable species in the gas phase. Structure **a9** is a deaminated guanine (C2-dehydrogenated inosine) anion/neutral ammonia complex, which is only 8.6 kcal/mol higher than **a8**. The significant geometry changes from **r9** (neutral) to **a9** (anion) explain the low VEA value (0.60 eV) of **r9** (Figure 3.3).

4. The geometrical distortions of $(G+H)^+$, $(G+H)^\bullet$ and anions $(G+H)^-$ with respect to ordinary guanine includes ring distortion, amino group pyramidalization, and the "butterfly" shape noted by Sevilla[30]. Generally, the $(G+H)^+$ minima favor the planar geometrical structures. The $(G+H)^-$ anions exhibit the largest geometrical distortions.
5. Among the hydrogenated guanine radicals, the carbon-centered formal radicals have the lowest AEA values (average 0.62 eV), while the two nitrogen-centered formal radicals have mid AEA values (average 1.59 eV), and the oxygen-centered formal radical **r7** has a 2.24 eV AEA value. The appearance of diverse AEA values related to different-centered radicals is one of the most fundamental elements of this research[17].
6. The present study indicates that $(G+H)^\bullet$ and $(G+H)^-$ readily exist as the products of consecutive electron attaching to $(G+H)^+$. The different energetic orderings for the $(G+H)^+$, $(G+H)^\bullet$ and $(G+H)^-$ structures (Figure 3.2) implies that there may exists intra-molecular hydrogen atom transfer among the different isomers during the electron attachment processes.

## 3.6 ACKNOWLEDGEMENTS

We appreciate the generous support of the U. S. National Science Foundation, Grant CHE-0451445.

## 3.7 REFERENCES


1. (a). O'Neill, P.; Fielden, M. *Advances in Radiation Biology* **1993**, vol. 17, pp 53-120 (b). Becker, D.; Sevilla, M.D. *Advances in Radiation Biology* **1993**, vol. 17 pp, 121-131 (c). Colson, A.O.; Sevilla, M.D. *Int. J. Radiat. Biol.* **1995**, *67*, 627 (d). Sanche, L. *Mass Spectrometry Reviews* **2002**, *21*, 349. (e). Kelly, S. O.; Barton, J. K. *Science* **1999**, *283*, 375. (f). Ratner, M. *Nature* **1999**, *397*, 480. (g). Huels, M. A.; Hahndorf, I.; Illenberger, E.; Sanche, L. *J. Chem. Phys.* **1998**, *108*, 1309.
2. (a). Cai, Z.; Dextraze, M.; Cloutier, P.; Hunting, D.; Sanche, L. *J. Chem. Phys.* **2006**, *124*, 024705. (b). Purkayastha, S.; Bernhard, W. A. *J. Phys. Chem. B* **2004**, *108*, 18377. (c). Li, X.; Sevilla, M. D.; Sanche, L. *J. Am. Chem. Soc.* **2003**, *5*, 13668. (d). Karagiannis, T.C.; El-Osta, A. *Cell. Mol. Life Sci.,* **2004**, *61*, 2137.
3. (a). Llano, J.; Eriksson, L. A. *Phys. Chem. Chem. Phys.* **2004**, *6*, 4707. (b). Cater, K. N.; Greenberg, M. M. *J. Am. Chem. Soc.* **2003**, *125*, 13376. (c). Cai, Z.; Sevilla, M. D. *Radiat. Res*. **2003**, *159*, 411.
4. (a). Hong, I. S.; Greenberg, M. M. *J. Am. Chem. Soc.* **2005**, *127*, 3692. (b). Hong, I. S.; Ding, H.; Greenberg, M. M. *J. Am. Chem. Soc.* **2006**, *128*, 2230.
5. (a). Abdoul-Carime, H.; Cloutier, P.; Sanche, L. *Radiat. Res.* **2001**, *155*, 625. (b). Huels, M. A.; Boudaiffa, B.; Cloutier, P.; Hunting, D.; Sanche, L. *J. Am. Chem. Soc.* **2003**, *125*, 4467. (c). Abdoul-Carime, H.; Gohlke, S.; Illenberger, E. *Phys. Rev. Lett.* **2004**, *92*, 168103.
6. (a). Pullman, B.; Pullman, A. *Proc. Natl. Acad. Sci. USA* **1958**, *44*, 1197. (b). Lin, J.; Yu, C.; Peng, S.; Akiyami, I.; Li, K.; Lee, L. K.; LeBreton, P. R. *J. Phys. Chem.* **1980**, *84*, 1006. (c). Steenken, S.; Jovanovic, S. V. *J. Am. Chem. Soc.* **1997**, *119*, 617.

7. (a). Giese, B. *Acc. Chem. Res.* **2000**, *33*, 631. (b). O'Neill, M. A.; Barton, J. K. *J. Am. Chem. Soc.* **2004**, *126*, 11471. (c). Lewis, F. D. *Photochem. Photobiol*. **2005**, *81*, 65. (d). Schuster, G. B. *Acc. Chem. Res.* **2000**, *33*, 253.

8. (a). Cadet, J.; Delatour, T.; Douki, T.; Gasparutto, D.; Pouget, J. P.; Sauvaigo, S. *Mutat. Res.* **1999**, *424*, 9. (b). Bruner, S. D.; Norman, D. P. G.; Verdine, G. C. *Nature* **2000**, *403*, 859. (c). Ober, M.; Linne, U.; Gierlich, J.; Carell, T. *Angew. Chem. Int. Ed.* **2003**, *42*, 4947. (d). Cheng, X.; Kelso, C.; Hornak, V.; de los Santos, C.; Grollman, A. P.; Simmerling, C. *J. Am. Chem. Soc.* **2005**, *127*, 13906. (e). Jena, N. R.; Mishra, P. C. *J. Phys. Chem. B* **2005**, *109*, 14205.

9. Ray, S. G.; Daube, S. S.; Naaman, R. *Proc. Natl. Acad. Sci. USA* **2005**, *102*, 15.

10. (a). Roehrig, G. H.; Oyler, N. A.; Adamowicz, L. *Chem. Phys. Lett.* **1994**, *225*, 265. (b). Wetmore, S. D.; Boyd, R. J.; Eriksson, L. A. *Chem. Phys. Lett.* **2000**, *322*, 129. (c). Wesolowski, S. S.; Leininger, M. L.; Pentchev, P. N.; Schaefer, H. F. *J. Am. Chem. Soc.* **2001**, *123*, 4023. (d). Li. X.; Cai, Z.; Sevilla, M. D. *J. Phys. Chem. A* **2002**, *106*, 1596. (e). Haranczyk, M.; Gutowski, M. *J. Am. Chem. Soc.* **2005**, *127*, 699.

11. Greco, F.; Liguori, A.; Sindona G.; Uccella, N. *J. Am. Chem. Soc.*, **1990**, *112*, 9092.

12. (a). Steenken, S. *Chem. Rev.* **1989**, *89*, 503. (b). Reynisson, J.; Steenken, S. *Phys. Chem. Chem. Phys.* **2002**, *4*, 527. (c). Giese, B.; McNaughton, D. *Phys. Chem. Chem. Phys.* **2002**, *4*, 5161.

13. Podolyan, Y.; Gorb, L.; Leszczynski, J. *J. Phys. Chem. A* **2000**, *104*, 7346.

14. Jang, Y. H.; Goddard, W. A.; Noyes, K. T.; Sowers, L. C.; Hwang, S.; Chung, D. S. *J. Phys. Chem. B* **2003**, *107*, 344.

15. Wetmore, S. D.; Boyd, R. J.; Eriksson, L. A. *J. Phys. Chem. B* **1998**, *102*, 9332.

16. (b). Luo, Q.; Li, Q. S.; Xie, Y.; Schaefer, H. F. *Collec. Czech. Chem. Comm.* **2005**, *70*, 6.

17. (a). Evangelista, F. A.; Paul, A.; Schaefer, H. F. *J. Phys. Chem. A*, **2004,** *108*, 3565. (b). Luo, Q.; Li, J.; Li, Q. S.; Kim, S.; Wheeler, S. E.; Xie, Y.; Schaefer, H.F. *Phys. Chem. Chem. Phys.* **2005**, *6*, 1. (c). Zhang, J. D.; Xie, Y.; Schaefer, H. F.; Luo, Q.; Li, Q. S. *Molecular Phys.* **2006**, in press.

18. (a). Boudaiffa, B.; Cloutier, P.; Hunting, D.; Huels, M. A.; Sanche, L. *Science* **2000**, *287*, 1658. (b). Zhang, Y.; Cloutier, P.; Hunting, D.; Wagner, J. R.; Sanche, L. *J. Am. Chem. Soc.* **2004**, *126*, 1002. (c). Cai, Z.; Cloutier, P.; Hunting, D.; Sanche, L. *J. Phys. Chem. B* **2005**, *109*, 4796. (d). Barrios, R.; Skurski, P.; Simons, J. *J. Phys. Chem. B* **2002**, *106*, 7991. (e). Anusiewicz, I.; Berdys, J.; Sobczyk, M.; Skurski, P.; Simons, J. *J. Phys. Chem. A* **2004**, *108*, 11381. (f). Gu, J.; Xie, Y.; Schaefer, H. F. *J. Am. Chem. Soc.* **2006**, *128*, 1250.

19. Rienstra-Kiracofe, J. C.; Tschumper, G. S.; Schaefer, H. F.; Nandi, S.; Ellison, G. B. *Chem. Rev.* **2002**, *102*, 231.

20. Becke, A. D. *J. Chem. Phys.* **1993**, *98*, 5648.

21. Lee, C.; Yang, W.; Parr, R. G. *Phys. Rev. B* **1988**, *37*, 785.

22. Frisch, M. J.; Trucks, G. W.; Schlegel, H. B.; Scuseria, G. E.; Robb, M. A.; Cheeseman, J. R.; Zakrzewski, V. G.; Montgomery, J. A.; Stratmann, R. E.; Burant, J. C.; Dapprich, S.; Millam, J. M.; Daniels, A. D.; Kudin, K. N.; Strain, M. C.; Farkas, O.; Tomasi, J.; Barone, V.; Cossi, M.; Cammi, R.; Mennucci, B.; Pomelli, C.; Adamo, C.; Clifford, S.; Ochterski, J.; Petersson, G. A.; Ayala, P. A.; Cui, Q.; Morokuma, K.; Salvador, P.; Dannenberg, J. J.; Malick, D. K.; Rabuck, A. D.; Raghavachari, K.; Foresman, J. B.; Cioslowski, J.; Ortiz, J. V.; Baboul, A. G.; Stefanov, B. B.; Liu, G.; Liashenko,

A.; Piskorz, P.; Komaromi, I.; Gomperts, R.; Martin, R. L.; Fox, D. J.; Keith, T.; Al-Laham, M. A.; Peng, C. Y.; Nanayakkara, A.; Challacombe, M.; Gill, P. M. W.; Johnson, B. G.; Chen, W.; Wong, M. W.; Andres, J. L.; Gonzalez, C.; Head-Gordon, M.; Replogle, E. S.; Pople, J. A. *Gaussian 94*, revision c.3; Gaussian, Inc.: Pittsburgh, PA, **1995**.

23. Huzinaga, S. *J. Chem. Phys*. **1965**, *42*, 1293.

24. Dunning, T. H. *J. Chem. Phys*. **1970**, *53*, 2823.

25. Lee, T. J.; Schaefer, H. F. *J. Chem. Phys*. **1985**, *83*, 1784.

26. Reed, A. E.; Weinstock, R. B.; Weinhold, F. *J. Chem. Phys*. **1985**, *83*, 735.

27. Reed, A. E.; Weinhold, F. *J. Chem. Phys*. **1985**, *83*, 1736.

28. Reed, A. E.; Curtiss, L. A.; Weinhold, F. *Chem. Rev*. **1988**, *88*, 899.

29. Reed, A. E.; Schleyer, P. R. *J. Am. Chem. Soc.* **1990**, *112*, 1434.

30. Colson, A. O.; Sevilla, M. D. *J. Phys. Chem.* **1996**, *100*, 4420.

Table 3.1: The Relative Energies of Protonated Guanine $(G + H)^+$ Structures and Proton Affinities (PA) in kcal/mol. See Figure 3.1 for the Labeling of the Different Protonated Structures **c1-c9**.

| Cations | Relative Energy | PA (with ZPVE) (B3LYP/DZP++) | PA (with ZPVE) (B3LYP/ 6-31++G[12b] | Experiment PA[11] |
|---|---|---|---|---|
| **c1** | 0.0 | 228.1 | 230 | 227.4 ± 0.1 |
| **c2** | 5.2 | 222.9 | 224 | |
| **c3** | 16.8 | 211.3 | 212 | |
| **c4** | 22.2 | 205.9 | | |
| **c5** | 25.2 | 202.8 | | |
| **c6** | 39.3 | 188.8 | 190 | |
| **c7** | 49.9 | 178.1 | | |
| **c8** | 52.0 | 176.1 | | |
| **c9** | 70.1 | 158.0 | | |

Table 3.2: The Relative Energies of Radicals Derived from Guanine $(G + H)^{\bullet}$. See Figure 3.1 for the Labeling of the Different Radicals **r1**-**r9**.

| Radicals | Relative Energies (kcal/mol) | ZPVE Corrected Relative Energies (kcal/mol) | Boyd's[a] Relative Energies[15] (kcal/mol) |
|---|---|---|---|
| **r2** | 0.0 | 0.0 | 0.0 |
| **r8** | 8.4 | 9.2 | |
| **r1** | 9.9 | 10.4 | 11.0 |
| **r6** | 13.6 | 13.9 | 14.8 |
| **r5** | 15.7 | 15.4 | 35.8[b] |
| **r3** | 16.4 | 16.9 | 19.5 |
| **r4** | 20.4 | 20.9 | 21.6 |
| **r7** | 30.7 | 31.1 | |
| **r9** | 40.1 | 40.6 | |

a. B3LYP/6-311G(2df,p)//B3LYP/6-31G(d,p) results with ZPVE corrections using the Bauschlicher and Partridge[BP] scaling factor (0.9804).

b. This earlier reported structure is qualitatively different from that predicted in the present research.

Table 3.3: The Relative Energies of Anions Derived from Guanine $(G+H)^-$ at the B3LYP/DZP++ Level. See Figure 3.1 for the Labeling of the Different Anions **a1**-**a9**.

| Anions | Relative Energy (kcal/mol) | ZPVE Corrected Relative Energy (kcal/mol) | ZPVE Corrected Guanine Hydride Affinities (kcal/mol) |
|---|---|---|---|
| **a8** | 0.0 | 0.0 | 51.8 |
| **a9** | 10.8 | 8.6 | 43.2 |
| **a7** | 18.9 | 17.9 | 33.9 |
| **a6** | 19.4 | 19.0 | 32.8 |
| **a2** | 20.6 | 19.5 | 32.3 |
| **a5** | 40.5 | 39.1 | 12.7 |
| **a4** | 46.9 | 46.0 | 5.8 |
| **a1** | 50.0 | 48.6 | 3.2 |
| **a3** | 53.7 | 52.5 | -0.7 |

Table 3.4: The Electron Attracting Properties of $(G + H)^{\bullet}$. See Figure 3.1 for the Labeling of the Different Radicals **r1**-**r9**.

| Radicals | Adiabatic Electron Affinity (eV) | | Vertical Electron Affinity (eV) |
|---|---|---|---|
| | AEA | ZPVE Corrected AEA | |
| **r1** | -0.01 | 0.07 | -0.47 |
| **r3** | 0.12 | 0.19 | -0.51 |
| **r4** | 0.58 | 0.64 | 0.11 |
| **r5** | 0.65 | 0.70 | 0.15 |
| **r2** | 0.84 | 0.88 | 0.49 |
| **r6** | 1.48 | 1.51 | 1.11 |
| **r8** | 2.10 | 2.13 | 1.90 |
| **r7** | 2.24 | 2.30 | 1.65 |
| **r9** | 3.00 | 3.12 | 0.60 |

Table 3.5: The Electron Ejecting Properties of $(G+H)^{-}$. See Figure 3.1 for the Labeling of the Different Anions **a1**-**a9**.

| Anions | Vertical Electron Detachment Energies (eV) |
|---|---|
| **a1** | 1.06 |
| **a3** | 1.20 |
| **a2** | 1.21 |
| **a5** | 1.23 |
| **a4** | 1.25 |
| **a6** | 1.83 |
| **a8** | 2.30 |
| **a7** | 2.72 |
| **a9** | 3.18 |

Figure 3.1. Geometries of Guanine and the Species $(G+H)^{+}$, $(G+H)^{\bullet}$ and $(G+H)^{-}$ at the B3LYP/DZP++ Level.

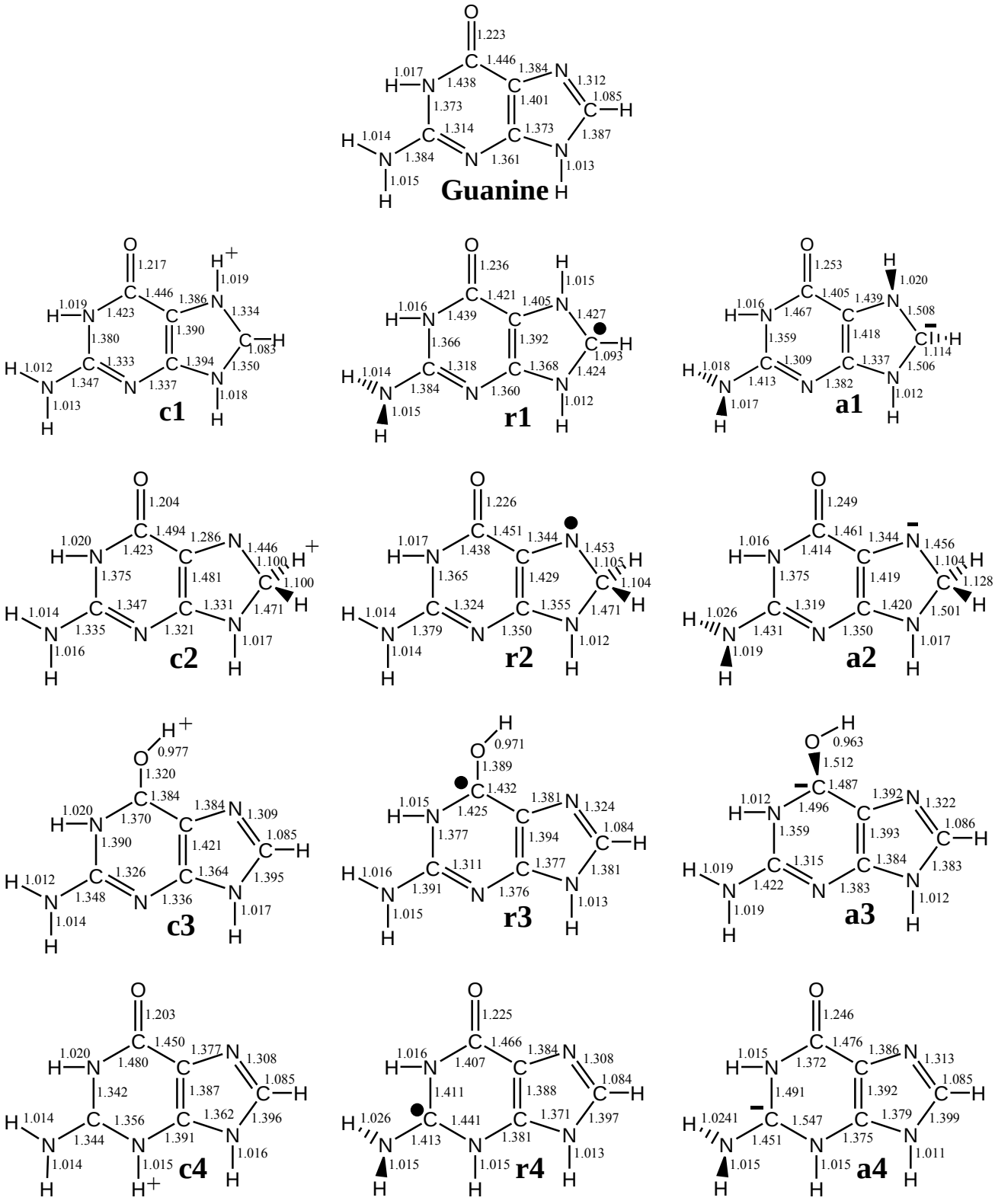

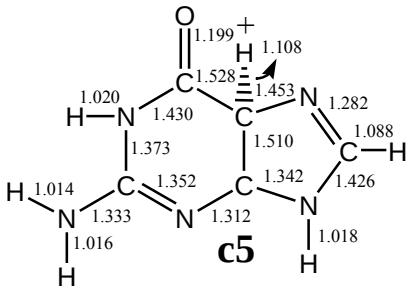
c5

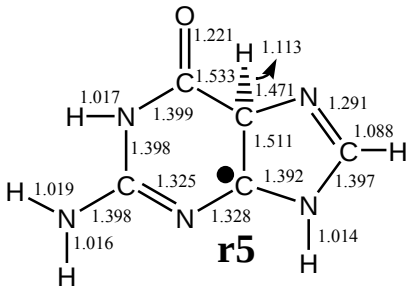
r5

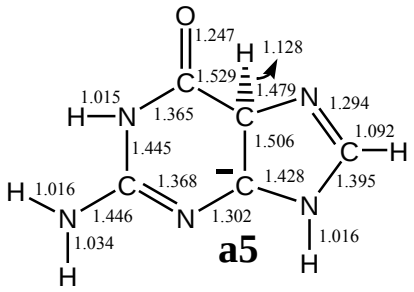
a5

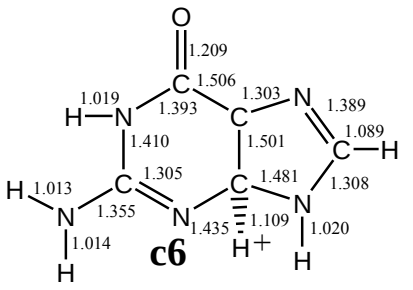
c6

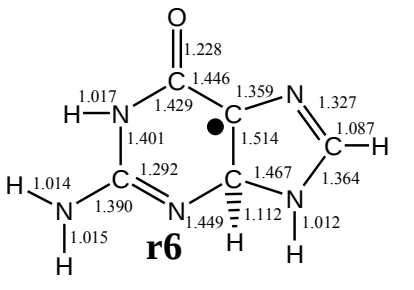
r6

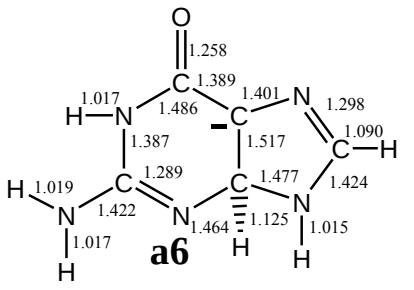
a6

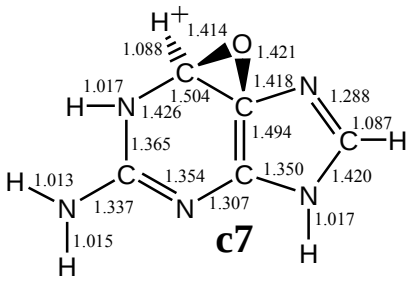
c7

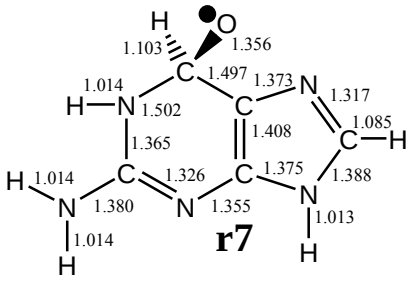
r7

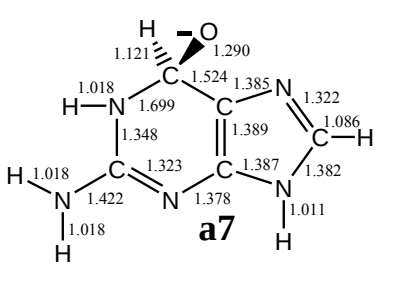
a7

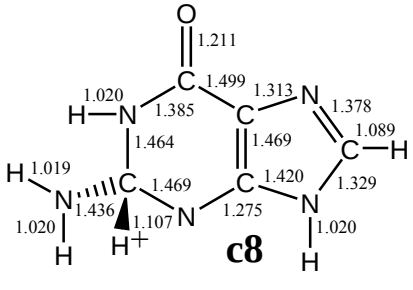
c8

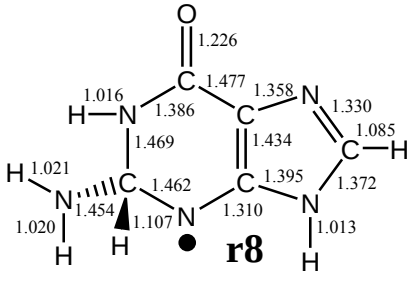
r8

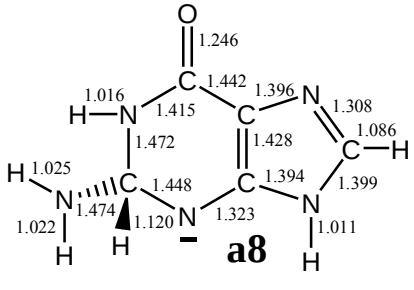
a8

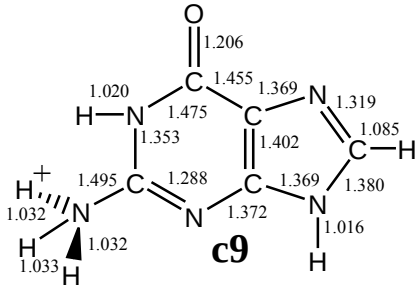
c9

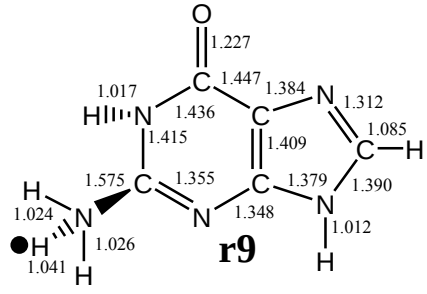
r9

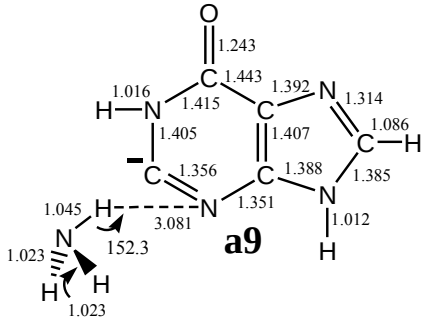
a9

Figure 3.2: Relative Energies of $(G+H)^+$, $(G+H)^\bullet$ and $(G+H)^-$ Derived from Guanine (G).

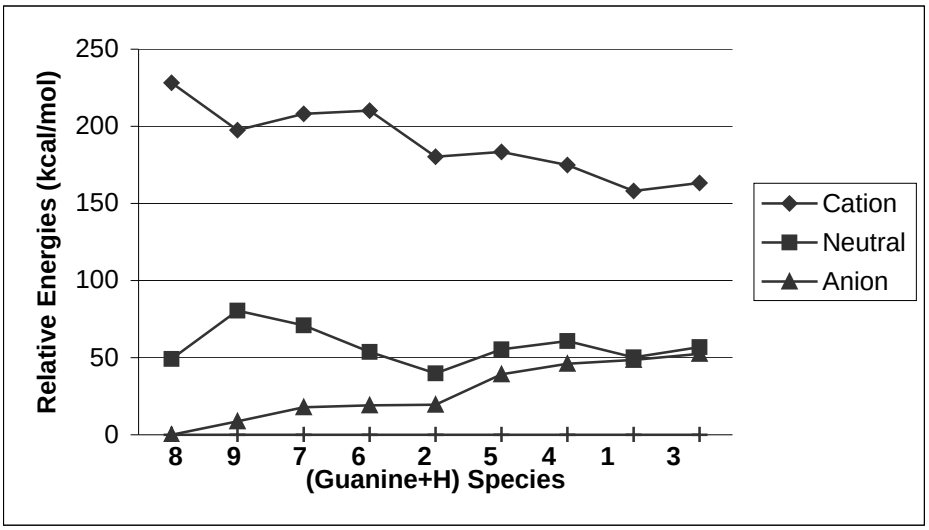

Figure 3.3: Electron Attracting Properties for $(G+H)^{\bullet}$ and $(G+H)^{-}$ Derived from Guanine.

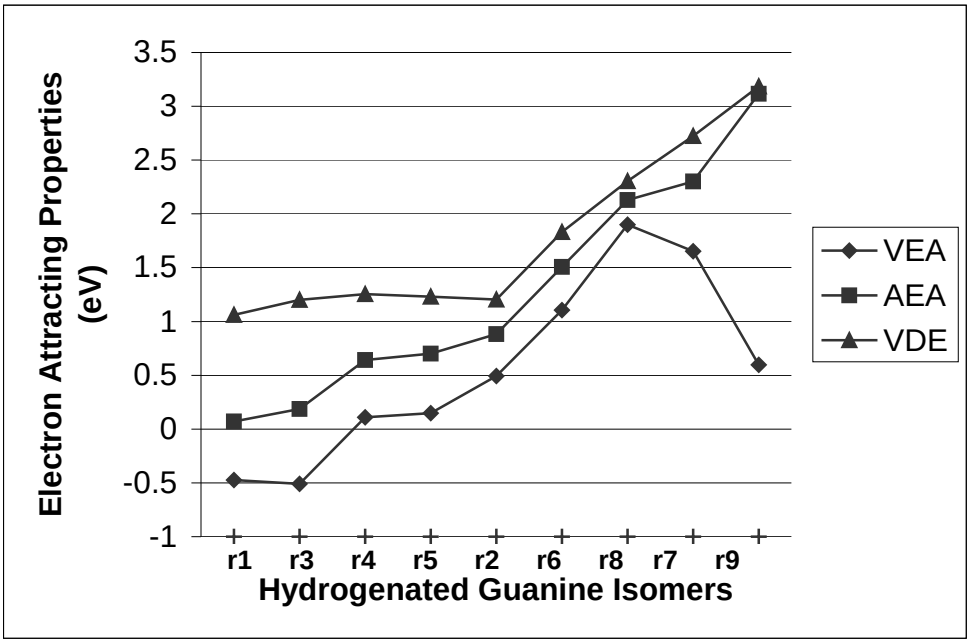

# CHAPTER 4

# ELECTRON ATTACHMENT TO THE HYDROGENATED WATSON-CRICK GUANINE CYTOSINE BASE PAIR (GC+H): CONVENTIONAL AND PROTON TRANSFERRED STRUCTURES[3]

[3] Zhang, J. D.; Schaefer, H. F., III. To be submitted to Journal of Physical Chemistry.

## 4.1 ABSTRACT

The anionic species resulting from hydride addition to the Watson-Crick Guanine-Cytosine (GC) DNA base pair are investigated theoretically. Proton transferred structures of GC hydride, in which proton H1 of guanine or proton H4 of cytosine migrates to the complementary base pair side, have been also studied. All optimized geometrical structures are confirmed to be minima via vibrational frequency analyses. The lowest energy structure places the additional hydride on the C6 position of Cytosine coupled with proton transfer, resulting in the closed-shell anion designated **1T** ($G^{-}C(C6)$). Energetically, the major groove side of the GC pair has a greater propensity toward hydride/hydrogen addition than does the minor grove side. The pairing (dissociation) energy and electron attracting ability of each anionic structure are predicted and compared with those of the neutral GC and the hydrogenated GC base pairs. Anion **8T** ($G(O6)C^{-}$) is a water-extracting complex and has the largest dissociation energy. Anion **2** ($GC(C4)^{-}$) and the corresponding open-shell radical GC(C4) have the largest vertical electron detachment energy and adiabatic electron affinity, respectively. From the difference between the dissociation energy and electron removal ability of the normal GC anion and the most favorable structure of GC hydride, it is clear that one may dissociate the GC anion and maintain the integrity of the GC hydride.

## 4.2 INTRODUCTION

DNA damage caused by ionizing radiation has been of continuing interest in recent decades. Generated from simple ionization processes, electrons are the most abundant secondary species in the living cell.[1-13] Both experimental and theoretical studies have revealed that even low-energy electrons (LEE) may attach to DNA nucleic acid bases (NABs) and induce either

sugar-backbone σ bond breakage or N1-glycosidic bond rupture (See Scheme 1 for IUPAC numbering scheme for the Watson-Crick guanine-cytosine base pair with backbones).[7,15-21] Furthermore, the radiation products of water, such as hydrogen atoms and hydroxl radicals, can react with charged NABs to cause base lesions. The stable lesion products, such as 8-oxo-guanine, resemble adenine instead of cytosine in the formation of mutagenic sequences.[22,23] If not repaired, a "bad" DNA sequence may be copied and translated to the next generation and cause potentially pathogenic cells. On the other hand, as a therapy to destroy tumor cells by damaging the cancerous DNA sequence, ionizing radiation can cause the demise of healthy cells. An always challenging question is whether one could design a medical radiation device to selectively break "bad" DNA molecules while keeping "good" species unchanged. Consequently, an understanding of differences in the molecular structures and electron attracting abilities of both DNA normal subunits and geometrically altered subunits might be useful in the future in designing nano-scale medical devices.

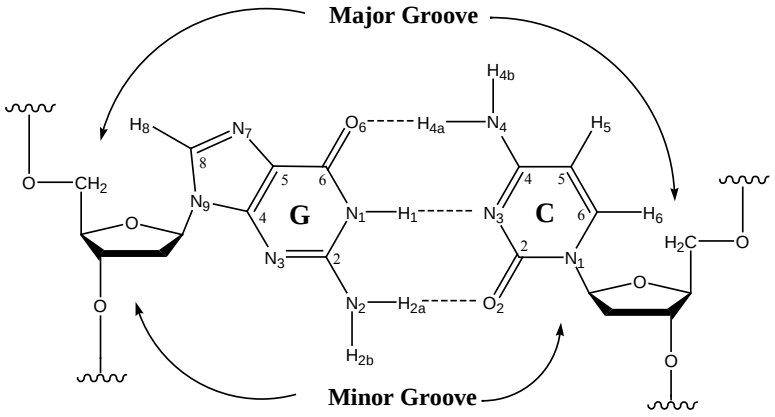


**Scheme 1. Guanine-Cytosine Base Pair with Backbone**

To understand the electron attracting ability of DNA subunits, the adiabatic electron affinities (AEAs) of these species should be determined. The valence-bound AEAs of individual NABs such as uracil(U), thymine(T), and cytosine(C) have been extrapolated from the AEAs of base-waters clusters measured by photodetachment-photoelectron (PD-PE) spectroscopy.[24]

Theoretical investigations have complemented experiments successfully, and experiment-consistent AEA values of the nucleobases, with the latest ordering U > T > C ~ G (guanine) > A (adenine), have been confirmed by density functional theory (DFT) approaches.[25] While the experimental determination of AEAs for the biologically related adenine-thymine (AT) and guanine-cytosine (GC) Watson-Crick base pairs still remains challenging, in 2005, Bowen and co-workers[26] reported the vertical detachment energy (VDE) of various AT and 9-methyladenine-1-methylthymine base pairs measured from photoelectron spectroscopy, in agreement with earlier theoretical predictions.[32] The canonical Watson-Crick base pairs AT and GC have been predicted by theory to have positive AEA values.[27-32] Recently, some disrupted DNA subunits such as de-hydrogenated bases[33-35] and base pairs,[36-38] and hydrogenated cytosine,[39-45] guanine,[46,47] and adenine,[48-53] have been detected experimentally, and the values of their AEAs have been also reported theoretically. The molecular structures of hydrogenated GC pairs have been reported recently,[54] while the AEA values have not been investigated yet. Meanwhile, it is well known that proton transfer (PT) plays an important role in stabilizing ionic DNA subunits upon radiation. Several theoretical studies have revealed that base pair anions are susceptible to PT.[55-58] It is thus important to consider PT structures in the present GC hydride study.

Here we selected the hydrogenated Watson-Crick GC base pairs as models of damaged DNA base pair to explore AEAs and dissociation energies and to compare with those of the parent Watson-Crick GC pair.[31] The overall effect of electron attachment to hydrogenated GC is a hydride adding to each of heavy atoms associated with seven double bonds of GC (1).

$$GC + H^- \rightarrow (GC+H)^- \text{ (fourteen isomers)} \qquad (1)$$

$$(GC+H)^- \rightarrow (G+H)^- + C \text{ or } (C+H)^- + G \qquad (2)$$

We optimized the molecular structure of each isomer and predicted the dissociation energy associated with each structure (2). Each "site-specific" AEA has been obtained by evaluating the energy difference between the hydrogenated GC and the corresponding GC hydride, where a hydrogen atom has been attached to a different site of GC. Furthermore, we investigated significant PT reaction (3) of each hydride GC isomer and compared with the PT process (4) for the GC anion.

$$(GC+H)^- \rightarrow (G+2H)(C-H)^- \text{ or } (G-H)^-(C+2H) \qquad (3)$$

$$GC^- \rightarrow (G-H)^-(C+H) \qquad (4)$$

The geometrical structures of Watson-Crick $GC^-$ and proton transferred $(G-H)^-(C+H)$ are shown in Figure 4.1. Transition states for the reactions (3) and (4) have been located. Two possible PT pathways are found. In one pathway the cytosine proton H4a transfers to guanine O6 (See Scheme 1 for numbering of atoms), where the anionic center resides on the guanine moiety. In the other pathway the guanine H1 transfers to the N3 site of cytosine, where the anionic center is located on the cytosine moiety. Knowledge of the electronic characteristics of DNA subunits may be useful in building more biologically relevant models in order to develop future techniques for separating and repairing damaged DNA sequences.

## 4.3 METHODS

Complete geometrical optimizations and vibrational frequency analyses were carried out using DFT methods, specifically the B3LYP functional with DZP++ basis sets.[59] This combination has been demonstrated to provide reasonable theoretical results for DNA subunits.[31,32,36,37,54] The B3LYP method is a hybrid of the HF and DFT methods, incorporating Becke's three-parameter exchange functional (B3)[60] with the Lee, Yang, and Parr (LYP)

correlation functional.[61] The DZP++ basis sets were constructed by augmenting the 1970 Huzinaga-Dunning contracted double-ζ basis with one set of five d-type polarization functions for each C, N and O atom, and a set of p functions on each H atom. In addition, even tempered s and p type diffuse functions were added to each C, N and O, and a diffuse s function on each H. The final DZP++ set contains nineteen functions per C, N and O atom (10s6p1d/5s3p1d) and six functions per H (5s1p/3s1p).[62-64] Vibrationally zero-point corrected relative energies and natural charges for the base pair were also determined using the same approach. Numerical integrations were performed using a fine grid of 75 radial and 302 angular points per shell.[65] Natural Population Atomic (NPA) charges were determined using the same level of theory with the Natural Bond Order (NBO) analysis of Reed and Weinhold.[66-69] The GAUSSIAN 94 and 03 systems of DFT programs were used for the computations.[70]

Critical energetic properties were determined as follows:

Adiabatic electron affinity (AEA)

AEA = *E*(optimized neutral) – *E*(optimized anion).

Anion vertical detachment energy (VDE)

VDE = *E*(neutral at optimized anion geometry) – *E*(optimized anion).

Dissociation energy (DE)

$DE = E[(G+H)-C]^- - E(G+H)^- - E(C)$ or,

$DE = E[G-(C+H)]^- - E(G) - E(C+H)^-$

## 4.4 RESULTS AND DISCUSSION

Hydrogenated and corresponding GC hydride structures have been selected herein as models to explore site-specific effects on damaged GC base pairs upon electron attachment. The formalism used to denote each hydrogenated/hydride GC structure is as follows: Addition of a hydrogen atom to one of the seven double bonds of the GC base pair, leading to open-shell radical structures, is denoted as $(GC+H)^{\bullet}$. There are a total of fourteen open-shell structures thus generated. The analogous closed-shell anions were formed by incoming electron attachment to each of the fourteen radicals, the anions thus are denoted as $(GC+H)^{-}$. More anionic structures, denoted as $(GC+H)^{-}_{PT}$ should be considered because of proton transfer (PT) processes triggered by electron attachment. The overall effect may be regarded as hydride addition to the GC base pair, as described by Scheme 2.

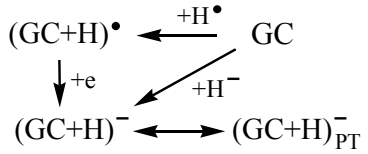


**Scheme 2. Reactions Associated with Hydrogen/Electron Attachment to the Guanine-Cytosine Base Pair**

The resulting anionic structures are specified using G for the parent guanine and C for the parent cytosine, followed by the atom in which the hydrogen atom is appended in parentheses. Thus $G(N3)^{-}C$ designates the anion generated by hydride addition to atom N3 of guanine, with the extra electron located on the G moiety; and the corresponding PT structure of this anion is denoted as $G(N3)C^{-}$, explicitly indicating that the negative charge has migrated to the C moiety in the course of the PT process. Structures **1** to **14** illustrate each of the hydride GC base pairs, while the designations **1T** to **13T** label the corresponding PT structures.

### 4.4.1 ENERGIES AND GEOMETRIES OF GC HYDRIDE SPECIES

In Table 4.1, relative energies of $(GC+H)^-$ and $(GC+H)^-_{PT}$ are presented. The total energies are shown in the Supporting Information Table A. All structures are local minima on the potential energy surfaces as demonstrated via vibrational frequency computations (Figure 5.2-4). The formal anionic center has been marked in each structure. All optimized structures of $(GC+H)^-$ and $(GC+H)^-_{PT}$ deviate from the planar symmetry of the neutral GC base pair in the gas phase. Two dihedral angles $\tau(C6\text{-}N1)_G\text{-}(N3\text{-}C4)_C$ and $\tau(C6\text{-}C2)_G\text{-}(C2\text{-}C4)_C$ were selected as indicators of the effects of anion formation on the overall base pair geometries (please see Supporting Information Table B).

There does not appear to be any systematic energetic preference in the addition of hydride to guanine rather than to the cytosine moiety. Among all isomers, PT structure **1T** with the hydride attached at cytosine C6 position has the lowest total energy. The non-PT structure **1** is predicted to lie only 3.7 kcal/mol above **1T**. Structure **2T,** donated as $G^-C(C4)$ implies a PT structure from hydride addition to atom C4 of cytosine and lies 5.3 kcal/mol above the global minimum **1T**. Meanwhile, the non-PT structure **2** [denoted as $GC(C4)^-$] has a total energy 5.4 kcal/mol higher than **2T**. In both the structures **2** and **2T**, hydride addition leads to a tetrahedral cytosine C4 structure, which causes significant strain on the base pairing, reflected by large dihedral angle $\tau(C6\text{-}N1)_G\text{-}(N3\text{-}C4)_C$ (-12.5 and –14.0 degree for **2** and **2T**, respectively, Table B of the Supporting Information). The five structures with lowest free energies (**1T**, **1**, **2T**, **2**, **3T**) are all formed by hydride addition on the major groove side of the GC double helix (Scheme 1). In the anionic structure **5** [$G(C2)^-C$, Figure 4.3], formation of a tetra-coordinated C2 atom reveals a loss of hydrogen bonding ability with cytosine, consistent with earlier predictions for the G(C2)C radical.[54]

Unlike the *radical* structure G(O6)C [54], the anion **8T**(G(O6)C$^-$) is predicted to have an unprecedented structure (Figure 4.3), lying 42.3 kcal/mol higher than the global minimum **1T**. In this complex, a water molecule is formed in which a hydride carbonyl group of guanine contributes OH and the amino group of cytosine provides an H atom. The negative charge in **8T** is mainly located at the dehydrogenated cytosine moiety, as indicated by both the Mulliken charge (-0.74 electrons) and the NBO charge (-0.86 electrons). However, structural analogues of **8**, **12** and **12T (**Figure 4.3) have not been located as water-extracted complexes. The C2-O2 distances are 1.451 Å and 1.453 Å for **12** and **12T**, respectively, both significantly longer than that in *radical* GC(O2) (1.371 Å)[54], but not sufficient for bond breakage.

Structure **10**[GC(N3)$^-$, Figure 4.4] lies 53.3 kcal/mol higher than **1T**, with a bifurcated hydrogen bond formed following hydride addition to N3 atom. There is an unusual hydrogen bond N2–H2···C2 in **12T** instead of the N2–H2···O2 in structure **12**. This may be because the cytosine C2 atom acquires substantial negative charge (-0.42 Mulliken "electrons"), as an anionic center at **12T**. Structure **14** is formed by addition of a hydride to the minor groove N3 atom of guanine. This structure has the highest total energy found for the (GC+H)$^-$ system, lying 78.9 kcal/mol above the global minimum **1T.** The PT structure for **14** was not found.

### 4.4.2 PROTON TRANSFER OF GC HYDRIDE SPECIES

Not all (GC+H)$^-$ isomers have both PT and non-PT structures, e.g., structures **3T**, **4T**, **7T**, **8T**, **10** and **14**. However, if both exist, the PT structure has a lower total energy than the corresponding non-PT structure, except for **6T**. This phenomenon implies that PT molecular structures may be generally more favorable to attachment of an electron.

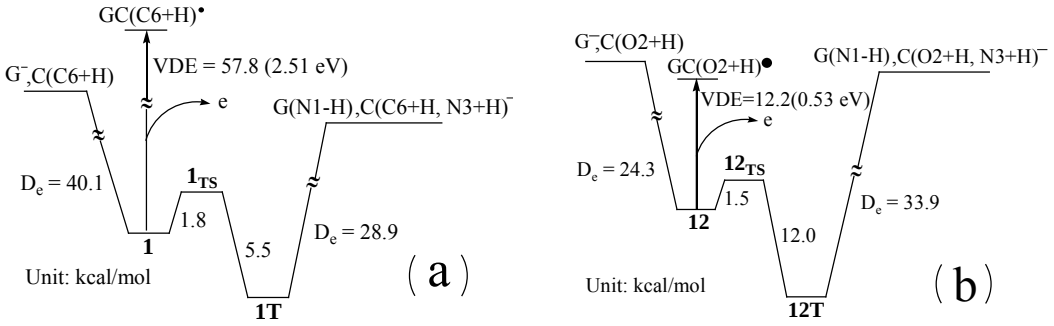


**Scheme 3. Energy profiles for the proton transfer, electron detachment, and dissociation reactions of (a) structure 1 to 1T and (b) structure 12 to 12T.**

To understand the mechanism of the PT process, two transition states ($\mathbf{1_{TS}}$ and $\mathbf{12_{TS}}$) corresponding to two PT process: **1** → **1T** and **12** → **12T**, respectively, were optimized. $\mathbf{1_{TS}}$ is probed because **1** and **1T** are the isomers with lowest total energy. In contrast, **12** and **12T** have the largest energy difference (10.6 kcal/mol) among all PT/non-PT pairs. The energy profiles are shown in Scheme 3. Dissociation energies and vertical electron detachment energies also included for comparison. The optimized structure of transition states is shown in Figure 4.5.

The $\mathbf{1_{TS}}$ vibrational analysis indicates that the imaginary vibrational frequency (1036i $cm^{-1}$) is the normal mode corresponding to the guanine N1-H1 stretching; in $\mathbf{12_{TS}}$ the analogous frequency is 1003i $cm^{-1}$. Two low energetic barriers are predicted, 1.8 kcal/mol for **1**→**1T** and 1.5 kcal/mol for **12**→**12T**. Compared to the higher dissociation energies and VDEs, these small barriers indicate that fast PT reactions may occur for **1** and **12**. The resulting PT products **1T** and **12T** are quite energetically favorable and, thus may have long enough lifetimes to cause further DNA damage reactions before dissociation. For comparison, the barrier for the analogous PT reaction of the base pair radical anion $GC^-$ is 2.3 kcal/mol at the same level of theory,[71] and 3.5 kcal/mol with the B3LYP/6-31+G(d) method.[56] The PT for the DNA nucleoside pair 2'-Deoxyguanosine(dG)-2'-Deoxycytidine(dC) anion also has been predicted to have a small barrier, 2.4 kcal/mol.[71]

### 4.4.3 DISSOCIATION ENERGIES

The dissociation energy discussed here is the energy required to separate the GC hydride pair into two monomers (guanine hydride + cytosine or cytosine hydride + guanine). For **8T** dissociation leads to three monomers: de-oxygened guanine + deprotonated cytosine + water molecule, respectively. There are some rules that should be noted from our findings. Firstly, the more hydrogen bonds formed, the larger the predicted dissociation energy. For example, the complex structure **8T** has the largest $D_e$ (49.1 kcal/mol, breaking four hydrogen bonds, Table 4.2), while **5** and **14** have quite low $D_e$ values (both have two hydrogen bonds, with $D_e$ = 13.5 and 12.0 kcal/mol, respectively, Table 4.2). Secondly, the formation of hydrogen bonds between two monomers may cause substantial strain for each of them. Hence, after dimer dissociation, the isolated monomer likely relaxes to the structure with the lowest free energy, thus decreasing the dissociation energy. For example, as the **6T** dissociation product ($D_e$ = 10.2 kcal/mol), compound **15** is an energeticly favored closed-shell structure (Figure 4.6), instead of the formal monomer of **6T** represented as a diradical structure of 3,5-dihydrogenated cytosine. Similarly, dissociation of **13T** ($D_e$ = 12.2 kcal/mol) yields a closed-shell structure **16** with a covalent bond forming between atoms C4 and C6 of the guanine moiety with two H atoms appended (Figure 4.6).

To separate a hydride GC pair, generally more energy is needed when the negative charge is primarily located on the cytosine part rather than the guanine moiety. The average $D_e$ for cytosine-centered anionic pairs is ~36 kcal/mol, whereas it is ~20 kcal/mol for guanine-centered pairs. This might be the case because cytosine represents a smaller conjugated system in which the extra electron is distributed. Hydrogen bonding is strengthened when the “last” electron is located near the hydrogen bond acceptor with higher electronegativity. On the other

hand, when the negative charge is located primarily on guanine, hydrogen bond acceptors receive less electron density due to the larger delocalized system. **1** and **1T** could be good examples here. There are three hydrogen bonds forming in both structures and no strain at each of four monomers. However, the dissociation energy $D_e$ of structure **1** is about 11 kcal/mol higher than that for **1T**. This significant $D_e$ difference may arise from the two H-bond acceptors O2 and N3 of cytosine in structure **1** having combined –0.96 Mulliken or –1.61 NBO populations. The latter electron densities are larger than those of O6 and N1 of guanine in **1T**, with combined –0.88 Mulliken or –1.50 NBO electrons. Qualitatively, the enhanced electrostatic interaction in hydrogen bonding caused by the excess electron on cytosine also appears to be an explanation of the lower $D_e$ of the neutral hydrogenated GC species. In Table 4.2, one observes that cytosine-centered anions are predicted to have larger $D_e$ values than those of the corresponding neutral radicals at the same theoretical level.

### 4.4.4 VDES OF GC HYDRIDE AND AEAS OF HYDROGENATED GC

All anionic structures of GC hydride have positive VDE values, ranging from 0.31 to 4.03 eV (Table 4.2). Generally, the PT anions have larger VDEs than the non-PT anions if both structures exist. Structure **2** has the largest VDE, indicating that the extra electron is least likely to be removed. The lowest total energy structure **1T** also has significant positive VDE 3.39 eV (78.2 kcal/mol), which is much larger than the analogous $D_e$ (28.9 kcal/mol), suggesting that anion **1T** may dissociate prior to ionization.

The predicted AEA values of hydrogenated GC (Table 4.2) are in the range from –0.16 to 3.45 eV. It may be interesting to compare the AEAs of $(GC+H)^{\bullet}$ with those of the hydrogenated G (denoted as $(G+H)^{\bullet}$) and C (denoted as $(C+H)^{\bullet}$) monomers.[45,47] For hydride GC

anions, if both non-PT and PT structures exist (Table 4.2) , the higher AEA is selected and shown in Figure 4.7 with the AEAs of the isolated $(G+H)^{\bullet}$ and $(C+H)^{\bullet}$. From Figure 4.7, the general trend of AEAs for $(GC+H)^{\bullet}$ is in consistent with those of isolated $(G+H)^{\bullet}$ and $(C+H)^{\bullet}$ systems. An exception occurs for G(O6), because the paired anion $G(O6)C^{-}$ has a complex structure with low free energy (Figure 4.3). Isolated $(C+H)^{\bullet}$ radicals have lower AEAs than the corresponding paired $(GC+H)^{\bullet}$ radicals. The AEAs of isolated $(G+H)^{\bullet}$ and the corresponding paired $(GC+H)^{\bullet}$ radicals display no clear pattern.

## 4.5 CONCLUSIONS

Hydride addition to the DNA Watson-Crick GC base pair generates 21 possible anionic structures. Generally, the proton transferred (PT) structures have lower free energies compared to the non-PT structures. This can be understood in light of theoretical results for GC and dGdC. Anion **1T** has been predicted to be the global minimum. Considering the double helix structure of the DNA sequence, hydride addition on the major grove side of the GC pair generates products with lower free energies than those generated on minor groove addition.

The adiabatic electron affinities (AEAs) of the hydrogenated GC radicals and the vertical detachment energies (VDEs) of the GC hydride anions range from –0.16 to 3.45 eV and 0.31 eV to 4.03 eV, respectively. The wide range predicted in our theoretical studies implies complicated photodetachment-photoelectron spectra for GC hydride species. Among all species, structure **11** has the lowest VDE and the corresponding lowest AEA for its neutral radical.

The answer to the first question posed in the present paper: “Can one find a substantial difference between the normal GC base pair and the hydrogenated GC under ionization radiation aim to separate normal and damaged DNA sequences?” is positive. For example, the

*hydrogenated* GC isomer with lowest free energy is structure G(C8)C (from reference 54), which has a very similar dissociation energy and AEA to the neutral Watson-Crick GC pair ($\Delta D_e$ = 0.9 kcal/mol, $\Delta$AEA = 0.13 eV, Table 4.2). However, with the electron attachment from ionization radiation, **9T** (G(C8)C$^-$) differs substantially in energy from either GC$^-$ or (G-H)$^-$(C+H). For example, an energy of 40 kcal/mol is adequate to dissociate both GC$^-$ and (G-H)$^-$(C+H) ($D_e$ values are 39.4 kcal/mol and 31.3 kcal/mol, respectively, Table 4.2). However, this amount of energy is not sufficient to separate the base pair anion G(C8)C$^-$ (the latter $D_e$ value is 45.2 kcal/mol, Table 4.2); instead, it is only enough to remove an electron from G(C8)C$^-$ [VDE value is 1.64 eV (37.8 kcal/mol), Table 4.2]; thus the G(C8)C$^-$ will remain bound.

## 4.6 ACKNOLEDGEMENTS

This research was supported by the National Science Foundation, Grant CHE-0451445 and CHE-0716718. ZFC thanks the Research Computing Center (RCC) at the University of Georgia for providing computation facilities.

## 4.7 REFERENCES

1. von Sonntag, C. *The Chemical Basis of Radiation Biology*, Taylor & Francis: New York, **1987**.
2. Becker, D.; Sevilla, M. D. *Advances in Radiation Biology*; Academic Press: New York, **1993**.
3. Colson, A. O.; Sevilla, M. D. *Int. J. Radiat. Biol.* **1995**, *67*, 627.
4. Steenken, S. *Chem. Rev.* **1989**, *89*, 503.

5. Steenken, S.; Telo, J. P.; Novais, H. M.; Candeias, L. P. *J. Am. Chem. Soc.* **1992**, *114*, 4701.
6. Steenken S.; Goldbergerova, L. *J. Am. Chem. Soc.* **1998**, *120*, 3928.
7. Boudaiffa, B.; Cloutier, P.; Hunting, D.; Huels, M. A.; Sanche, L. *Science* **2000**, *287*, 1658.
8. Li, X.; Sevilla, M. D.; Sanche, L. *J. Am. Chem. Soc.* **2003**, *125*, 13668.
9. Caron, L. G.; Sanche, L. *Phys. Rev. Lett.* **2003**, *91*, 113201.
10. Huels, M. A.; Boudaiffa, B.; Cloutier, P.; Hunting, D.; Sanche, L. *J. Am. Chem. Soc.* **2003**, *125*, 4446.
11. Sanche, L. *Eur. Phys. J. D* **2005**, *35*, 367.
12. Ptasińska, S.; Denifl, S.; Gohlke, S.; Scheier, P.; Illenberger, E.; Märk, T. D. *Angew. Chem. Int. Ed.* **2006**, *45*, 1893.
13. Simons, J. *J. Acc. Chem. Res.* **2006**, *39*, 772.
14. Barriors, R.; Skurski, P.; Simons, J. *J. Phys. Chem. B* **2002**, *106*, 7991.
15. Berdys, J.; Ansiewicz, I.; Skurski, P.; Simons, J. *Acc. Chem. Res.* **2004**, *126*, 6441.
16. Berdys, J.; Skurski, P.; Simons, J. *J. Phys. Chem. B* **2004**, *108*, 5800.
17. Li, X.; Sanche, L.; Sevilla, M. D. *Rediation Research* **2006**, *165*, 721.
18. Gu, J.; Wang, J.; Leszczynski, J. *J. Am. Chem. Soc.* **2006**, *128*, 9322.
19. Gu, J.; Xie, Y.; Schaefer, H. F. *J. Am. Chem. Soc.* **2005**, *127*, 1053.
20. Gu, J.; Xie, Y.; Schaefer, H. F. *J. Am. Chem. Soc.* **2006**, *128*, 1250.
21. Bao, X.; Wang, J.; Gu, J.; Leszcynski, J. *Proc. Nat. Acad. Sci. USA* **2006**, *103*, 5658.
22. Malins, D. C.; Polissar, N. L.; Ostrander, G.K.; Vinson, M.A. *Proc. Natl. Acad. Sci. USA* **2000**, *97*, 12442.

23. Cheng, X.; Kelso, C.; Hornak, V.; de los Santos, C.; Grollman, A. P.; Simmerling, C. *J. Am. Chem. Soc.* **2005**, *127*, 13906.

24. Schiedt, J.; Weinkauf, R.; Neumark, D. M.; Schlag, E. W. *Chem. Phys.* **1998**, *239*, 511.

25. Wesolowski, S. S.; Leininger, M. L.; Pentchev, P. N.; Schaefer, H. F. *J. Am. Chem. Soc*. **2001**, *123*, 4023.

26. Radisic, D.; Bowen, K. H.; Dabkowska, I.; Storoniak, P.; Rak, J.; Gutowski, M. *J. Am. Chem. Soc*. **2005**, *127*, 6443.

27. Li, X.; Cai, Z.; Sevilla, M. D. *J. Phys. Chem. B* **2001**, *105*, 10115.

28. Li, X.; Cai, Z.; Sevilla, M. D. *J. Phys. Chem. A* **2002**, *106*, 9345.

29. Li, X.; Sevilla, M. D.; Sanche, L. *J. Am. Chem. Soc*. **2003**, *125*, 8916.

30. Reynisson, J.; Steenken, S. *Phys. Chem. Chem. Phys*. **2002**, *4*, 5353.

31. Richardson, N. A.; Wesolowski, S. S.; Schaefer, H. F. *J. Am. Chem. Soc*. **2002**, *124*, 10163.

32. Richardson, N. A.; Wesolowski, S. S.; Schaefer, H. F. *J. Phys. Chem. B* **2003**, *107*, 848.

33. Liu, B.; Hvelplund, P.; Nielsen, S. B.; Tomita, S. *J. Chem. Phys.* **2004**, *121*, 4175.

34. Denifl, S.; Ptasinska, S.; Probst, M.; Hrusak, J.; Scheier, P.; Mark, T. D. *J. Phys. Chem. A* **2004**, *108*, 6562.

35. Abdoul-Carime, H.; Langer, J.; Huels, M. A.; Illenberger, E. *Eur. Phys. J. D* **2005**, *35*, 399.

36. Bera, P. P.; Schaefer, H. F. *Proc. Natl. Acad. Sci. USA* **2005**, *102*, 6698.

37. Lind, M. C.; Bera, P. P.; Richardson, N. A.; Wheeler, S. E.; Schaefer, H. F. *Proc. Natl. Acad. Sci. USA* **2006**, *103*, 7554.

38. Lind, M. C.; Richardson, N. A.; Wheeler, S. E.; Schaefer, H. F. *J. Phys. Chem. B* **2007**, *111*, 5525.

39. Colson, A.O.; Becker, D.; Eliezer, I.; Sevilla, M.D. *J. Phys. Chem. A* **1997**, *101*, 8935.

40. Debije, M.D.; Bernhard, W.A. *J. Phys. Chem. A* **2002**, *106*, 4608.

41. Debije, M. G.; Close, D. M.; Bernhard, W. A. *Radiation Research* **2002**, *157*, 235.

42. Turecek, F.; Yao, C. *J. Phys. Chem. A* **2003**, *107*, 9221.

43. Chen, X.; Syrstad, E. A.; Nguyen, M. T.; Gerbaux, P. G.; Turecek, F. *J. Phys. Chem. A* **2005**, *109*, 8121.

44. Yao, C.; Cuadrado-Peinado, M. L.; Polasek, M.; Turecek, F. *Angew. Chem. Int. Ed.* **2005**, *44*, 6708.

45. Zhang, J. D.; Xie, Y.; Schaefer, H. F.; Luo, Q.; Li, Q.-S. *Molecular Phys.* **2006**, *104*, 2347.

46. Wetmore, S. D.; Boyd, R. J.; Eriksson, L. A. *J. Phys. Chem. B* **1998**, *102*, 9332.

47. Zhang, J. D.; Xie, Y.; Schaefer, H. F. *J. Phys. Chem. A* **2006**, *110*, 12010.

48. Lichter, J. J.; Gordy, W. *Proc. Natl. Acad. Sci. USA* **1968**, *60*, 450.

49. Close, D. M.; Nelson, W. H.; Sagstuen, E.; Hole, E. O. *Radiation Research* **1994**, *137*, 309.

50. Colson, A. O.; Sevilla, M. D. *J. Phys. Chem.* **1995**, *99*, 13037.

51. Colson, A. O.; Becker, D.; Eliezer, I.; Sevilla, M. D. *J. Phys. Chem. A* **1997**, *101*, 8941.

52. Wetmore, S. D.; Boyd, R. J.; Eriksson, L. A. *J. Phys. Chem. B* **1998**, *102*, 10614.

53. Reynisson, J.; Steenken, S. *Phys. Chem. Chem. Phys.* **2005**, *7*, 665.

54. Zhang, J. D.; Schaefer, H. F. *J. Chem. Theory Comput.* **2007,** *3,* 115.

55. Colson, A. O.; Besler, B.; Close, D. M.; Sevilla, M. D. *J. Phys. Chem.***1992**, *96*, 661.

56. Li, X.; Cai, Z.; Sevilla, M. D. *J. Phys. Chem. B* **2001**, *105*, 10115.

57. Gorb, L.; Podolyan, Y.; Dziekonski, P.; Sokalski, W. A.; Leszczynski, J. *J. Am. Chem. Soc.* **2004**, *126*, 10119.

58. Zoete, V.; Meuwly, M. *J. Chem. Phys*. **2004**, *121*, 4377.

59. Rienstra-Kiracofe, J. C.; Tschumper, G. S.; Schaefer, H. F.; Nandi, S.; Ellison, G. B. *Chem. Rev.* **2002**, *102*, 231.

60. Becke, A. D. *J. Chem. Phys.* **1993**, *98*, 5648.

61. Lee, C.; Yang, W.; Parr, R. G. *Phys. Rev. B* **1988**, *37*, 785.

62. Huzinaga, S. *J. Chem. Phys*. **1965**, *42*, 1293.

63. Dunning, T. H. *J. Chem. Phys*. **1970**, *53*, 2823.

64. Lee, T. J.; Schaefer, H. F. *J. Chem. Phys*. **1985**, *83*, 1784.

65. Papas, B. N.; Schaefer, H. F. *J. Mol. Struct.* **2006**, *768*, 175.

66. Reed, A. E.; Weinstock, R. B.; Weinhold, F. *J. Chem. Phys*. **1985**, *83*, 735.

67. Reed, A. E.; Weinhold, F. *J. Chem. Phys*. **1985**, *83*, 1736.

68. Reed, A. E.; Curtiss, L. A.; Weinhold, F. *Chem. Rev*. **1988**, *88*, 899.

69. Reed, A. E.; Schleyer, P. R. *J. Am. Chem. Soc.* **1990**, *112*, 1434.

70. (a) Frisch, M. J. et al. *Gaussian 94,* Revision B.3; Gaussian Inc., Pittsburgh, PA, 1995; used by J. D. Zhang. (b) Frisch, M. J. et al. *Gaussian 03*, Gaussian, Inc., Wallingford CT, 2004; used by Z. Chen.

71. Gu, J.; Xie, Y.; Schaefer, H. F. *J. Chem. Phys*, AIP ID: 303736JCP Issue: 28 Sept **2007**.

Table 4.1: Zero point vibrational energy (ZPVE) un-corrected and corrected relative energies (kcal/mol) of hydride GC base pair system.

| GC base pair hydride $(GC+H)^-$ | | | GC base pair hydride with proton transferred $(GC+H)^-_{PT}$ | | |
|---|---|---|---|---|---|
| Anion Structures | Relative Energies | Relative Energies (ZPVE corrected) | Anion Structures | Relative Energies | Relative Energies (ZPVE corrected) |
| **1** GC(C6)$^-$ | 3.7 | 3.3 | **1T** G$^-$C(C6) | 0.0 | 0.0 |
| **2** GC(C4)$^-$ | 10.7 | 10.2 | **2T** G$^-$C(C4) | 5.3 | 5.8 |
| | Collapses to **3T** | | **3T** G(C6)C$^-$ | 18.4 | 18.7 |
| | Collapses to **4T** | | **4T** G$^-$C(C2) | 22.0 | 22.0 |
| **5** G(C2)$^-$C | 30.5 | 29.4 | | Collapses to **5** | |
| **6** GC(C5)$^-$ | 36.6 | 35.2 | **6T** G$^-$C(C5) | 37.1 | 35.7 |
| | Collapses to **7T** | | **7T** G(C4)C$^-$ | 36.7 | 35.9 |
| | Collapses to **8T** | | **8T** G(O6)C$^-$ | 42.3 | 40.6 |
| **9** G(C8)$^-$C | 42.7 | 40.6 | **9T** G(C8)C$^-$ | 39.7 | 38.4 |
| **10** GC(N3)$^-$ | 53.3 | 52.1 | — | — | — |
| **11** G(N7)$^-$C | 70.3 | 67.5 | **11T** G(N7)C$^-$ | 69.9 | 67.7 |
| **12** GC(O2)$^-$ | 71.8 | 69.7 | **12T** G$^-$C(O2) | 61.2 | 59.4 |
| **13** G(C5)$^-$C | 72.3 | 69.1 | **13T** G(C5)C$^-$ | 71.4 | 69.2 |
| **14** G(N3)$^-$C | 78.9 | 76.9 | | Collapses to **14** | |

Table 4.2: Dissociation energies ($D_e$), anion vertical detachment energies (VDE), and adiabatic electron affinities (AEA) of radicals for GC and hydrogenated/hydride GC species. The values inside parentheses are $D_e$ for the corresponding neutral radicals at the same level of theory (from ref. 54).

| GC base pair hydride | | | | GC base pair hydride with proton transferred | | | |
|---|---|---|---|---|---|---|---|
| Anion Structures | $D_e$ (kcal/mol) | VDE (eV) | AEA (eV) | Anion Structures | $D_e$ (kcal/mol) | VDE (eV) | AEA (eV) |
| $GC^-$ | 39.4 | 1.20 | 0.44 | $(G\text{-}H)^-(C+H)$ | 31.3 | 2.03 | 0.57 |
| **1** $GC(C6)^-$ | 40.1(27.7) | 3.07 | 2.51 | **1T** $G^-C(C6)$ | 28.9 | 3.39 | 3.18 |
| **2** $GC(C4)^-$ | 40.7(20.7) | 4.03 | 3.45 | **2T** $G^-C(C4)$ | 24.8 | 3.56 | 3.19 |
| | | | | **3T** $G(O6)C^-$ | 38.9(41.1) | 3.31 | 2.85 |
| | | | | **4T** $G^-C(C2)$ | 21.5(27.2) | 3.21 | 2.95 |
| **5** $G(C2)^-C$ | 13.5(14.8) | 2.47 | 2.04 | | | | |
| **6** $GC(C5)^-$ | 36.3(27.9) | 1.64 | 0.99 | **6T** $G^-C(C5)$ | 10.2 | 2.24 | 1.23 |
| | | | | **7T** $G(C4)C^-$ | 41.2(24.3) | 2.85 | 1.58 |
| | | | | **8T** $G(O6)C^-$ | 49.1(19.7) | 3.89 | 2.39 |
| **9** $G(C8)^-C$ | 21.9(28.1) | 0.90 | 0.57 | **9T** $G(C8)C^-$ | 45.2 | 1.64 | 0.70 |
| **10** $GC(N3)^-$ | 24.6(22.1) | 1.46 | 0.24 | | | | |
| **11** $G(N7)^-C$ | 23.7(25.9) | 0.31 | -0.16 | **11T** $G(N7)C^-$ | 46.3 | 1.22 | -0.14 |
| **12** $GC(O2)^-$ | 24.3(8.3) | 1.36 | 0.52 | **12T** $G^-C(O2)$ | 33.9 | 2.90 | 0.98 |
| **13** $G(C5)^-C$ | 12.2(23.8) | 0.44 | 0.15 | **13T** $G(C5)C^-$ | 12.2 | 1.52 | 0.19 |
| **14** $G(N3)^-C$ | 12.0(20.1) | 1.21 | 0.23 | | | | |

Figure 4.1: Optimized structures of non-proton transferred Guanine-Cytosine base pair anions ($GC^-$) and proton transferred ($(G-H)^-(C+H)$) anions. The unit of bond distance is the angstrom (Å).

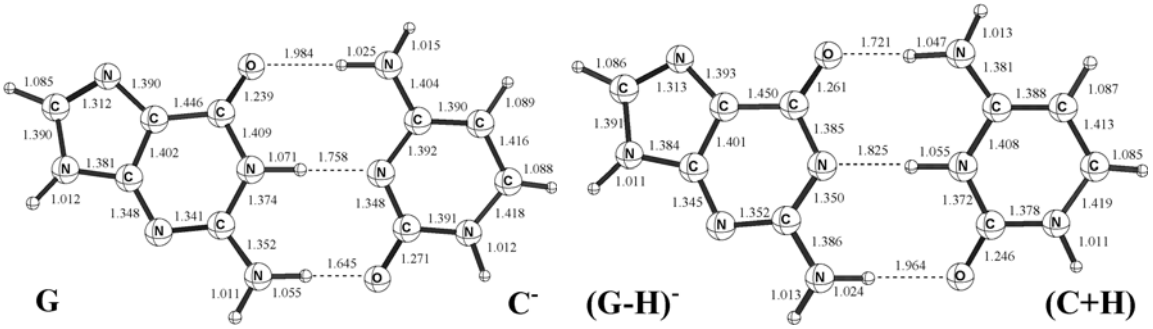

Figure 4.2: Optimized structures of GC hydrides from **1** to **4T**. A minus sign (–) shows the formal negative charge position. The unit of bond distance is the angstrom (Å).

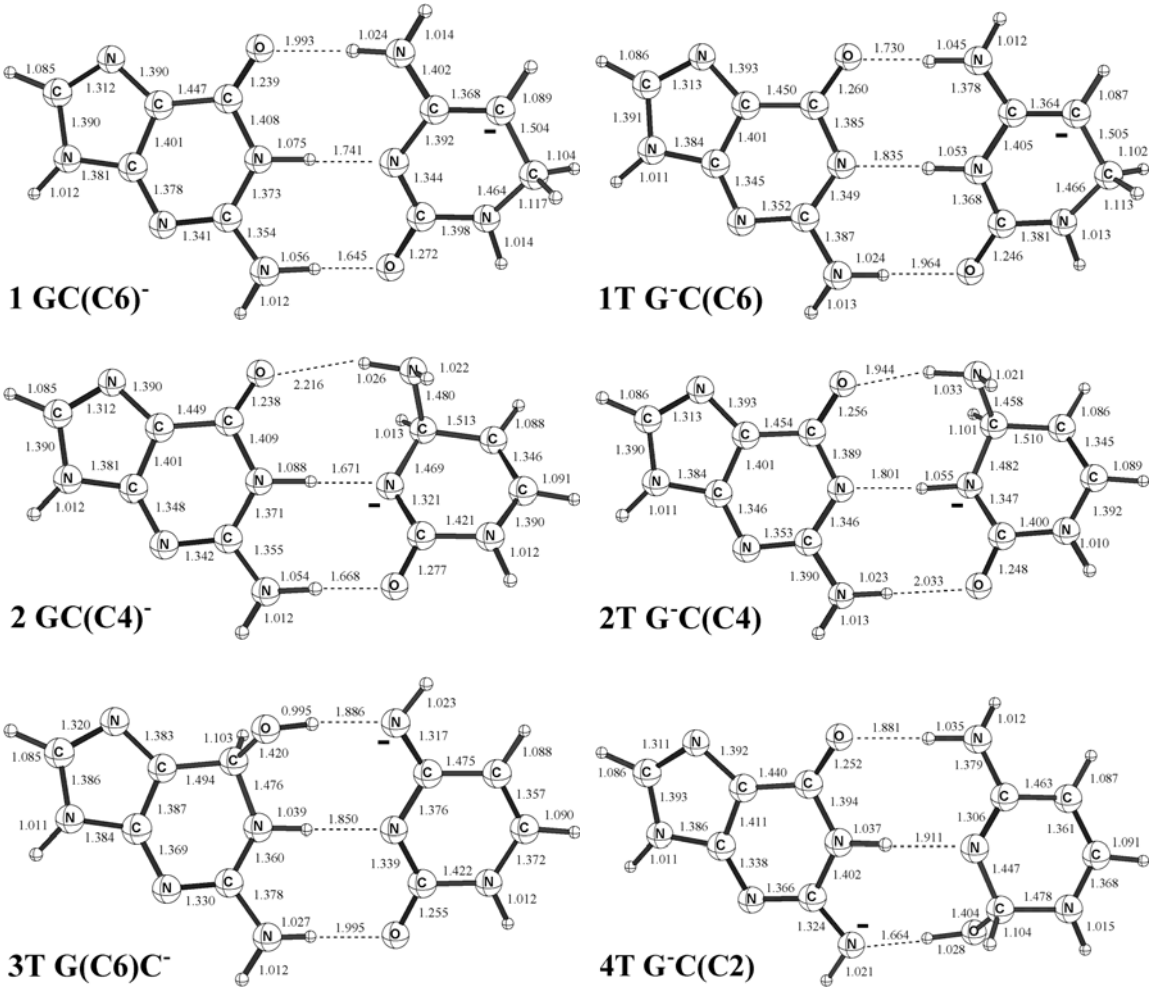

Figure 4.3: Optimized structures of GC hydrides from **5** to **9T**. A minus sign (–) shows the formal negative charge position. The unit of bond distance is the angstrom (Å).

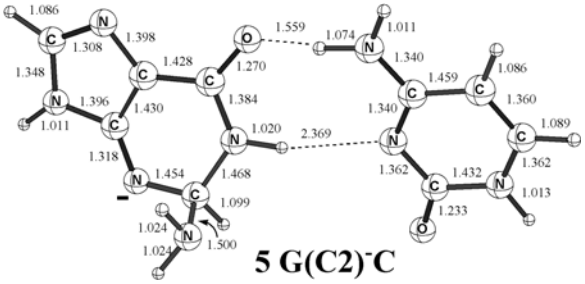

**5 G(C2)$^-$C**

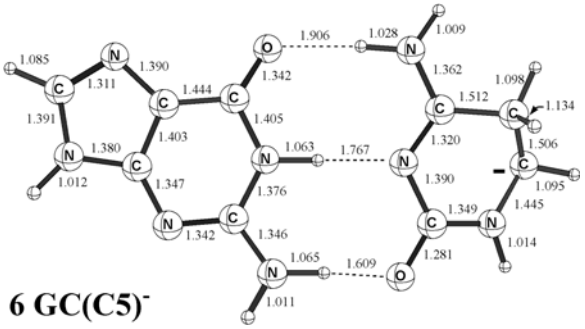

**6 GC(C5)$^-$**

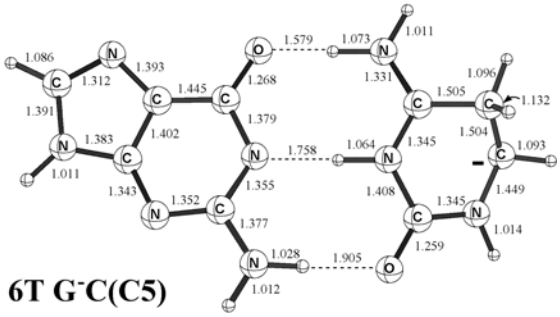

**6T G$^-$C(C5)**

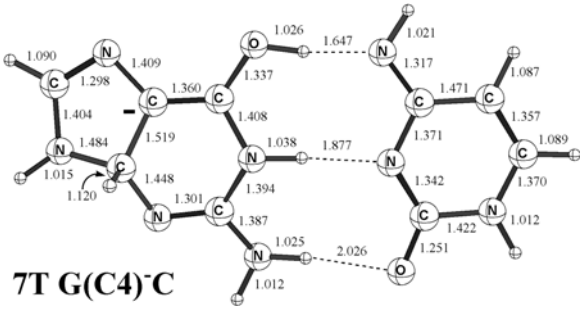

**7T G(C4)$^-$C**

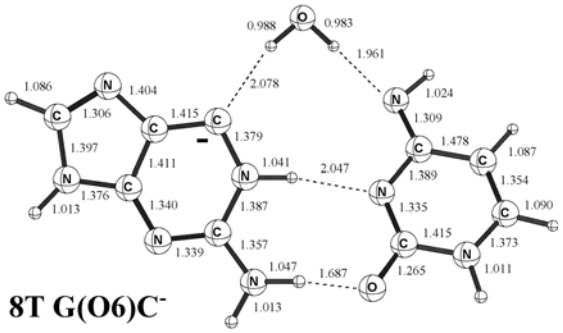

**8T G(O6)C$^-$**

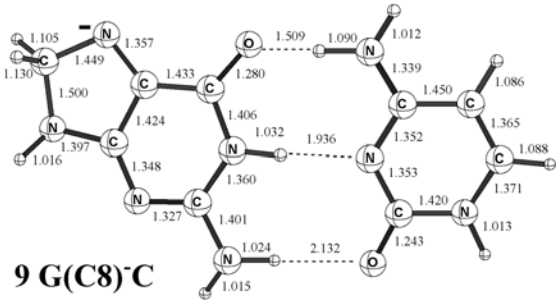

**9 G(C8)$^-$C**

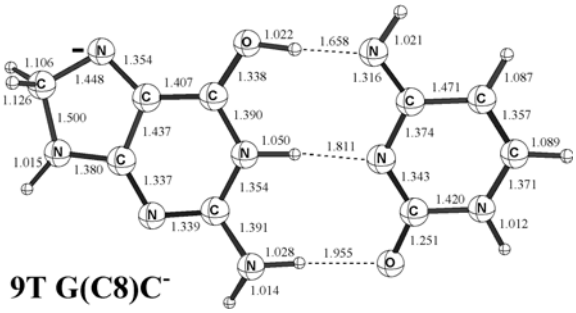

**9T G(C8)C$^-$**

Figure 4.4: Optimized structures of GC hydrides from **10** to **14T**. A minus sign (–) shows the formal negative charge position. The unit of bond distance is the angstrom (Å).

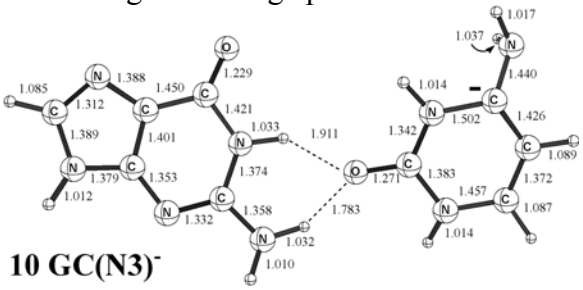

**10 GC(N3)⁻**

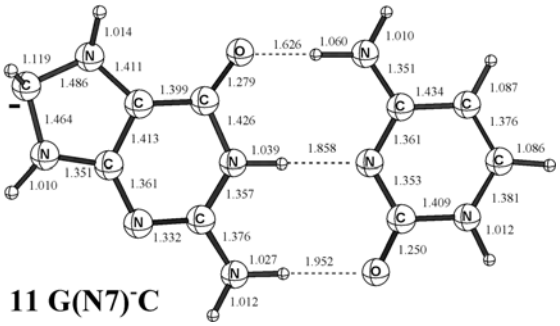

**11 G(N7)⁻C**

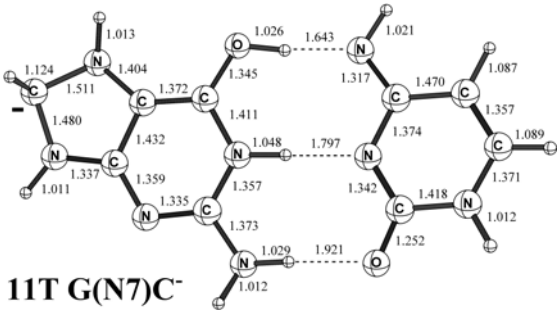

**11T G(N7)C⁻**

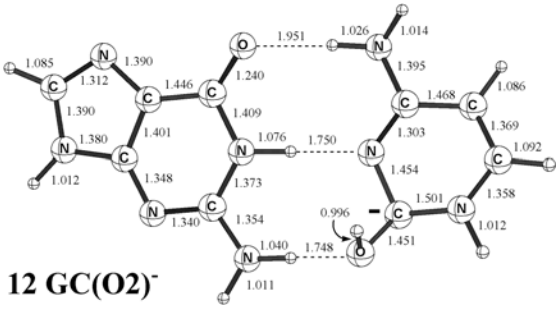

**12 GC(O2)⁻**

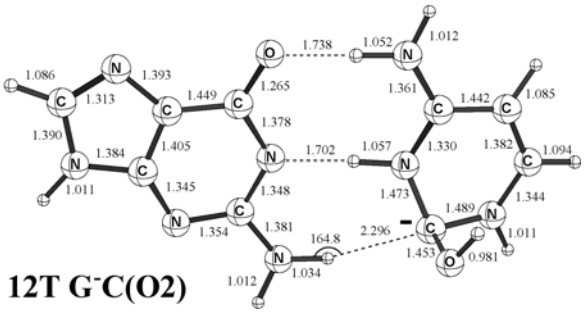

**12T G⁻C(O2)**

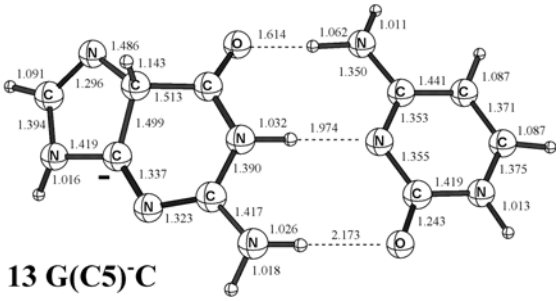

**13 G(C5)⁻C**

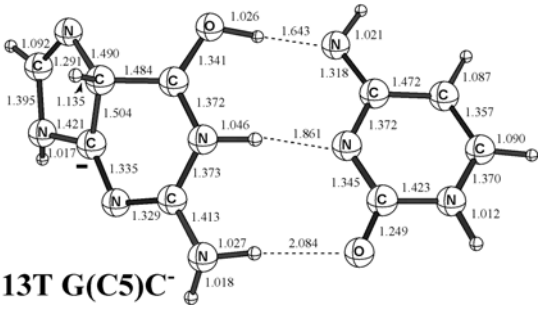

**13T G(C5)C⁻**

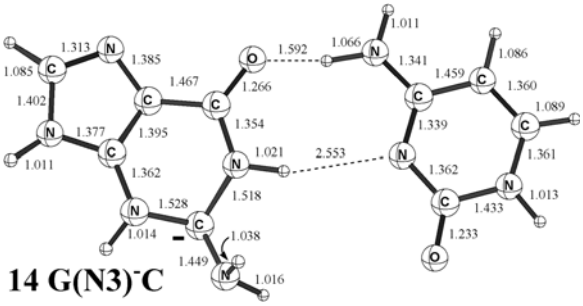

**14 G(N3)⁻C**

Figure 4.5: Optimized structures of transition states $\mathbf{1}_{TS}$ and $\mathbf{12}_{TS}$. A minus sign (–) shows the formal negative charge position. The unit of bond distance is the angstrom (Å).

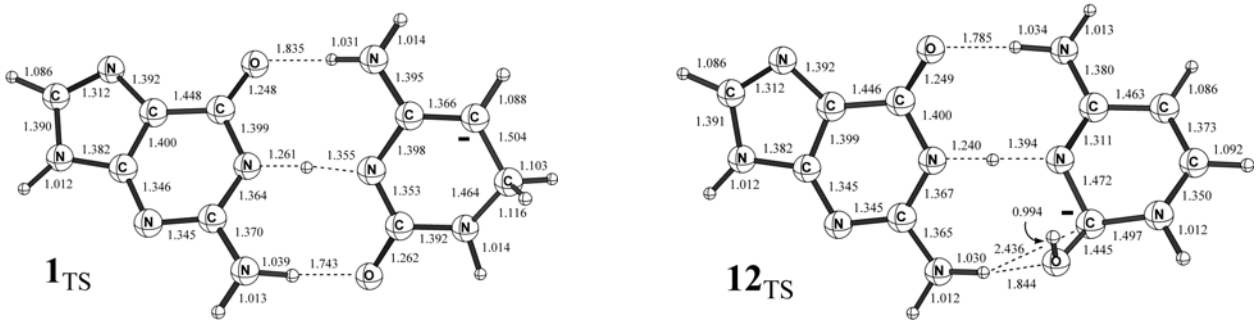


$\mathbf{1}_{TS}$ $\mathbf{12}_{TS}$

Figure 4.6: Dissociation reactions of structure **6T** and **13T**.

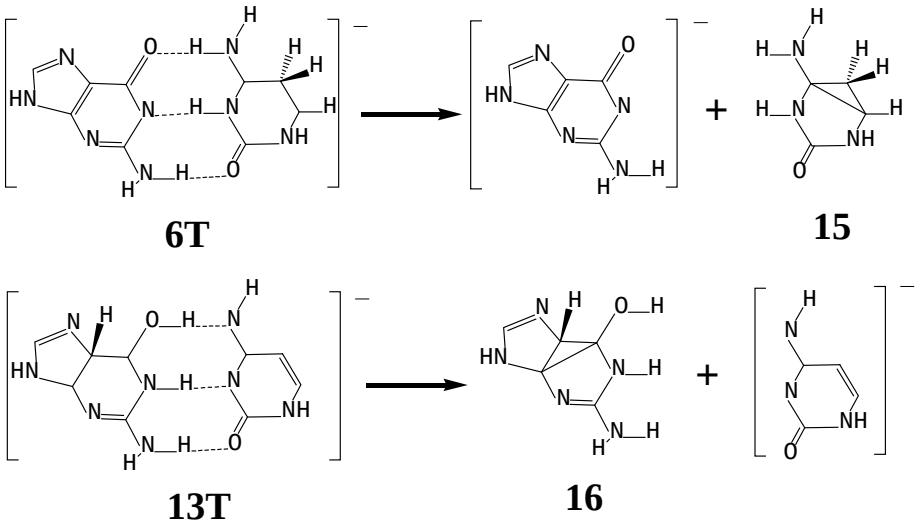

**6T** **15**

**13T** **16**

Figure 4.7: (a) Comparison of AEA predictions between the isolated (G+H) and the paired (G+H)C at the same level of theory. The AEA results for (G+H) are from reference 47. (b) Comparison of AEA predictions between the isolated (C+H) and the paired G(C+H) at the same level of theory. The AEA results for (C+H) are from reference 45.

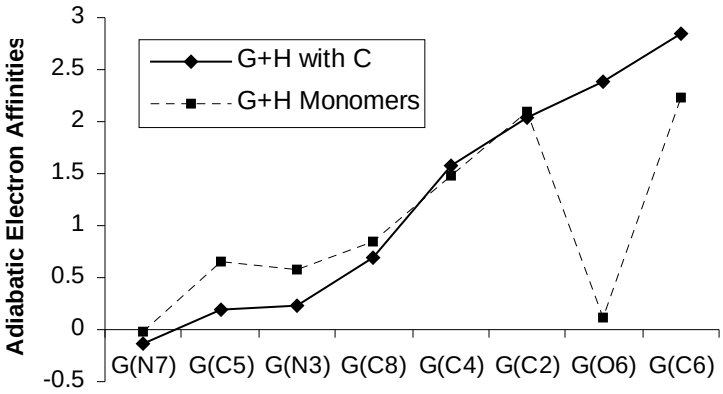


**(a) Hydrogenated Guanine Radicals**

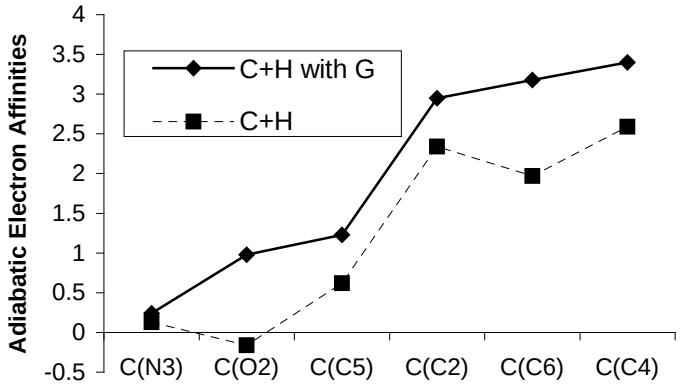


**(b) Hydrogenated Cytosine Radicals**

# CHAPTER 5

# COMPARISON OF ISOELECTRONIC HETEROMETALLIC AND HOMOMETALLIC BINUCLEAR CYCLOPENTADIENYLMETAL CARBONYLS: THE IRON-NICKEL VERSUS THE DICOBALT SYSTEMS[4]

[4] Zhang, J. D.; Chen, Z.; King, R. Bruce; Schaefer, H. F., III. To be submitted, Inorganic Chemistry.

## 5.1 ABSTRACT

The heterometallic binuclear cyclopentadienylironnickel carbonyls $Cp_2FeNi(CO)_n$ ($n$ = 3, 2, 1; Cp = $\eta^5$-$C_5H_5$) have been studied by density functional theory (BP86) for comparison with the isoelectronic homometallic dicobalt derivatives $Cp_2Co_2(CO)_n$. The FeNi tricarbonyl is shown to be the doubly bridged isomer $Cp_2Fe(CO)Ni(\mu\text{-}CO)_2$ with an Fe–Ni distance of 2.455 Å (BP86), in accord with experiment and in contrast to $Cp_2Co_2(CO)_3$ where singly and triply bridged but not doubly bridged isomers are found. The dicarbonyls $Cp_2FeNi(\mu\text{-}CO)_2$ and $Cp_2Co_2(\mu\text{-}CO)_2$ both have analogous doubly bridged structures with M=M distances around 2.35 Å, suggesting formal M=M double bonds. The monocarbonyls have analogous singly bridged axial structures $Cp_2FeNi(\mu\text{-}CO)$ and $Cp_2Co_2(\mu\text{-}CO)$ with metal-metal distances in the range 2.05 Å ($M_2$ = $Co_2$) to 2.12 Å ($M_2$ = FeNi) consistent with the formal M≡M triple bonds required for the favored 18-electron configuration. Open-shell states of $Cp_2FeNi(\mu\text{-}CO)$ are found to have even lower energies than the closed-shell structure, which indicates that the ground state of $Cp_2FeNi(\mu\text{-}CO)$ might be a high spin structure. However, the global minimum for the monocarbonyl is found to be a singlet "hot dog" perpendicular $Cp_2NiFe(CO)$ structure with a terminal CO group bonded to the iron atom. Other higher energy perpendicular structures are also found for $Cp_2FeNi(CO)_n$ ($n$ = 3, 2, 1) with terminal CO groups and bridging Cp rings.

## 5.2 INTRODUCTION

A variety of unsaturated homonuclear cyclopentadienylmetal carbonyls have been prepared since the original report[1] of $(\eta^5\text{-}Me_5C_5)_2Mo_2(CO)_4$ in 1967, including $Cp_2V_2(CO)_5$,[2] $Cp_2M_2(CO)_4$ (M = Cr,[3] Mo[4]), and $Cp_2M'_2(CO)_3$ (M' = Mn,[5] Re[6]) with formal M≡M triple bonds and $Cp_2Re_2(CO)_4$,[7] $Cp_2Fe_2(CO)_3$,[8] and $Cp_2M''_2(CO)_2$ (M'' = Co,[9] Rh[10]) with formal M=M double

bonds (Cp = $\eta^5$-$C_5H_5$ or substitution product thereof). In addition, a variety of heteronuclear cyclopentadienylmetal carbonyls are known with heteronuclear metal-metal single bonds.[11] However, no unsaturated heteronuclear cyclopentadienylmetal carbonyls have been prepared containing formal heteronuclear metal-metal multiple bonds. A possible explanation, which has yet to be explored, is that these unsaturated transition metal complexes may prefer ground state structures with open-shell high spin metal atoms rather than closed-shell structures with formal metal-metal multiple bonds.

This paper describes the use of density functional theory (DFT) to investigate possible binuclear cyclopentadienylmetal carbonyl derivatives containing either multiple iron-nickel bonds or open-shell iron-nickel pairs. The iron-nickel system was chosen for this initial study for the following reasons: (1) The "saturated" derivative $Cp_2FeNi(CO)_3$ has been known since 1960[12,13] as well as its phosphine substitution products of the type ($\eta^5$-$C_5H_5)_2FeNi(CO)_2L$ (L = $PPh_3$, $PPh_2CH_2$, $PPh(CH_3)_2$, $P(CH_3)_3$ and $P(OPh)_3$)[14,15]; (2) The isoelectronic dicobalt derivatives are well-characterized experimentally with the isolation and structural characterization of both $Cp_2Co_2(CO)_3$ [16] and $Cp_2Co_2(CO)_2$[9], with formal Co–Co single and Co=Co double bonds, respectively, as well as theoretically using DFT methods.[17] Furthermore, $Cp_2Co_2(CO)$, with a formal Co≡Co triple bond, is a probable intermediate in the formation of its dimer, namely $Cp_4Co_4(\mu_3\text{-}CO)_2$, in the pyrolysis of $Cp_3Co_3(CO)_3$.[18] We focus on the competition between high-spin structures and multiple metal-metal bonds in the formation of "unsaturated" $Cp_2FeNi(CO)$ and the isoelectronic $Cp_2Co_2(CO)$.

## 5.3 THEORETICAL METHODS

DFT is a powerful tool in computational transition metal chemistry,[19] since it provides reliable and useful predictions for the structures and electronic properties of naked transition metal dimers,[20] trimers,[21] and organometallic compounds.[22-30] Extensive experience suggests that the pure GGA functional BP86 is often more reliable for many organometallic systems than the popular hybrid functional B3LYP when compared with available experimental results.[17,31-33] In the present study, complete geometrical optimization and vibrational frequency analyses were carried out using the DFT functional BP86 with DZP basis sets. The BP86 functional combines Becke's 1988 exchange functional (B) with Perdew's 1986 correlation functional.[34,35] Both restricted and unrestricted DFT methods were used to explore the singlet and high spin ground states, respectively. Computational results using the B3LYP functional with a DZP basis set are presented as Supporting Information for comparison.

In this work, the DZP basis set used for carbon and oxygen adds one set of pure spherical harmonic d functions with orbital exponents $\alpha_d(C) = 0.75$ and $\alpha_d(O) = 0.85$ to the Huzinaga-Dunning standard contracted DZ sets[36,37] and is designated as (9s5p1d/4s2p1d). For H, a set of p polarization functions, $\alpha_p(H) = 0.75$, is added to the set to give H(4s1p/2s1p). For Fe and Ni, a loosely contracted DZP basis set, the Wachters primitive set[38] augmented by two sets of p functions and a set of d functions, contracted following Hood, Pitzer and Schaefer,[39] and designated as (14s11p6d/10s8p3d), was used.

Geometrical optimizations and vibrational frequency analyses were performed at the same level of theory discussed above. The second derivatives of the system energy with respect to the nuclear coordinates were evaluated analytically to determine vibrational frequencies. The corresponding infrared intensities were also evaluated analytically. All of the computations were

carried out with the Gaussian 94 and Gaussian 03 programs,[40] in which the Ultrafine grid consisting of 99 radical shells with 590 angular points per shell is chosen for evaluating integrals numerically in order to eliminate low magnitude imaginary frequencies caused by numerical error.[41] Both closed-shell singlet and open-shell triplet electronic states were investigated for each $Cp_2FeNi(CO)_n$ structure ($n$ = 3, 2, 1). The lowest quintet state was also investigated for the $Cp_2FeNi(CO)$ structures.

In the search for minima, low magnitude imaginary vibrational frequencies are suspicious, because the numerical integration procedures used in existing DFT methods have significant limitations. Thus, an imaginary vibrational frequency of magnitude less than $10i$ $cm^{-1}$ should imply that there is a minimum with energy identical to or close to that of the stationary point in question. In most cases we do not follow the eigenvectors corresponding to imaginary vibrational frequencies less than $10i$ $cm^{-1}$ in search of another minimum.[42]

## 5.4 RESULTS AND DISCUSSION

In general the molecular structures of singlet and higher spin electronic states of $Cp_2FeNi(CO)_n$ isomers are found for each formula to have related geometrical frameworks using the BP86 method. Information on the optimized structures (Figures 1 to 4) is reported in Tables 1 to 3 accordingly. The listed information includes the dihedral angle $\tau_{(H1\text{-}C2\text{-}H3\text{-}C4)}$ indicating the relative orientation of the two cyclopentadienyl rings. For example, a dihedral angle of 0° indicates an eclipsed structure and an angle of 36° indicates a staggered structure. Singlet, triplet, and quintet electronic states are designated by **S**, **T**, and **Q**, respectively.

### 5.4.1 STRUCTURES AND ENERGETICS

#### 5.4.1.1 $Cp_2FeNi(CO)_3$

The beautiful coaxial structure **3-1** with two bridging CO groups and one terminal CO group bonded to the iron atom is found to be the global minimum for $Cp_2FeNi(CO)_3$ (Figure 5.1 and Table 5.1). The Fe–Ni distance in **3-1** of 2.46 Å is consistent with a single bond. No experimental crystal structure on the known $Cp_2FeNi(CO)_3$ is available for comparison with these theoretical results. However, this calculated Fe–Ni distance for **3-1** is consistent with the Fe–Ni distances in the range 2.43 to 2.56 Å found[43] by X-ray crystallography in the $NiFe_3C_2$ octahedron of $CpNiFe_3(CO)_7(\mu\text{-}PPh_2)(\mu_4,\eta^2\text{-}HC{\equiv}CPr^i)$. Thus the FeNi bond in **3-1** may be considered to be a formal single bond.

The theoretical infrared active ν(CO) frequencies for structure **3-1S** at 1815 and 1984 $cm^{-1}$ agree well with the experimental[44] values of 1816 and 1998 $cm^{-1}$ and correspond to the antisymmetrical stretching mode of the two bridging CO groups and the stretching mode of the terminal CO group, respectively. The symmetrical stretching mode of the two bridging CO groups is predicted at 1845 $cm^{-1}$, with an infrared intensity too weak to be observed.

Structures of $Cp_2FeNi(CO)_3$ were also investigated in which the Fe-Ni bond is parallel to the Cp rings so that each metal atom is bonded to both Cp rings. However, such structures were found to lie more than 35 kcal/mol above **3-1**.

#### 5.4.1.2 $Cp_2FeNi(CO)_2$

Two optimized structures (**2-1** and **2-2** in Figure 5.2) are predicted for $Cp_2FeNi(CO)_2$. Structure **2-1** is a coaxial structure, $Cp_2FeNi(\mu\text{-}CO)_2$, with terminal $\eta^5$-Cp rings and two bridging CO ligands. Structure **2-2** is a perpendicular structure with two bridging Cp rings and two

terminal CO ligands, namely $(\mu\text{-}Cp)_2FeNi(CO)$. This structure resembles a "hot dog" in which the "buns" are the Cp rings and the OCNiFeCO chain is the "meat." The Fe-Ni distances are longer in the triplet structures of $Cp_2FeNi(CO)_2$ than in the singlet isomers. The Fe–CO distances are generally smaller than the Ni–CO distances in all structures. This is consistent with the previous observation of shorter Fe-CO distances in $Fe(CO)_5$, namely 1.807 Å (axial) and 1.827 Å (equatorial),[45] than in $Ni(CO)_4$, namely 1.838 Å.[46] The energies of the "hot dog" singlet and triplet structures **2-2** are significantly higher than those of structure **2-1** (27.0 and 38.8 kcal/mol for singlet and triplet states, respectively). The global minimum for $Cp_2FeNi(CO)_2$ was found to be the singlet structure **2-1S**. The triplet structure **2-1T** is predicted to lie 5.5 kcal/mol higher than **2-1S**.

5.4.1.3 $Cp_2FeNi(CO)$

Three possible structures for $Cp_2FeNi(CO)$ (Figure 5.3) have been found. Structure **1-1** is a coaxial dimetallocene $Cp_2FeNi(\mu\text{-}CO)$ with a bridging CO group. The other two structures **1-2** and **1-3** have the metal-metal bond axis approximately perpendicular to the Cp ring axes (Figure 5.3) forming a "hot dog" shape perpendicular structure $(\mu\text{-}Cp)_2FeNi(CO)$ with bridging Cp ligands and a terminal CO group. The triplet and quintet electronic states of each structure have also been investigated, since the monocarbonyl complex represents a highly unsaturated molecular structure. Structure **1-2S** has $C_s$ symmetry with the CO group bonded to iron, while structure **1-3S** has no symmetry with the CO group bonded to nickel. The energetic trend for each structure is quite different with respect to the singlet, triplet, and quintet electronic states. Thus for structure **1-1**, the quintet state has the lowest total energy. However, the singlet and triplet states are of the lowest energy for the two perpendicular structures **1-2** and **1-3**,

respectively. The global minimum for all $Cp_2FeNi(CO)$ species is the singlet perpendicular structure **1-2S** with the CO group terminally bonded to the iron atom.

The Ni-Fe bond distances in the $Cp_2FeNi(CO)$ isomers are predicted to be longer in the high spin states than in the singlet states except for **1-2**. For example, the Fe-Ni distances in **1-1** follow a trend **1-1Q** (2.267 Å**) > 1-1T** (2.217 Å) > **1-1S** (2.123 Å). The same trend is found for isomer **1-3**, but not for **1-2** (Table 5.3). The orientation of the two Cp rings is quite different in the different electronic states for geometry **1-1**. In **1-1S**, the two rings are nearly staggered ($\tau_{(H1\text{-}C2\text{-}H3\text{-}C4)}$ is 32.6°). However, in **1-1T** and **1-1Q**, the two rings prefer only partially staggered conformations ($\tau_{(H1\text{-}C2\text{-}H3\text{-}C4)}$ is 16.6° and 11.9°, respectively). A very small imaginary frequency of 2*i* for **1-1T** arises from numerical integration errors.

In the perpendicular "hot dog" structures **1-2** and **1-3**, the Ni-Fe distances are significantly longer then those in the coaxial structure **1-1** for both the singlet and triplet isomers. Moreover, the terminal CO group binds more tightly to iron than to nickel as reflected implicitly by the shorter Fe-CO distance in **1-2** than the Ni-CO distance in **1-3** in both the singlet and triplet states. A similar trend is noted in comparing the first metal carbonyl dissociation energies of 41 ± 1 kcal/mole[47,48] in $Fe(CO)_5$ versus 25 ± 2 kcal/mole[49] in $Ni(CO)_4$.

The **1-2Q** quintet state structure is special (Figure 5.4) with a non-linear Ni-Fe-CO unit (121.8°) in contrast to **1-2S** and **1-2T** with linear Ni-Fe-CO units. Structure **1-2Q** is also anomalous by having a predicted Ni-Fe distance shorter rather than that in the corresponding singlet **1-2S**.

### 5.4.2 DISSOCIATION ENERGIES

The CO dissociation energies for the $Cp_2FeNi(CO)_n$ complexes are listed in Table 5.4 based on the global minima and with the $Cp_2FeNi(CO)_{n-1}$ product in the same spin state as the reactant $Cp_2FeNi(CO)_n$. The positive CO dissociation energies indicate these reactions to be endothermic. Furthermore, the triplet isomers are found to have lower CO dissociation energies than the corresponding singlet isomers.

#### 5.4.2.1 $Cp_2FeNi(CO)_3$ VERSUS $Cp_2Co_2(CO)_3$

The asymmetry of the dimetal unit in $Cp_2FeNi(CO)_3$ leads to a different structure than that found for the isoelectronic $Cp_2Co_2(CO)_3$ in order for both metal atoms to have the favored 18-electron configurations with a formal metal-metal single bond (Figure 5.5). Thus for $Cp_2Co_2(CO)_3$ the experimentally known structure is $Cp_2Co_2(CO)_2(\mu\text{-}CO)$ with a single bridging CO group. However, an alternative structure $Cp_2Co_2(\mu\text{-}CO)_3$ with three bridging CO groups is predicted to have a similar energy. For the isoelectronic $Cp_2FeNi(CO)_3$ the global minimum is $Cp_2Fe(CO)Ni(\mu\text{-}CO)_2$ with two bridging CO groups rather than one or three bridging CO groups. The third CO group in this $Cp_2Fe(CO)Ni(\mu\text{-}CO)_2$ structure is a terminal CO group bonded to the iron atom, so that both the iron and nickel atoms have equivalent electronic configurations, namely the favored 18-electron configuration. Thus the asymmetry of the metal-metal bond in $Cp_2FeNi(CO)_3$ relative to $Cp_2Co_2(CO)_3$ leads to a redistribution of the metal carbonyl groups.

The metal-metal bond distances in $Cp_2MM'(CO)_3$ derivatives decrease monotonically as the number of bridging CO groups increases in the series $Cp_2Co_2(CO)_2(\mu\text{-}CO) > Cp_2Fe(CO)Ni(\mu\text{-}CO)_2 > Cp_2Co_2(\mu\text{-}CO)_3$ irrespective of whether the dimetal unit is $Co_2$ or FeNi with BP86 values of 2.506 Å, 2.455 Å, and 2.352 Å, respectively. The available information

does not provide information as to whether the metal-metal interactions in these binuclear compounds are direct interactions or occur through the carbonyl bridges. Even for the less complicated homoleptic analogue $Fe_2(CO)_9$, detailed studies[50] do not provide clear and definitive insight into this question.

#### 5.4.2.2 $Cp_2FeNi(CO)_2$ VERSUS $Cp_2Co_2(CO)_2$

The global minima for the isoelectronic dicarbonyls $Cp_2Co_2(\mu\text{-}CO)_2$ and $Cp_2FeNi(\mu\text{-}CO)_2$ are coaxial structures with the same arrangements of their two CO groups, namely as two bridging groups. The metal-metal distances (2.346 Å for $Cp_2Co_2(\mu\text{-}CO)_2$ and 2.353 Å for $Cp_2FeNi(\mu\text{-}CO)_2$) are essentially identical and enough less than the 2.455 Å Fe–Ni doubly bridged single bond distance in $Cp_2Fe(CO)Ni(\mu\text{-}CO)_2$ to be regarded as the M=M double bonds needed to give both metal atoms the favored 18-electron configurations. The perpendicular "hot dog" isomers $(\mu\text{-}Cp)_2M_2(CO)_2$ ($M_2 = Co_2$ or FeNi) have essentially similar structures with metal-metal distances (BP86) of 2.427 Å for $(\mu\text{-}Cp)_2Co_2(CO)_2$ and 2.468 Å for $(\mu\text{-}Cp)_2FeNi_2(CO)_2$.

#### 5.4.2.3 $Cp_2FeNi(CO)$ VERSUS $Cp_2Co_2(CO)$

The isoelectronic species $Cp_2Co_2(CO)$ was reinvestigated for comparison with $Cp_2FeNi(CO)$ using the same level of theory. The singlet states of $Cp_2Co_2(CO)$ were studied in the previous work using a coarser integration grid (75,302) than the (99,590) integration grid used in this work; this leads to some significant imaginary frequencies.[17] Our new results on $Cp_2Co_2(CO)$ including not only recomputed singlet electronic states but also the first investigations of triplet and quintet electronic states are listed at Table 5.5 and Figure 5.6. The energetic trend of different electronic states for both the coaxial dimetallocene $Cp_2Co_2(\mu\text{-}CO)$

**Co-1** and the perpendicular dimetallocene $(\mu\text{-Cp})_2Co_2(CO)$ **Co-2** is consistent with singlet < triplet < quintet. The isomer **Co-1S** is again found to be a global minimum. The metal-metal distances are longer in the perpendicular structure than those in the coaxial structure of the homometallic $Cp_2Co_2(CO)$, as found here for the heterometallic $Cp_2FeNi(CO)$.

Plots of the spin densities of all open-shell species of the $Cp_2FeNi(CO)$ and $Cp_2Co_2(CO)$ isomers are displayed in Table 5.6. In the $Cp_2FeNi(CO)$ triplet states, the spin densities are almost exclusively concentrated on the iron atom, consistent with a 16-electron configuration for the iron atom and an 18-electron configuration for the nickel atom.. Even in the quintet states, the spin density is still concentrated largely on iron. However, in the homometallic binuclear $Cp_2Co_2(CO)$ structures, the unpaired electron density is evenly distributed on each cobalt atom. None of the triplet or quintet isomers of $Cp_2FeNi(CO)_n$ ($n$ = 3, 2, 1) or $Cp_2Co_2(CO)$ exhibits any significant spin contamination as indicated by approximate $<S^2>$ values close to the ideal values of 2 and 6 for the triplets and quintets, respectively.

The isoelectronic pair of monocarbonyls $Cp_2Co_2(CO)$ and $Cp_2FeNi(CO)$ have qualitatively similar structures. The CO group in the coaxial isomers (e.g., **1-1**) bridges the metal-metal bond, which is short enough by BP86 (2.050 Å for $Cp_2Co(\mu\text{-CO})$ and 2.123 Å for $Cp_2FeNi(\mu\text{-CO})$) to be considered to be the triple bond required to give both metal atoms the favored 18-electron configurations for the singlet state. Compared to the energetic trend of singlet < triplet < quintet for the $Cp_2Co_2(\mu\text{-CO})$ coaxial isomer (**Co-1**), a reversed energetic trend is found for the $Cp_2FeNi(\mu\text{-CO})$ coaxial isomer (**1-1**), in which a quintet state has relatively the lowest energy. This indicates that for heterometallic complexes, a high spin state with unbalanced density distribution between two metals (Table 5.6) might be favored instead of a multiple metal-metal bond. The isoelectronic set of three perpendicular complexes $Cp_2Co_2(CO)$,

$Cp_2Fe(CO)Ni$ (**1-2** in Figure 5.3) and $Cp_2FeNi(CO)$ (**1-3** in Figure 5.3) all have essentially the same structures with metal-metal distances in the narrow range 2.29 – 2.33 Å.

## 5.5 CONCLUSION

A coaxial structure $Cp_2Fe(CO)Ni(\mu\text{-}CO)_2$ with two bridging carbonyls and one terminal carbonyl has been found to be the global minimum for the tricarbonyl $Cp_2FeNi(CO)_3$. Compared with $Cp_2FeNi(CO)_3$, the isoelectronic $Cp_2Co_2(CO)_3$ has two coaxial minima with different structures, namely $Cp_2Co_2(CO)_2(\mu\text{-}CO)$ with a single bridging carbonyl and $Cp_2Co_2(\mu\text{-}CO)_3$ with all three carbonyls in bridging positions. The isoelectronic pair of dicarbonyls $Cp_2FeNi(CO)_2$ and $Cp_2Co_2(CO)_2$ have essentially the same structures for both coaxial and perpendicular isomers. The coaxial structure of the monocarbonyl $Cp_2FeNi(CO)$ prefers an open-shell high spin state whereas the isoelectronic $Cp_2Co_2(CO)$ prefers a closed shell state with a Co≡Co triple bond. However, the global minimum for the monocarbonyl is a singlet perpendicular $Cp_2FeNi(CO)$ structure with a terminal CO group bonded to the iron atom.

## 5.6 .ACKNOWLEDGMENTS

We are grateful to the National Science Foundation for support of this work under grants CHE-0209857 and CHE-0451445. J. D. Zhang thanks Dr. Jiande Gu for help in preparing spin density plots.

## 5.7 LITERATURE REFERENCES

1. King, R.B.; Bisnette, M.B. *J. Organometal. Chem.* **1967**, *8*, 287.
2. Cotton, F. A.; Kruczynski, L. *J. Organometal. Chem.* **1978**, *160*, 93.

3. Curtis, M. D.; Butler, W. M. *J. Organometal. Chem.* **1978**, *155*, 131.
4. Klingler, R. J.; Butler, W. M.; Curtis, M. D. *J. Am. Chem. Soc.* **1978**, *100*, 5034.
5. Bernal, I.; Korp, J. D.; Herrmann, W. A.; Serrano, R. *Chem. Ber.* **1984**, *117*, 434.
6. Hoyano, J. K.; Graham, W. A. G. *Chem. Comm.* **1982**, 27.
7. Casey, C. P.; Sakaba, H.; Hazin, P. N.; Powell, D. R. *J. Am. Chem. Soc.* **1991**, *113*, 8165.
8. Blaha, J. P.; Bursten, B. E.; Dewan, J. C.; Frankel, R. B.; Randolph, C. L.; Wilson, B. A.; Wrighton, M. S. *J. Am. Chem. Soc.* **1985**, *107*, 4561.
9. Bailey, W. I. Jr.; Collins, D. M.; Cotton, F. A.; Baldwin, J. C. *J. Organometal. Chem.* **1979**, *165*, 373.
10. Green, M.; Hankey, D. R.; Howard, J. A. K.; Louca, P.; Stone, F. G. A. *Chem. Comm.* **1983**, 757.
11. Madach, T.; Vahrenkamp, H. *Chem. Ber.* **1980**, *113*, 2675.
12. Tilney-Bassett, J. F. *Proc. Chem. Soc.* **1960**, 419.
13. Tilney-Bassett, J. F. *J. Chem. Soc.* **1963**, 4784.
14. Yasufuku, K.; Yamazaki, H. *J. Organometal. Chem.* **1971**, *28*, 415.
15. Yasufuku, K.; Yamazaki, H. *J. Organometal. Chem.* **1972**, *38*, 367.
16. Anderson, F. R.; Wrighton, M. S. *Inorg. Chem.* **1986**, *25*, 112.
17. Wang, H.; Xie, Y.; King, R. B.; Schaefer, H. F. *J. Am. Chem. Soc.* **2005**, *127*, 11646.
18. Vollhardt, K. P. C.; Bercaw, J. E.; Bergmann, R. G. *J. Organometal. Chem.* **1975**, *97*, 283.
19. Davidson, E. R. (guest editor) Chem. Rev. Special issue on Computational Transition Metal Chemistry, February, **2000**.
20. Barden, C. J.; Rienstra-Kiracofe, J. C.; Schaefer, H. F. *J. Chem. Phys.* **2000**, *113*, 690.

21. Papas, B. N.; Schaefer, H. F. *J. Chem. Phys.* **2005**, *123*, 074321.

22. Ehlers, A. W.; Frenking, G. *J. Am. Chem. Soc.* **1994**, *116*, 1514.

23. Delley, B.; Wrinn, M.; Lüthi, H. P. *J. Chem. Phys*. **1994**, *100*, 5785.

24. Li, J.; Schreckenbach, G.; Ziegler, T. *J. Am. Chem. Soc.* **1995**, *117*, 486.

25. Jonas, V.; Thiel, W. *J. Chem. Phys.* **1995**, *102*, 8474.

26. Barckholtz, T. A.; Bursten, B. E. *J. Am. Chem. Soc.* **1998**, *120*, 1926.

27. Niu, S.; Hall, M. B. *Chem. Rev.* **2000**, *100*, 353.

28. Macchi, P.; Sironi, A. *Coord. Chem. Rev.* **2003**, *238*, 383.

29. Carreon, J.-L.; Harvey, J. N. *Phys. Chem. Chem. Phys.* **2006**, *8*, 93.

30. Bühl, M.; Kabrede, H. *J. Chem. Theory Comput.* **2006**, *2*, 1282.

31. Furche, F.; Perdew, J. P. *J. Chem. Phys.* **2006**, *124*, 044103.

32. Feng, X.; Gu, J.; Xie, Y.; King, R. B.; Schaefer, H. F. *J. Chem. Theory Comput.* **2007**, *3*, 1580.

33. Wang, H.Y.; Xie, Y.; King, R.B.; Schaefer, H. F. *J. Am. Chem. Soc.* **2006**, *128*, 11376.

34. Becke, A. D. *Phys. Rev. A* **1988**, *38*, 3098.

35. Perdew, J. P. *Phys. Rev. B* **1986**, *33*, 8822.

36. Dunning, T. H. *J. Chem. Phys*. **1970**, *53*, 2823.

37. Huzinaga, S. *J. Chem. Phys*. **1965**, *42*, 1293.

38. Wachters A. J. H. *J. Chem. Phys*. **1970**, *52*, 1033.

39. Hood, D. M.; Pitzer, R. M.; Schaefer, H. F. *J. Chem. Phys*. **1979**, *71*, 705.

40. (a) Frisch, M. J. et al. *Gaussian 94,* Revision B.3; Gaussian Inc.: Pittsburgh, PA, 1995. Used by J. D. Zhang. (b) Frisch, M. J. et al. *Gaussian 03*, Gaussian, Inc., Wallingford CT, 2004. Used by Z. Chen.

41. Papas, B. N.; Schaefer, H. F. *J. Mol. Struct. THEOCHEM* **2006**, *768*, 175.

42. Xie, Y.; Schaefer, H. F.; King, R. B. *J. Am. Chem. Soc.* **2000**, *122*, 8746.

43. Sappa, E.; Belletti, D.; Tiripicchio, A.; Tiripicchio Camellini, M. *J. Organometal. Chem.* **1989**, *359*, 419.

44. McArdle, P.; Manning, A. R. *J. Chem. Soc. (A)* **1971**, 717.

45. Lüthi, H. P.; Siegbahn, P. E. M.; Almlöf, J. *J. Phys. Chem.* **1985**, *89*, 2156.

46. Hedberg, L.; Iijima, T.; Hedberg, K. *J. Chem. Phys.* **1979**, *70*, 3224.

47. Lewis, K. E.; Golden, D. M.; Smith, G. P. *J. Am. Chem. Soc.* **1984**, 106, 3905.

48. Huq, R.; Pöe, A. J.; Chawla, S. *Inorg. Chim. Acta* **1979**, *38*, 121.

49. Stevens, A. E.; Feigerle, C. S.; Lineberger, W. C. *J. Am. Chem. Soc.* **1982**, *104*, 5026.

50. Rosa, A.; Baerends, E. J. *New J. Chem.* **1991**, *125*, 815.

Table 5.1: Bond distances (in Å), dihedral angles $\tau_{(H1\text{-}C2\text{-}H3\text{-}C4)}$ (in degrees), relative energies ΔE (in kcal/mol), approximate $<S^2>$ values, and ν(CO) frequencies (in $cm^{-1}$) for the $Cp_2FeNi(CO)_3$ isomers at the BP86/DZP level of theory. Infrared intensities in parentheses are in km/mol.

| | **3-1S** | **3-1T** |
|---|---|---|
| Symmetry | $C_1$ | $C_1$ |
| Fe-Ni | 2.455 | 2.459 |
| Fe-CO (bridge) | 1.911 | 1.850 |
| | 1.911 | 1.850 |
| Fe-CO (non-bridge) | 1.755 | 1.850 |
| Ni-CO | 1.877 | 1.950 |
| | 1.877 | 1.950 |
| $\tau_{(H1\text{-}C2\text{-}C3\text{-}H4)}$ | 32.2 | -3.1 |
| ΔE | 0.0 | 26.3 |
| $<S^2>$ | 0.00 | 2.04 |
| ν(C-O) | 1815 (842)<br>1845 (10)<br>1984 (780) | 1813 (866)<br>1835 (10)<br>1965 (809) |
| Imaginary Frequency | none | none |

Table 5.2: Bond distances (in Å), relative energies ΔE (in kcal/mol), approximate $<S^2>$ values, and ν(CO) frequencies (in $cm^{-1}$) for the $Cp_2FeNi(CO)_2$ isomers at the BP86/DZP level of theory. Infrared intensities in parentheses are in km/mol.

| | **2-1S** | **2-1T** | **2-2S** | **2-2T** |
|---|---|---|---|---|
| Symmetry | $C_s$ | $C_1$ | $C_s$ | $C_s$ |
| Fe-Ni | 2.353 | 2.389 | 2.475 | 2.555 |
| Fe-CO (bridge) | 1.831<br>1.830 | 1.847<br>1.848 | 1.732 | 1.748 |
| Ni-CO (bridge) | 1.948<br>1.943 | 1.926<br>1.927 | 1.805 | 1.783 |
| ΔE | 0.0 | 5.5 | 27.0 | 38.8 |
| $<S^2>$ | 0.00 | 2.05 | 0.00 | 2.06 |
| ν(CO) | 1811 (944)<br>1836 (18) | 1803 (911)<br>1838 (9) | 1921 (1062)<br>1979 (874) | 1928 (1149)<br>1982 (784) |
| Imaginary Frequencies | none | none | none | none |

Table 5.3: Bond distances (in Å), bond angles $\theta_{(Fe\text{-}C5\text{-}O)}$ (in degrees), dihedral angles $\tau_{(H1\text{-}C2\text{-}H3\text{-}C4)}$ (in degrees), relative energies ΔE (in kcal/mol), approximate $<S^2>$ values, and ν(CO) frequencies (in $cm^{-1}$) for the $Cp_2FeNi(CO)$ isomers at the BP86/DZP level of theory. Infrared intensities in parentheses are in km/mol.

| | **1-1S** | **1-1T** | **1-1Q** | **1-2S** | **1-2T** | **1-2Q** | **1-3S** | **1-3T** | **1-3Q** |
|---|---|---|---|---|---|---|---|---|---|
| Symmetry | $C_1$ | $C_1$ | $C_1$ | $C_s$ | $C_1$ | $C_1$ | $C_1$ | $C_1$ | $C_1$ |
| Fe-Ni | 2.123 | 2.217 | 2.267 | 2.323 | 2.364 | 2.310 | 2.325 | 2.464 | 2.473 |
| Fe-CO | 1.868 | 1.917 | 2.104 | 1.731 | 1.744 | 1.850 | | | |
| Ni-CO | 1.923 | 1.858 | 1.764 | | | | 1.805 | 1.800 | 1.773 |
| $\theta_{(Fe\text{-}C5\text{-}O)}$ | 150.4 | 145.7 | 131.2 | 179.2 | 179.4 | 172.0 | 179.6 | 179.2 | 175.6 |
| $\tau_{(H1\text{-}C2\text{-}C3\text{-}H4)}$ | 32.6 | 16.6 | 11.9 | 0.0 | 36.1 | -23.1 | 0.0 | 0.0 | -15.7 |
| ΔE | 4.6 | 4.1 | 2.1 | 0.0 | 11.3 | 26.8 | 25.1 | 11.9 | 15.2 |
| $<S^2>$ | 0.00 | 2.26 | 6.04 | 0.00 | 2.05 | 6.07 | 0.00 | 2.05 | 6.03 |
| ν(CO) | 1856 (561) | 1829 (590) | 1867 (602) | 1918 (855) | 1920 (891) | 1921 (1115) | 1975 (1014) | 1963 (1101) | 1965 (1211) |
| Imaginary Frequecy | none | 2*i* | none | none | none | none | none | none | none |

Table 5.4: Dissociation energies (kcal/mol) for the successive removal of carbonyl groups from $Cp_2FeNi(CO)_3$.

| | B3LYP | BP86 |
|---|---|---|
| $Cp_2FeNi(CO)_3$ (**3-1S**) $\rightarrow Cp_2FeNi(CO)_2$ (**2-1S**) + CO | 34.8 | 40.6 |
| $Cp_2FeNi(CO)_3$ (**3-1T**) $\rightarrow Cp_2FeNi(CO)_2$ (**2-1T**) + CO | 9.5 | 19.8 |
| $Cp_2FeNi(CO)_2$ (**2-1S**) $\rightarrow Cp_2FeNi(CO)$ (**1-1S**) + CO | 49.5 | 65.3 |
| $Cp_2FeNi(CO)_2$ (**2-1T**) $\rightarrow Cp_2FeNi(CO)$ (**1-1T**) + CO | 36.2 | 59.3 |

Table 5.5: Bond distances (in Å), approximate $<S^2>$ values, and ν(CO) frequencies (in $cm^{-1}$) for the $Cp_2Co_2(CO)$ isomers at the BP86/DZP level of theory. Infrared intensities in parentheses are in km/mol.

| | **Co-1S** | **Co-1T** | **Co-1Q** | **Co-2S** | **Co-2T** | **Co-2Q** |
|---|---|---|---|---|---|---|
| Symmetry | $C_{2v}$ | $C_1$ | $C_1$ | $C_s$ | $C_1$ | $C_1$ |
| Co-Co | 2.050 | 2.144 | 2.242 | 2.295 | 2.384 | 2.355 |
| Co-CO | 1.905 | 1.831 | 1.921 | 1.741 | 1.737 | 1.776 |
| | 1.905 | 1.953 | 1.868 | | | |
| ΔE | 0.0 | 7.3 | 9.6 | 6.3 | 20.0 | 28.3 |
| $<S^2>$ | 0.00 | 2.06 | 6.04 | 0.00 | 2.04 | 6.05 |
| ν(CO) | 1870 (583) | 1840 (593) | 1837 (574) | 1939 (933) | 1936 (1000) | 1932 (1241) |
| Imaginary Frequecy | no | no | no | no | no | no |

Table 5.6: The spin densities of triplet and quintet states of $Cp_2Co_2(CO)$ and isoelectronic species $Cp_2FeNi(CO)$ at the BP86/DZP level. Positive and negative values are represented by purple and green, respectively. Atoms are identified by colors as: O (red), Ni (yellow), Fe (brown), Co (blue), C (gray) and H (white).

| **Compound** | **Triplet** | **Quintet** |
|---|---|---|
| $Cp_2FeNi(\mu\text{-}CO)$ **1-1** |  | 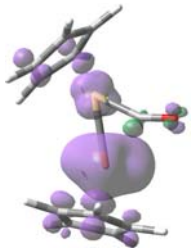 |
| $Cp_2NiFe(CO)$ **1-2** | 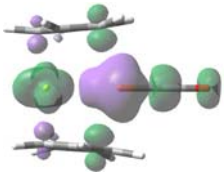 | 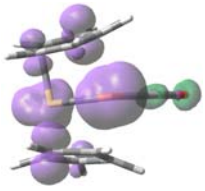 |
| $Cp_2FeNi(CO)$ **1-3** | 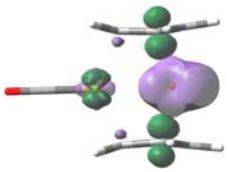 | 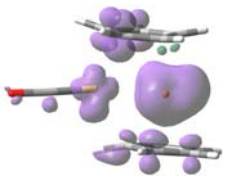 |
| $Cp_2Co_2(\mu\text{-}CO)$ **Co-1** | 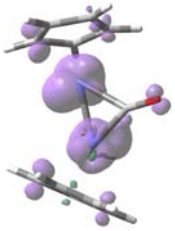 | 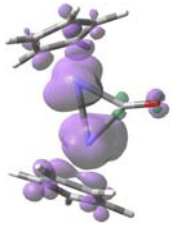 |
| $Cp_2Co_2(CO)$ **Co-2** | 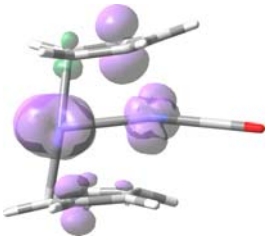 | 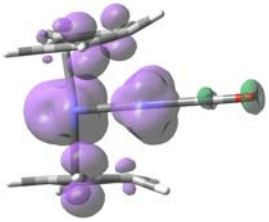 |

Figure 5.1: The structure of $Cp_2FeNi(CO)_3$ found in this work.

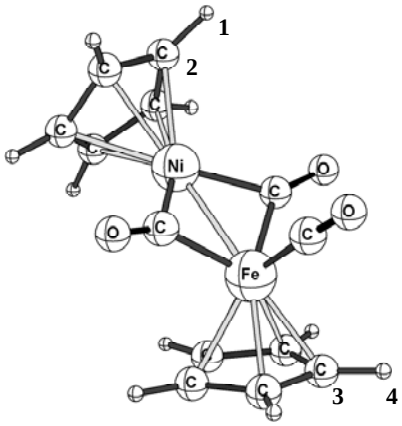


**3-1**

Figure 5.2: The two geometrical structures of $Cp_2FeNi(CO)_2$ found in this work.

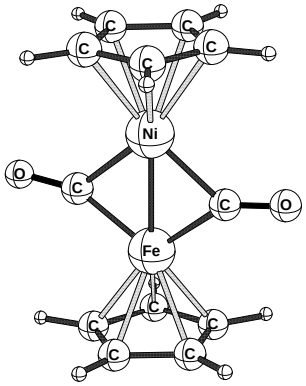


**2-1**

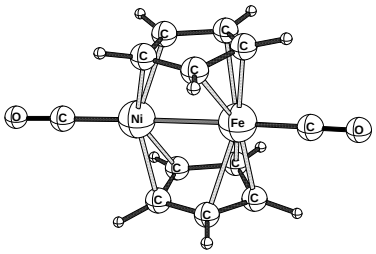


**2-2**

Figure 5.3: The three structures of $Cp_2FeNi(CO)$ found in this work. The numbers on atoms relate to the definitions of bond angles θ and dihedral angle τ in Table 5.3.

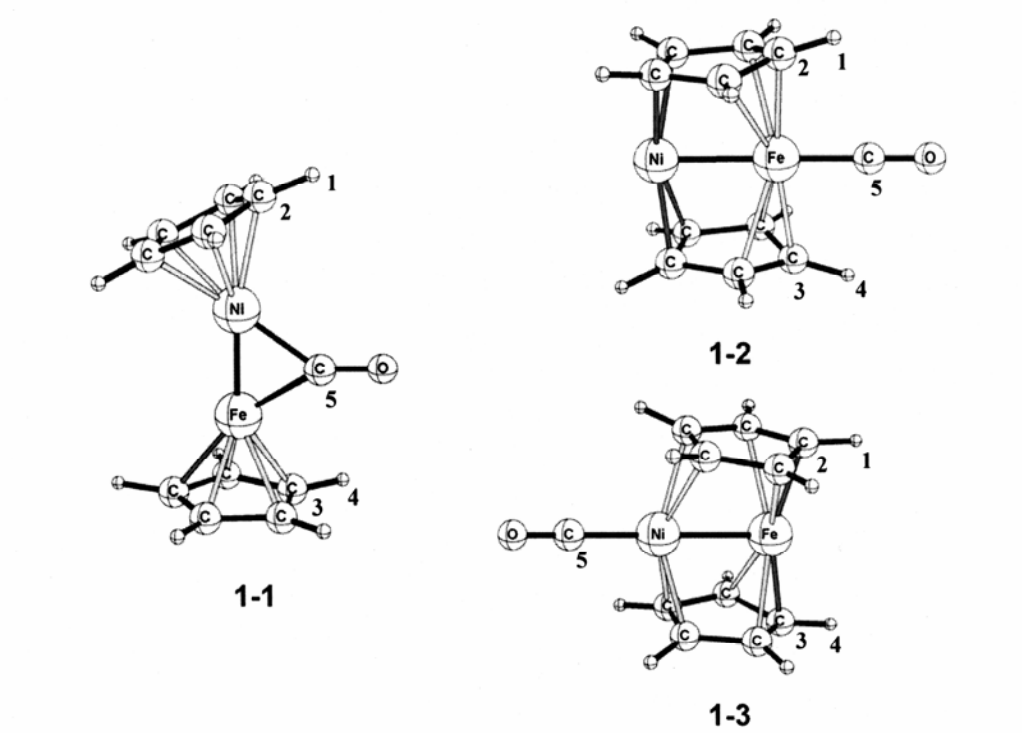

Figure 5.4: The anomalous structure of the quintet state **1-2Q** with a bent Ni–Fe–CO unit found in this work.

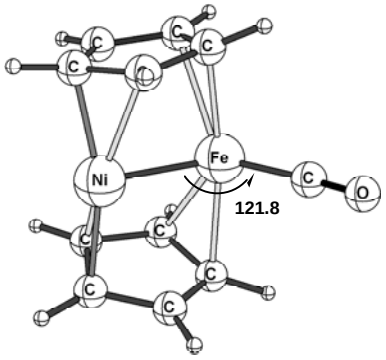


**1-2 Quintet**

Figure 5.5: Alternative structures for $Cp_2MM'(CO)_3$ derivatives.

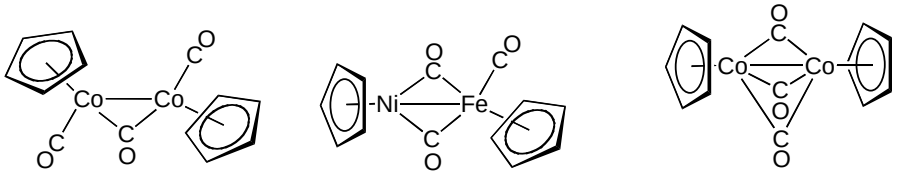


$Cp_2Co_2(CO)_2(\mu\text{-}CO)$ $Cp_2Fe(CO)Ni(\mu\text{-}CO)_2$ $Cp_2Co_2(\mu\text{-}CO)_3$

Figure 5.6: The two structures of $Cp_2Co_2(CO)$ with high spin states (triplet and quintet) investigated in this work.

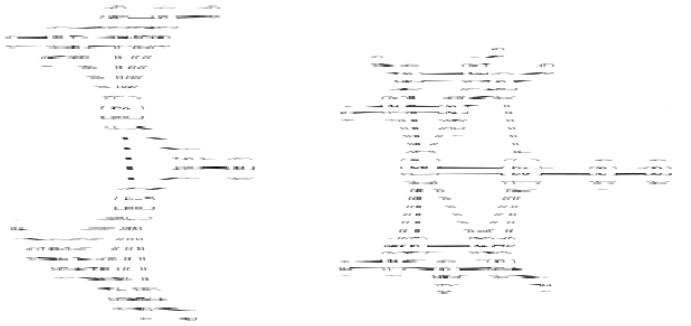

**Co-1** **Co-2**

# CHAPTER 6

# CONCLUDING REMARK

The application of the density functional theory (DFT) has been made to various chemistry problems in this dissertation. These chemical systems include biochemical DNA base pairs and transitional metal clusters. The choice of theoretical methods depends on the interests of chemical system and the size of molecule. Compared to the DFT, the high-level *ab initio* electron correlation methods play significant role in determining molecular structure, vibrational spectrums and potential energy surfaces of very small molecules with less than 10 atoms by given high accurate results, but they are formidable to compute larger molecular systems because of their high demanding for computer memory and CPU time. For example, the state-of-the-art *ab initio* method CCSDT scales $O(N^9)$ computation time consuming, which means when the size of basis sets N (or size of atoms if keeping same basis sets for each atom) doubles, the CPU usage of computation will increase up to $2^9$ times! Thus the DFT is the proper choice to carry out all my theoretical computations involved more than 20 atoms in this dissertation.

In the damaged DNA base and base pair research, I focused on the molecular structures, dissociation energy of base pairs, electron affinities and electron detachment energies. The studies aim to investigate the difference between normal and damaged bases/base pairs in the nascent stage of DNA radiation ionization. A series studies, reported in the Chapter 2 ~ 4, indicates that hydrogenated DNA bases and base pairs have significant positive electron affinities, while the normal bases have near zero electron affinities. The normal base pair and damaged base pairs have similar dissociation energy in the neutral state. However, the incident electron, once bound to base pair valently, can cause significant decrease of dissociation energy for damaged base pairs with lowest free energy, but increase dissociation energy for normal base pair. These fundamental findings may propose a possible way to separate damaged DNA subunits and shed a light in the future development of DNA repair technology.

Theoretical computation of molecules composed of transition metals has been a headache for people to use *ab initio* methods. With proper selection of functional, reliable results can be generated from DFT computations efficiently. Both the heterometallic $Cp_2FeNi(CO)_n$ ($n$ = 3, 2, 1; Cp = $\eta^5$-$C_5H_5$) and homometallic $Cp_2Co_2(CO)_n$ transition metal complexes are thus theoretically practical for the DFT method. In Chapter 6, results of theoretical computation from BP86 functional were elucidated. We discovered that inexistence of heterometallic Cp carbonyls with metal-metal multiple bonds dues to these compounds have even higher free energy than unstable high spin compounds.

Through these studies, the importance of DFT method in computational chemistry has been clearly demonstrated. The applications also show that while DFT provides approximate answers, further improvements are needed for better answers leading to wider applicability. As the computing power continuously to increase, computational chemistry will play a more and more important role in chemistry.